Theses and Dissertations

2019

Behavior and Analysis of Blast-Resistant Precast Concrete Wall Panels with Realistic Boundary Conditions and Openings

Omar Mohammed Alawad
Lehigh University

Follow this and additional works at: https://preserve.lehigh.edu/etd

 Part of the Civil Engineering Commons

Behavior and Analysis of Blast-Resistant Precast Concrete Wall Panels with Realistic

Boundary Conditions and Openings

by

Omar Mohammed Alawad

Presented to the Graduate and Research Committee

of Lehigh University

in Candidacy for the Degree of

Doctor of Philosophy

in

Structural Engineering

Lehigh University

May 2019

Approved and recommended for acceptance as a dissertation in partial fulfillment of the requirements for the degree of Doctor of Philosophy

_____
Date

_____
Clay Naito, Dissertation Co-Advisor

_____
Spencer Quiel, Dissertation Co-Advisor

_____
Accepted Date

Committee Members:

_____
Stephen Pessiki, Committee Chair

_____
Paolo Bocchini, Committee Member

_____
Ned Cleland, External Member

iii

ACKNOWLEDGEMENTS

TABLE OF CONTENTS

LIST OF TABLES

LIST OF FIGURES

ABSTRACT

This dissertation presents a comprehensive assessment of the flexural resistance of non-loadbearing, blast-resistant precast concrete wall panels. A major focus of this research is quantifying the expected response of these panels, considering realistic response mechanisms, boundary conditions, and constitutive properties, in comparison to conventional design standards and prescriptive guidelines. A preliminary study focused on the implementation of a simplified methodology for the rapid assessment of blast-induced damage during the construction bidding process and early design stages. Using this simplified approach, in conjunction with conventional design assumptions, an interactive spreadsheet was developed which facilitates the inclusion of a broad range of panel constitutive parameters while maintaining ease of implementation for precast concrete producers and design engineers. A series of subsequent studies focused on examining the flexural response of panels with realistic boundary conditions, geometric arrangements, material properties, and panel types. These three studies, focused on precast concrete wall panels with discrete connections, openings, and insulated wall panels, respectively, examined realistic failure mechanisms, material-based limit states, flexural capacity and ductility, relative to conventional design assumptions. These examinations were conducted using a finite element modeling approach, validated against several experimental test programs. The results of this study show that, depending upon constitutive properties and panel geometry, conventional design limitations facilitate unexpected failure mechanisms and significant reductions in ductility in many cases. Lastly, design recommendations and detailing strategies for mitigating these adverse consequences are numerically evaluated and discussed herein. The research presented in this study facilitates enhanced detailing of realistic blast-resistant cladding panel configurations while targeting a specific limit state for government, military, or other high risk facilities.

1. INTRODUCTION

Panelized precast concrete facades are commonly used for buildings subject to extreme lateral loads including accidental or intentional blast pressure demands. Precast concrete panels offer several advantages over other conventional façade systems for protective design applications due to their inertial mass and ability to be customized to provide elevated levels of stiffness and strength. Precast panels are produced in a controlled environment and have high quality control, and they can be erected more rapidly than other systems such as cast-in-place reinforced concrete, reinforced masonry, or stick-built metal stud construction.

Due to the dynamic nature of blast loading conditions, specialized design and analysis methods are needed to quantify structural response and determine the extent of component damage following a blast event. These methods can be computationally expensive and require the knowledge and expertise of a blast design consultant. For these reasons, it is not always feasible for precast concrete producers to readily assess the blast-resistant performance of a wall panel system during the early design stages and bidding processes. Chapter 2 evaluates two simplified methodologies for the preliminary design of one-way precast concrete wall panels to resist blast loading. Additionally, an interactive design tool based on these methods has been developed to facilitate the evaluation of a broad range of panel constitutive parameters and increase the ease of implementation for precast concrete producers.

Precast concrete panels are attached to the main structural system, typically at the floor diaphragms, using discretely welded or bolted connections. Therefore, the potential of non-one-way mechanism may occur, yet the current design assumption consider discrete connection to behave as a line support and thus one-way action. Chapter 3 investigate the influence of discrete connections and the current practice design assumptions on the flexural performance of solid non-loadbearing precast concrete cladding panels under uniform lateral pressure due to blast.

When opening is included in blast-resistance wall panels, current practice design assumes that discrete connections behave as a continuous line support thus implying one-way flexural behavior and that continuous regions adjacent to a blast resistant opening act to resist all the demands imparted across the entire surface area of the panel. Chapter 4 examines the implication of discrete connections and the current practice design assumptions on the flexural performance of solid non-loadbearing precast concrete cladding panels with opening(s) under uniform lateral pressure due to blast.

When analyzing insulated panels for blast. Based on this assumption, the current practice design also assumes one-way behavior and the shear ties are considered to provide the composite flexural behavior along the assumed one-way direction (primary direction). Chapter 5 illustrates the effect of discrete connections and the current design assumptions on the flexural performance of insulated non-loadbearing precast concrete cladding panels under uniform lateral pressure due to blast.

2. SIMPLIFIED METHODOLOGIES FOR PRELIMINARY BLAST-RESISTANT DESIGN OF PRECAST CONCRETE WALL PANELS

2.1. Introduction

Precast concrete wall panels are commonly used for exterior building envelopes due to their installation efficiency, high quality control, and design flexibility. For facilities that are vulnerable to explosive threats, these panels often serve as the first line of defense against blast loading and are commonly detailed to resist these severe impulsive loads in addition to conventional loading requirements. Blast demands are considered for anti-terrorism and force protection applications, such as government buildings and military installations, or for facilities at risk of accidental vapor cloud explosions, such as petrochemical or industrial processing facilities. Due to the dynamic nature of blast loading conditions, specialized design and analysis methods are needed to quantify structural response and determine the extent of component damage following a blast event. These methods can be computationally expensive and require the knowledge and expertise of a blast design consultant. For these reasons, it is not always feasible for precast concrete producers to readily assess the blast-resistant performance of a wall panel system during the early design stages and bidding processes. This study evaluates two simplified methodologies for the preliminary design of one-way precast concrete wall panels to resist blast loading. Using efficient and computationally inexpensive approaches, these methods allow the user to rapidly assess the blast resistance of a given panel design, thereby facilitating a more accurate estimation of fabrication and installation costs during the bidding phase. An interactive design tool based on these methods has been developed to facilitate the evaluation of a broad range of panel constitutive parameters and increase the ease of implementation for precast concrete producers.

Precast concrete wall panels provide an attractive design solution for blast resistant applications due to their flexural performance, inertial mass, and customizability. When developing a bid for a facility with blast design requirements, precast producers must rely on previous

experience, internal expertise, or preliminary analyses from a specialized blast design consultant to develop a reliable cost estimate. If the bid is successful, the full extent of blast resistant design calculations is then typically performed by an external consultant. In addition to determining expected deformations and corresponding damage to the panel in accordance with specified performance levels, the blast consultant must calculate the resulting reaction forces which are then used by the precast producer to design appropriate connection details. Large blast-induced reaction forces often lead to unexpectedly large and expensive connections. Since this information usually becomes apparent once the project has already been awarded, cost estimates that were initially provided by the precast producer may no longer be representative of actual construction costs. To address these issues, two simplified blast evaluation methods are presented herein which allow for rapid preliminary design of precast concrete wall panels. The approaches utilize pressure-impulse (P-I) diagrams, i.e. iso-damage curves which represent the potential combinations of reflected pressure and impulse demands that produce a given level of component response. Once P-I curves are determined at critical response levels for a panel design configuration (e.g., at low, medium or high level of damage), the performance of the panel under an array of potential blast hazards can be rapidly assessed. This process facilitates a cost-effective estimation of expected panel response and eliminates the need for complicated dynamic analyses during the bidding phase.

2.2.   Background

2.2.1. SDOF Analysis Methodology

Explosive events generate a shock or pressure wave which radiates outward from the point of detonation. Blast pressure loading initiates when the shock wave makes contact with the surface of the component. A realistic representative blast loading pressure time history, illustrated in Figure 1a, is comprised of a large impulse of positive pressure which then rapidly decays (over a time scale of milliseconds) until a small negative blast pressure region is produced as the shock wave clears. Since it is small and can slightly counteract deformation induced by the larger positive

pressure, the negative phase is often conservatively neglected for simplicity. For further simplicity, the positive phase is often idealized as a triangular pulse function as shown in Figure 1b. This representation of blast loading is widely used in design and will therefore be used for the study presented in this study. The magnitude of the peak reflected pressure and duration of the positive phase are a function of the charge size and standoff distance in accordance with empirical relationships documented in Unified Facilities Criteria (UFC 3-340-02) [1]. The UFC 3-340-02 document used to design construction, includes reinforced concrete and steel structural members, to resist the effects of accidental explosions. Within this dissertation the UFC 3-340-02 is henceforth referred to as UFC for simplicity. The impulse of the blast loading is calculated as the area under the positive pressure time history.
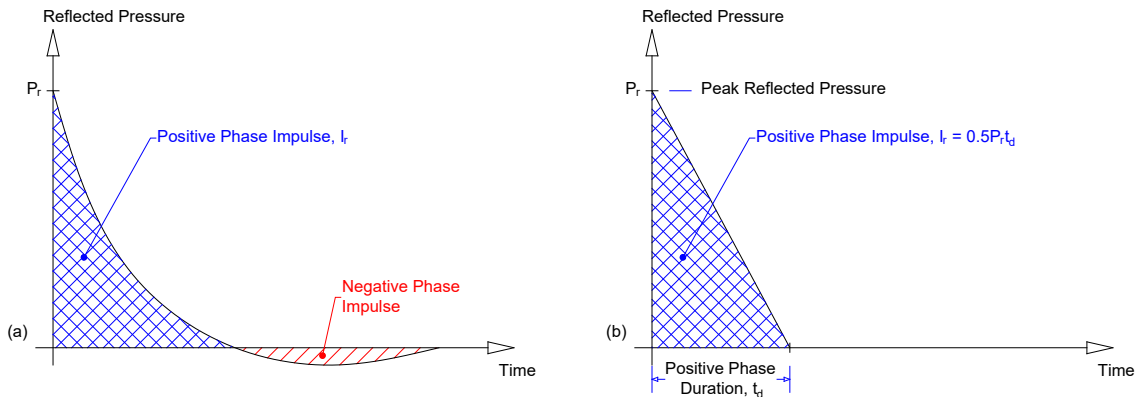
Figure 1 - Blast pressure time histories: (a) realistic representation of both positive and negative pressure phases, and (b) idealized, conservative triangular pulse function with positive phase only

To properly determine the response of structural components to blast events, dynamic analysis methods are used which consider the characteristics of the blast-induced shock wave as well as the flexural behavior of the structural component. Flexural performance is assessed using idealized resistance functions [1] with a generalized single degree of freedom (SDOF) analysis approach as outlined in Biggs [2]. Each component is equilibrated to a mass-spring system (Figure 2b) and allowed only one translational degree of freedom normal to the span length as illustrated in Figure 2a. This approach relies on the assumption of far-field explosive conditions, which implies that the component of interest is far enough from the epicenter of the explosion to justify

the approximation of uniform pressure demands along the entire span length. The response of elements to near-field explosions, which is typically governed by brittle mechanisms such as spall and breach, are not included in the scope of this study since the majority of precast façade panels are designed for far-field hazards.
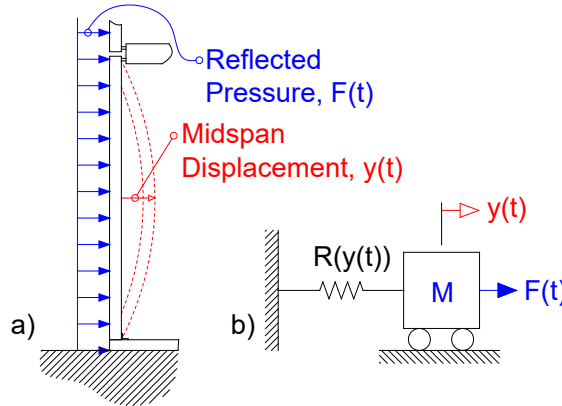
Figure 2 – Building component subject to blast (a) and idealized SDOF system (b)

Wall panels on a building can be modeled with idealized boundary conditions such as fixed-fixed, fixed-simple, or simple-simple depending on the connection detailing of the system and the goals of the analysis. For example, elements being evaluated for maximum deflection under blast loading are commonly analyzed with simple-simple boundary conditions, and evaluations for maximum shear may be performed using fixed supports at one or both ends. Once the component is idealized as a generalized SDOF system, its deformation history can be calculated by solving the dynamic equation of motion as shown in Equation 1, where M is the lumped mass of the system, K_{LM} is the load-mass transformation factor, $R(y(t))$ is the resistance function of the component, $y(t)$ is the midspan displacement of the panel as a function of time, t, and $F(t)$ is the blast pressure versus time history.

$$K_{LM} \, M \, y''(t) + R \, (y(t)) = F(t)$$

Equation 1

The load-mass transformation factor (K_{LM}) is used to equate the distribution of mass and applied blast pressure along the span of the component as a SDOF system. This factor is calculated

via Equation 2 as the ratio of the load and mass factors (K_L and K_M, respectively). For uniform mass and pressure, these factors are calculated using an appropriate shape function for the actual element, $\phi(x)$ and the span length, L, of the member as shown in Equation 3 and Equation 4. Values of K_{LM} that are commonly used in SDOF analyses are presented in Table 1 and assume that a blast-loaded element will experience the same deflected shape as for static loading [2]. The mechanical behavior of the component is represented using the resistance function, R, which describes the relationship between the magnitude of applied load and the resulting midspan deformation. R can be calculated using traditional structural analysis approaches which incorporate the constitutive properties of the materials, compatibility, and force equilibrium. In this approach, it is commonly assumed that a discrete plastic hinge will form at locations where the cross-section yields. An idealized elastic-perfectly-plastic resistance function is often used by assuming a linear elastic response up to the point of component yield, after which the resistance remains constant for all subsequent values of plastic deformation. For reinforced concrete components, the elastic stiffness is calculated assuming a moment of inertia equal to the average of values for gross cross-section and fully cracked behavior. This assumption does not consider the effects of strain hardening in the reinforcing steel or the softening that occurs once the concrete crushing strength is reached. After determining the mass of the component, resistance function, transformation factors, and blast loading demands, midspan deformation of the SDOF model is generated as a function of time using any numerical method suited for dynamic structural analyses. The maximum displacement is then converted to either a ductility ratio or equivalent support rotation for comparison with appropriate blast response criteria to determine the extent of damage to the component.

$$K_{LM} = \frac{K_M}{K_L} \qquad\qquad \text{Equation 2}$$

$$K_L = \frac{1}{L}\int_0^L \phi(x)\,dx \qquad\qquad \text{Equation 3}$$

8

$$K_M = \frac{1}{L} \int_0^L [\phi(x)]^2 \, dx \qquad\qquad\qquad \text{Equation 4}$$

Table 1 Load-mass factors for one-way components blast-loaded with uniform pressure

Boundary condition	Range of behavior	K_{LM}
Simple-simple	Elastic	0.78
	Plastic	0.66
Simple-fixed	Elastic	0.78
	Elastic-plastic	0.78
	Plastic	0.66
Fixed-fixed	Elastic	0.77
	Elastic-plastic	0.78
	Plastic	0.66

2.2.2. *Pressure-Impulse (P-I) Capacity Curves*

It is possible for a structural element to experience the same maximum response (and therefore the same level of protection (LOP)) when subjected to various combinations of reflected pressure and impulse. A series of these combinations can be identified via SDOF analyses and assembled together to produce a *P-I* capacity curve for a component at a given LOP. *P-I* diagrams are commonly utilized in blast-resistant applications such as determining safe standoff distances and establishing acceptable thresholds for human injuries. An early application of obtaining safety distances in this manner was initiated following World War II where buildings damaged by blast loading in the United Kingdom were analyzed for different response limits [3]. Currently, *P-I* diagrams are commonly used as a design tool for a wide array of building façade components, including proprietary window systems, curtain walls, and concrete wall systems.

Generating a *P-I* curve requires multiple iterations of SDOF analyses to identify the relevant response limit, which can be tedious especially in a preliminary design phase. For this reason, several recent research efforts have introduced multiple ways of developing normalized *P-I* diagrams for blast loaded components. Li and Meng [4] developed a normalized *P-I* curve for an elastic SDOF system that is compatible with varying pulse loading shapes. Fallah and Louca [5] approximated the *P-I* curves of idealized structural components by deriving analytical formulas. The formulas depend on a SDOF system with a bilinear resistance deflection curve subjected to different pulse loading shapes. Using this method, the curve can be generated by using one known point in the dynamic range of the plot. Shi et al. [6] derived analytical formulas as a function of constitutive properties to develop a normalized *P-I* curve for reinforced concrete columns. Dragos and Wu [7] proposed an analytical methodology to develop a normalized curve for any pulse loading shape and any bilinear resistance function based on an empirical approach. Dragos et al. [8] derived two equations that can be used to normalize a *P-I* curve for simply supported, one-way, and ultra-high performance concrete slab. Wang et al. [9] developed an analytical formula to generate *P-I* curves for a one-way reinforced concrete slab using pressure and impulse asymptotes. The aforementioned methodologies have certain limitations: Li and Meng [4] can only be used for elastic SDOF systems; Shi et al.[6] and Dragos et al. [8] work for a relatively small set of components; Fallah and Louca [5] requires a SDOF model to be analyzed for at least one point on the dynamic region; and Dragos and Wu [7] requires iteration and integration, which increases the computational cost of developing a point on the normalized *P-I* curve. Two simplified approaches are therefore developed in this study that allow for rapid initial assessment of a wide array of reinforced concrete blast loaded components for a wide range of far-field blast loads. The approaches presented in this study builds upon these previous studies and is tailored specifically to precast concrete wall panels.

A canned set of *P-I* diagrams for use as a prescriptive design aid can be readily developed via a limited set of one-time SDOF analyses if the user is only concerned with a narrow set of design parameters. However, if a designer must consider a broader range of parameters in their blast-resistant projects, the possible variation of *P-I* diagrams can increase significantly due to a large range of available component types, design configurations, and detailing schemes. For example, solid concrete non-load bearing wall panels analyzed for possible combinations consisting of three response limits, three boundary conditions, five span lengths, five concrete compressive strengths and thirteen reinforcement ratios would require 2,925 unique *P-I* diagrams. To more efficiently represent these combinations of possible curves, two simplified approaches are evaluated in this study to calculate *P-I* curves for solid non-prestressed concrete wall panels: (1) a *P-I* normalization approach, and (2) a curve fitting methodology. The effectiveness of each method is examined in comparison to conventional SDOF analyses. A spreadsheet-based tool was developed in conjunction with this study to facilitate seamless integration of one of the simplified design methodologies into preliminary design practices. This tool was developed for use in preliminary design phases and is not intended for preparing official engineering calculations in applications where blast-resistant design provisions are required. The approach will, however, facilitate increased accuracy when estimating panel design and detailing requirements during the bidding phase. These tools can thereby allow precast concrete producers to gain a competitive advantage when considering projects involving blast-resistant facilities.

2.3. Calculation of Minimum Pressure and Impulse Asymptotes

A *P-I* curve consists of three regions: impulsive, dynamic and quasi-static as illustrated in Figure 3. For increased computational efficiency, each region can be calculated separately and then assembled together to complete the full curve. The quasi-static and impulsive regions can be characterized by the minimum pressure (P_0) and impulse (I_0) that the component can resist. These limits can be represented as asymptotes using Equation 5 and Equation 6, respectively, where *E* is

the strain energy of the resistance function (i.e., the area under the curve in Figure 4) up to the deformation corresponding to the desired LOP at y_{Limit}. K_{LM} is the load-mass transformation factor corresponding to the range of the resistance function (i.e., elastic or plastic) in which the desired LOP falls.

The minimum pressure and impulse asymptotes serve as the baseline for properly calculating the entire *P-I* curve for both simplified methods that are evaluated in this study. The dynamic region, which provides connectivity between these asymptotes, can be generated using one of two simplified approaches detailed in this study. The first method, a normalization approach, uses two dimensionless factors to shift the asymptotes of a control P-I curve, which has been obtained from a single SDOF calculation of a "control element" (which has representative characteristics of a blast-resistant precast panel). Using the *P-I* curve from the control element provides appropriate curvature to the dynamic region of a *P-I* curve for the panel of interest. The second method, a curve fitting approach, is performed by first calculating both asymptotes and then using an analytical formula, which considers the magnitude of each asymptote, to define the dynamic region of the *P-I* curve between those asymptotes. For these reasons, careful consideration is given to properly characterizing and calculating the asymptotes.
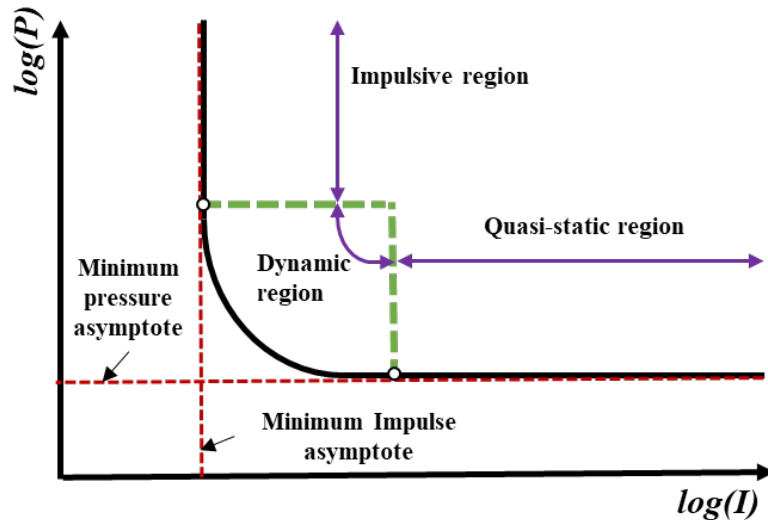
Figure 3 - Representative loading regions of a *P-I* curve

12
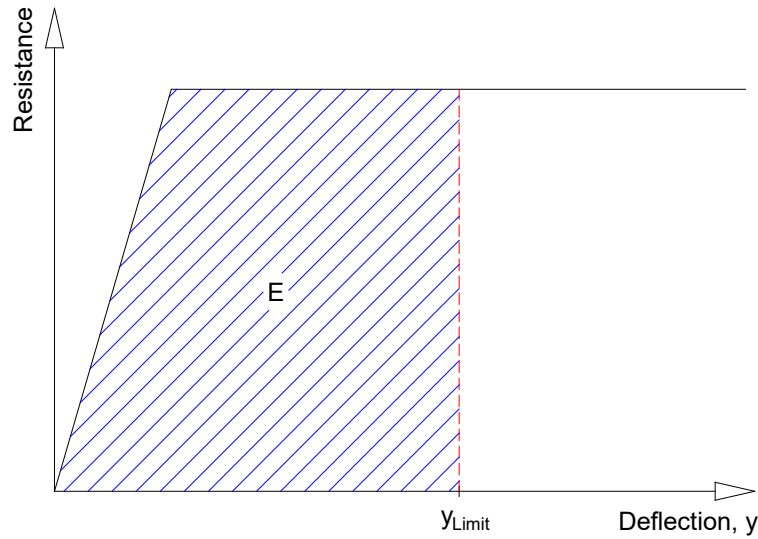
Figure 4 Representative elastic-perfectly-plastic resistance-deflection function

$$I_0 = \sqrt{2 \times E \times K_{LM} \times M}$$ Equation 5

$$P_0 = \frac{E}{y_{Limit}}$$ Equation 6

Both methods are applicable for one-way, single span, non-load bearing reinforced concrete solid wall panels with simple-simple, simple-fixed, and fixed-fixed boundary conditions. The proposed approach can be extended for use on prestressed and insulated wall panels, but only with further development. Like most simplified blast design calculations, far-field explosive conditions are assumed, and the blast-pressure versus time history is idealized as a triangular pulse load (neglecting the negative phase). A more detailed discussion of each simplified method is presented in the following sections of this study.

2.4. Simplified Method 1: Normalization Approach

The first approach generates the *P-I* curve for a given wall panel by shifting a baseline P-I curve for a control component according to the ratio the pressure and impulse asymptotes between the element of interest and the control component. This approach builds on a "normalization" analysis strategy from Dragos et al. [8] and introduces additional features to facilitate ease of implementation and use with precast concrete wall panels. To provide a basis for the normalization

13

strategy, a control component is introduced. A *P-I* curve for the control component is developed using traditional SDOF methodology and acts as a baseline for generating curves for other component configurations. Since it is fully defined, the control curve can be scaled to determine the *P-I* curve for the component of interest. The shift between the *P-I* curves for the control component and the component of interest is based on the ratio of the asymptotes calculated using Equation 7 and Equation 8 for impulse (ψ_I) and pressure (ψ_P), respectively. The control asymptotes are defined as $P_{0,c}$, $I_{0,c}$, and those for the component of interest are identified as P_0, I_0. These factors will be used to shift the control *P-I* curve and generate the *P-I* curve for the component of interest at the desired LOP. The control component is shifted by multiplying the respective control component impulse and pressure vectors, I_c, P_c, by these factors as shown in Equation 9 and Equation 10, resulting in the *P-I* curve for the component of interest as shown in Figure 5. For the purposes of this study, the control wall panel component illustrated in Figure 6 was selected. The P-I curve data points for the control component are summarized in Table 2. The associated $I_{0,c}$ and $P_{0,c}$ are 403.62 kPa-ms and 15.86 kPa (58.54 psi-ms and 2.30 psi).

$$\psi_I = \frac{I_0}{I_{0,c}} \qquad\qquad \text{Equation 7}$$

$$\psi_P = \frac{P_0}{P_{0,c}} \qquad\qquad \text{Equation 8}$$

$$I = \psi_I \times I_c \qquad\qquad \text{Equation 9}$$

$$P = \psi_P \times P_c \qquad\qquad \text{Equation 10}$$
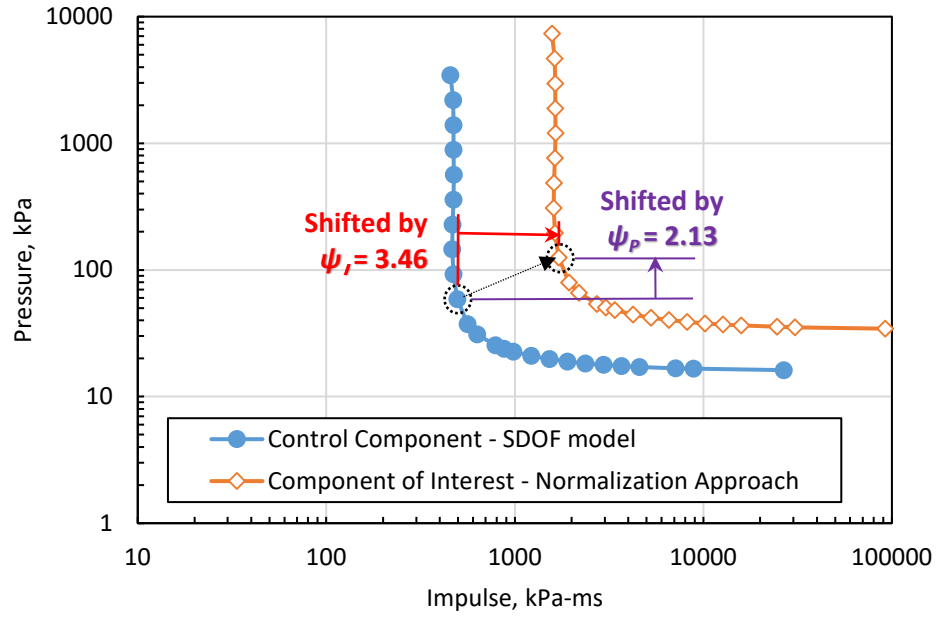
Figure 5 Example of shifting control component. Note: 1 kPa = 0.1450 psi

a)

b)
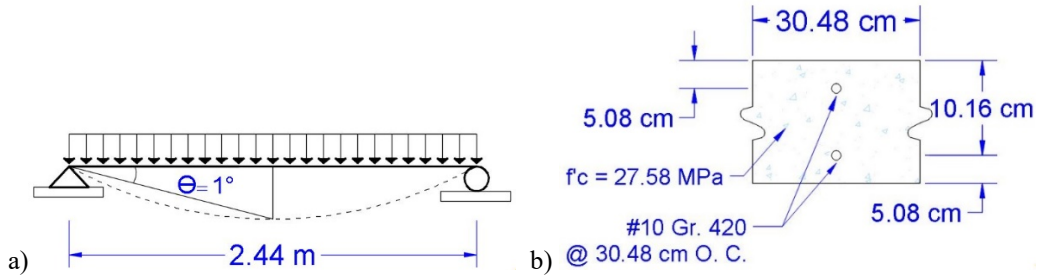
Figure 6 Selected control component data; (a) span and response limit and (b) cross-section properties.
Note: 1 kPa = 0.1450 psi and 2.54 cm = 1 in

Table 2 Impulse and pressure values of the control component

Impulse [psi-ms]	Pressure [psi]	Impulse [psi-ms]	Pressure [psi]	Impulse [psi-ms]	Pressure [psi]
66.07	500.00	71.77	8.52	343.53	2.65
68.27	318.04	81.47	5.42	428.07	2.58
68.67	202.30	91.76	4.49	533.42	2.53
68.67	128.67	114.34	3.68	664.69	2.49
68.97	81.85	127.37	3.45	1032.11	2.43
68.57	52.06	142.48	3.28	1286.12	2.40
67.77	33.11	177.54	3.03	3864.07	2.34
67.47	21.06	221.24	2.87	n.d.	n.d.
68.47	13.40	275.68	2.74	n.d.	n.d.

Note: 1 psi = 6.8948 kPa

The accuracy of the normalization approach is evaluated by comparing the resulting shifted P-I curves to traditional SDOF analyses. A case study of 9,450 wall panel design configurations was performed. Errors between the normalization approach and the SDOF analyses were calculated for each wall panel design and LOP. For each design, the error was calculated over the three separate regions: impulsive, dynamic and quasi-static as shown in Figure 7a. The total error for each curve was determined using a root mean square calculation. The errors calculated in the impulsive and quasi-static (i.e. pressure governed) regions were determined by simply calculating the horizontal or vertical difference, respectively, between the normalization and SDOF *P-I* curves at each discrete point in those regions. For the dynamic region, the differences between the curves were determined using a radial distance approach. To do this, the central point of the radial curve must first be determined. For this evaluation, this point was chosen as the intersection of the minimum pressure value, $P_{impulsive}$, in the impulsive region and the minimum impulse value, $I_{quasi-static}$, for the quasi-static region as illustrated in Figure 7a. $P_{impulsive}$ is located where the slope of the *P-I* curve, as you move from the impulsive to dynamic region, exceeds an angle of 15°. In a similar

16

manner $I_{quasi\text{-}static}$ is located where the slope of the *P-I* curve, as you move from the quasi-static to dynamic region, exceeds an angle of $0.015°$. A smaller angle change is used for this region because the overall slope of the transition between the quasi-static and dynamic regimes is more gradual than for the impulsive to quasi-static region. Due to the shift, the points on the normalized curve do not align perfectly with their SDOF counterparts along the radial line intersections. To compute the error along the radial lines, the normalized curve is re-discretized relative to points on the SDOF curve as illustrated in Figure 7b. The error between the normalized curve and the SDOF solution was calculated using Equation 11, where subscripts labeled "SDOF" and "NM" represent the values for the SDOF and normalization curves, respectively. Total errors are illustrated using a probability density function (PDF) in Figure 8. Approximately 95% of the examined cases have error percentages between +/- 6%. This simplified approach has acceptable accuracy as preliminary design tool for precast concrete wall panels under blast loads. The method is also found to be well-suited for computer-based computations and was therefore deployed as a spreadsheet-based design tool, which is presented later in this study.
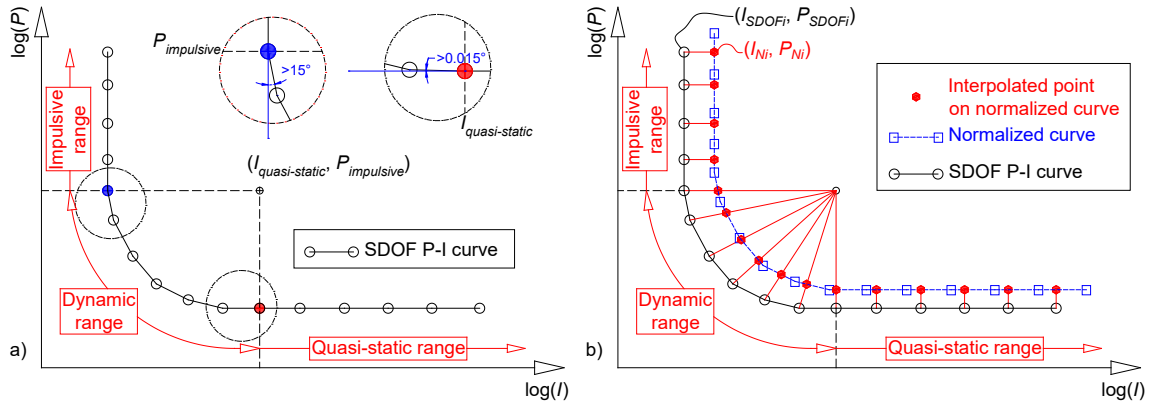
Figure 7 Graphical representation of the error calculation for the normalization approach

$$Error\ (\%) = \sqrt{\left(\frac{I_{SDOF} - I_{NM}}{I_{SDOF}}\right)^2 + \left(\frac{P_{SDOF} - P_{NM}}{P_{SDOF}}\right)^2} \times 100 \qquad \text{Equation 11}$$
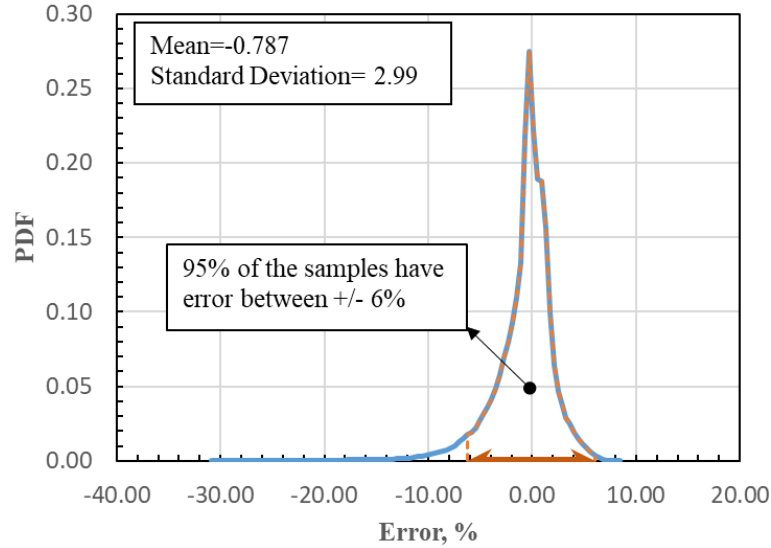
Figure 8 PDF of errors for the normalization approach

2.5.   Simplified Method 2: explicit Curve Fitting approach

The second approach explicitly links the pressure and impulse asymptotes using a closed-form analytical expression. This "explicit curve fitting" approach builds upon work previously conducted by Wang et al. [9], which developed an analytical formula to generate P-I curves for one-way reinforced concrete slabs. The original formula by Wang et al. [9] is shown in Equation 12,d where n is equal to 0.6 and 0.5 for flexural and shear failure modes, respectively. This approach allows reflected pressure, P, to be defined as a function of impulse, I, or vice-versa. A plot of this equation will directly connect the pressure and impulse asymptotes, thereby forming the dynamic region of the P-I diagram (see Figure 7).

$$(P - P_0)(I - I_0)^n = 0.33(\frac{P_0}{2} + \frac{I_0}{2})^{1.5}$$

Equation 12

The pressure and impulse asymptotes are calculated using Equation 5 and Equation 6 as shown previously. The minimum pressure asymptote lies in the semi-static region and therefore shows a consistent strong agreement (i.e. with errors generally less than 15%) with that calculated via SDOF methods. As shown in Figure 9, however, the minimum impulse asymptote obtained from Equation 6 can exhibit slightly more error versus that calculated via SDOF methods. Recall

18

that the minimum impulse asymptote is calculated using a K_{LM} that assumes quasi-static deflected shapes for blast loaded elements (see Equation 5). As the *P-I* calculations trend towards an increasingly impulsive response at the corresponding minimum asymptote, the assumed quasi-static formulation of K_{LM} may not capture realistic variations in the shape function due to higher order modal vibration effects. As the response of the component becomes more impulse-dominant, it is expected that the value of K_{LM} would increase, thereby increasing the minimum impulse asymptote (i.e. shifting it to the right) and move closer to the limits of the *P-I* curve. An impulse asymptote modification factor, γ, is proposed to mitigate this effect as shown in Equation 13. I_{min_SDOF} represents the minimum impulse value of the *P-I* curve generated using traditional SDOF methods. An evaluation of precast panels was performed to determine optimal values for this factor. Natural period, T_n, are calculated using Equation 14 where *k* is the elastic stiffness of the component and K_{LM} corresponds to the elastic range. Factors were calculated for three different antiterrorism response limits for non-prestressed concrete components [10] and are plotted in Figure 10. From these plots, conservative values of γ can be selected for several ranges of natural periods. For components with low natural periods (below 50-100 ms), γ ranges from 1.07 to 1.18. For higher natural periods, γ has a much wider distribution. Conservative floor values for these modification factors are marked with a solid orange line in Figure 10 and are summarized in Table 3 for relevant ranges of natural periods and response limits.
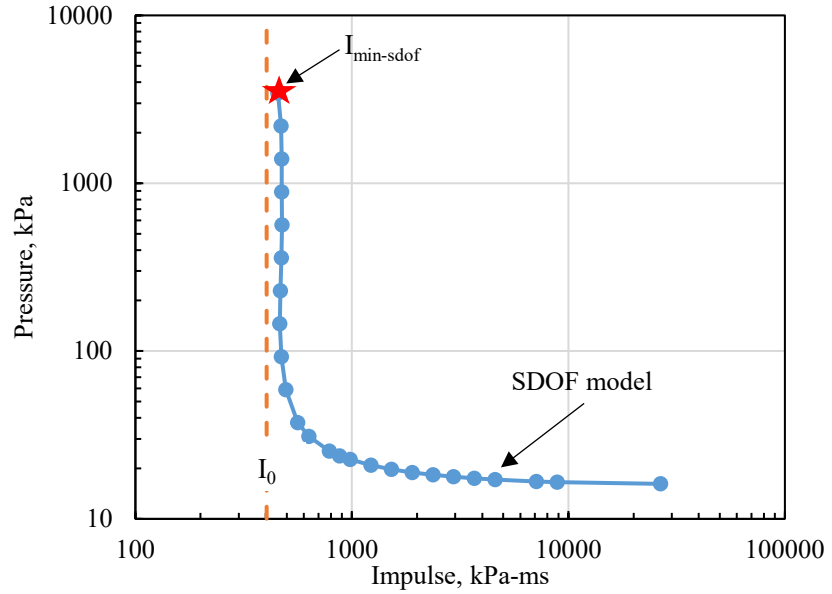
Figure 9 Divergence of P-I curve on impulsive range from impulse asymptote. Note: 1 kPa = 0.1450 psi

$$\gamma = \frac{I_{\min\_sdof}}{I_0}$$

Equation 13
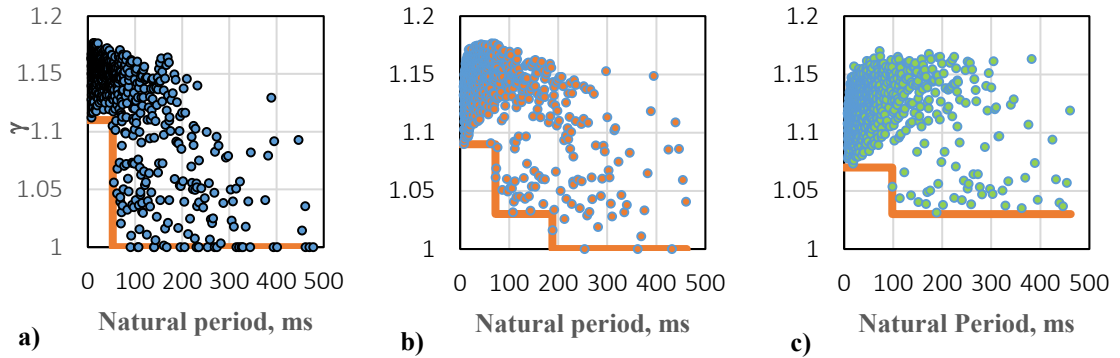
Figure 10 Impulse asymptote modification factor; a) $\theta=1°$, b) $\theta=2°$, and c) $\theta=5°$

$$T_n = \frac{2\pi}{\sqrt{\dfrac{k}{K_{LM} \times M}}}$$

Equation 14

20

Table 3 Recommended impulse asymptote modification factor

Support rotation response limit, θ [deg]	Natural period of component, T_n [ms]	Impulse modification factor, γ
1	$T_n \leq 53$	1.11
	$T_n > 53$	1.00
2	$0 < T_n \leq 72$	1.09
	$72 < T_n \leq 188$	1.03
	$T_n > 188$	1.00
5	$T_n \leq 98$	1.07
	$T_n > 98$	1.03

To better capture wall panel response, Equation 12 is modified such that two new parameters, a and b, replace the numeric coefficients of the equation. The new formulation in Equation 15 also includes the impulse modification factor, γ, which is multiplied to the impulse asymptote I_0. Optimal values for a and b were determined by examining 630 different panel configurations. *P-I* curves that are generated via the curve fitting approach for each trial combination of a and b were investigated and compared with curves generated using traditional SDOF methods. Figure 11 shows a surface plot of the average *P-I* error for a single panel configuration over relevant ranges of a and b values. The combination of a and b which resulted in the lowest average error for each panel configuration was selected and added to a frequency histogram in Figure 12. Recommended values of $a = 0.35$ and $b = 0.80$ are the combination that most often resulted in the lowest error in Figure 12 across the 630 panel configurations.

$$(P - P_0)(I - \gamma I_0)^b = \text{a}(P_0 + \gamma I_0) \qquad \text{Equation 15}$$
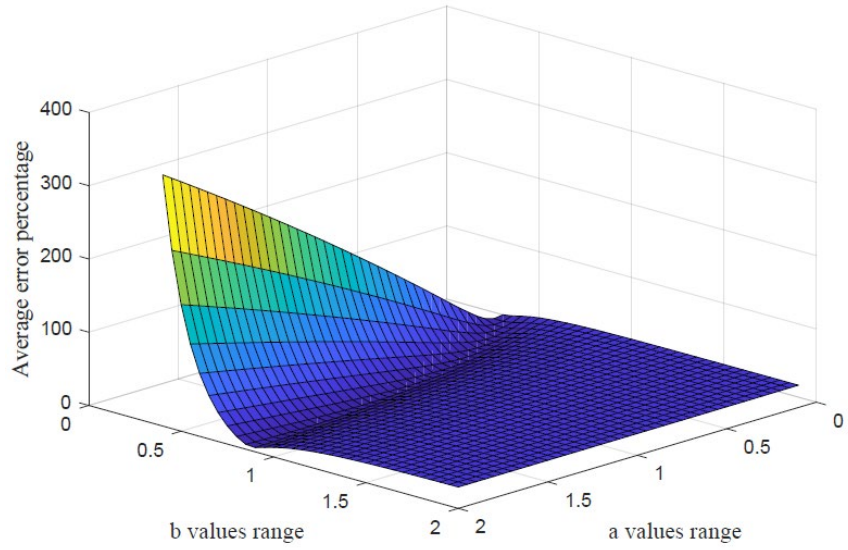
Figure 11 Average error percentage for *a* and *b* values for a representative panel
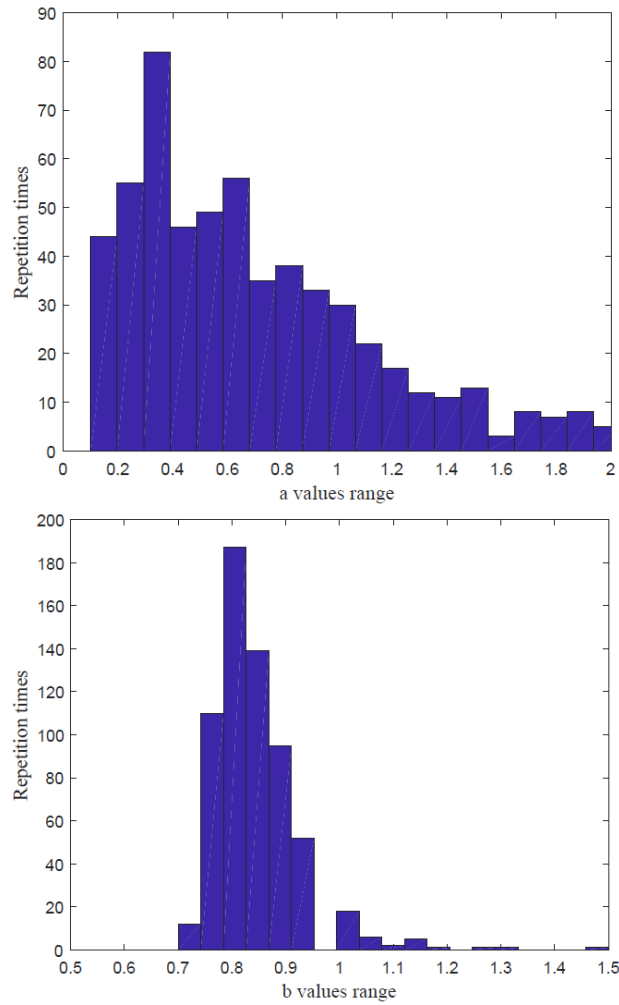
Figure 12 Frequency histograms of *a* and *b* values which result in minimum error for all panel configurations

For verification, *P-I* curves that are generated using Equation 15 with the recommended values of *a, b,* and γ were compared with SDOF solutions for the 630 panel configurations. The error percentage of each point along the *P-I* curves across all panel configurations is summarized as a PDF in Figure 13. The PDF shows that error percentages range from approximately -20% to 200%. Approximately 70% of the examined cases have error percentages between -13% and 27%. Although this approach results in a wider range of potential error than the normalization method, the curve fitting method still enables an efficient and reasonably accurate generation of *P-I* curves for preliminary design of blast resistant precast panels via a closed-form equation rather than SDOF analyses, which have higher computational expense. Because it is closed form, the curve fitting method is well suited for implementation in design handbooks.
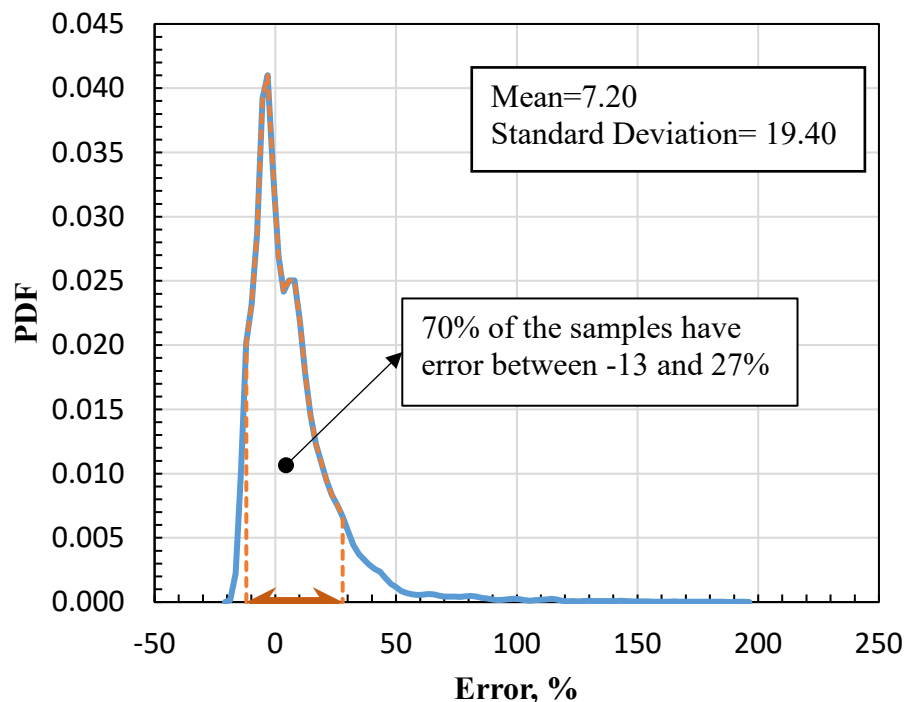
Figure 13 PDF of errors (curve fitting vs. SDOF) across all panel configurations for the curve fitting approach

2.6. P-I Curve Development Illustration

An example which implements the two proposed approaches is provided below as a demonstration.

Required: Develop a *P-I* curve for the wall component outlined below with a support rotation limit of 1° using (a) the normalization approach, and (b) the curve fitting approach.

Given: A simply supported 3657.6 mm (12 ft) tall and 203.2 mm (8 in). thick wall panel with 16M (#5) rebar at 304.8mm (12 in). on center. The tension reinforcement is located at a depth of 152.4 mm (6 in) with a 50.8 mm (2 in) cover to center of bars. The concrete has a compressive strength of 27.58 MPa (4 ksi), and grade 420 (60) reinforcement is used. The concrete density is 2403 kg/m³ (150 pcf). Static and dynamic increase factors for the steel reinforcement are 1.10 and 1.17, respectively. The dynamic increase factor for concrete is 1.19.

Note: A unit width will be analyzed, and top reinforcement is neglected

Procedure: Part (a) normalization approach

Step 1.	Obtain given parameters of the control component
Step 2.	Establish given parameters of the targeted component
Step 3.	Determine dynamic moment capacity of the targeted component
Step 4.	Compute elastic stiffness and ultimate resistance at mid-span for the targeted component
Step 5.	Compute the impulse and pressure asymptotes of the targeted component using Equation 5 and Equation 6
Step 6.	Compute impulse and pressure normalization factors using Equation 7 and Equation 8, respectively
Step 7.	Develop the impulse and pressure curve for the targeted component using Equation 9 and Equation 10, respectively

Procedure: Part (b) the curve fitting approach

Step 1.	Same as in step 2 of part (a)
Step 2.	Same as in step 3 of part (a)
Step 3.	Same as in step 4 of part (a)

24

Step 4.   Same as in step 5 of part (a)

Step 5.   Determine the impulse asymptote modification factor from Table 3

Step 6.   Develop the impulse and pressure curve for the targeted component using

            Equation 15

Solution: Part (a) – normalization approach

Step 1. Given parameters of the control component:

Boundary conditions:	Simply supported
Area of #3 bar:	$As_c = 0.11$ in^2
Span length:	$L_c = 8$ ft
Depth of reinforcement:	$d_c = 4$ in
Concrete compressive strength	$fc'_c = 4$ ksi
Thickness	$h_c = 6$ in
Concrete unit weight	$\gamma_c = 150$ pcf
Minimum impulse asymptote	$I_{0,c} = 58.54$ psi-ms
Minimum pressure asymptote	$P_{0,c} = 2.30$ psi
Impulse and pressure for response limit	See Table 3

1°

Step 2. Given parameters of the targeted component:

Boundary conditions:	Simply supported
Area of #5 bar:	$As_T = 0.31$ in^2
Span length:	$L_T = 12$ ft
Depth of reinforcement:	$d_T = 6$ in
Concrete compressive strength:	$fc'_T = 4$ ksi
Thickness:	$h_T = 8$ in

Concrete unit weight:	$\gamma = 150 \text{ pcf}$
Concrete elastic modulus:	$E_c = 33 \times 150^{1.5} \times \sqrt{4000} = 3834 \ ksi$
Dynamic steel tensile strength:	$fdy_T = 1.17 \times (1.10 \times 60) = 77.22 \ ksi$
Dynamic steel tensile strength:	$fdc_T = 1.19 \times 4 = 4.76 \ ksi$

Step 3. Determine dynamic moment capacity of the targeted component:

Dynamic moment capacity:

$$M_{du} = As_T \times fdy_T \times \left(0.5 \times \frac{As_T \times fdy_T}{0.85 \times fdc_T \times b}\right)$$

$$M_{du} = 0.31 \times 77.22 \times \left(0.5 \times \frac{0.31 \times 77.22}{0.85 \times 4.76 \times 12}\right)$$

$$= 137.73 \ kip - in$$

Step 4. Compute elastic stiffness and ultimate resistance at mid-span of the targeted component:

Average moment of inertia:

$$I_{av} = \frac{I_g + I_{cr}}{2} = \frac{512 + 60.54}{2} = 286.27 \ in^4$$

Elastic stiffness:

$$k = \frac{384 \times E_c \times I_{av}}{5 \times L_T{}^4 \times b}$$

$$k = \frac{384 \times 3834000 \times 286.27}{5 \times 144^4 \times 12} = 16.34 \ psi/in$$

Ultimate resistance:

$$r_u = \frac{8 \times M_{du}}{L_T^2 \times b}$$

$$r_u = \frac{8 \times 137730}{144^2 \times 12} = 4.43 \ psi$$

Step 5. Compute the impulse and pressure asymptotes of the targeted component

Elastic and plastic load mass factor:	$K_{LM} = 0.78$ (elastic), $K_{LM} = 0.66$ (plastic)

Mass:

$$M = \frac{h_T \times \gamma}{g} = \frac{8 \times 0.08681}{386 \times 60^2} = 1799 \ psi \cdot ms^2/in$$

Mid-span displacement at 1°:

$y_{limit} = \tan(\theta) \times L_T \times 0.5 = 1.26 \ in$ (larger than

y_e)

Strain energy:

$$E = 0.5 \times r_u \times y_e + r_u \times (y_{limit} - y_e)$$

$$= 4.97 \ lb/in$$

Impulse asymptote:

$$I_0 = \sqrt{2 \times E \times K_{LM} \times M}$$

$$= \sqrt{2 \times 4.97 \times 0.66 \times 1799} = 108.57 \ psi \cdot ms$$

Pressure asymptote

$$P_0 = E/y_{limit} = 4.97/1.26 = 3.95 \ psi$$

Step 6. Compute impulse and pressure normalization factors

Impulse normalization factor:

$$\psi_I = I_0/I_{0,c} = 108.57/58.54 = 1.86$$

Pressure normalization factor:

$$\psi_P = P_0/P_{0,c} = 3.95/2.30 = 1.72$$

Step 7. Develop the impulse and pressure curve for the targeted component

Impulse:

$$I = \psi_I \times I_c \text{ (see Table 4)}$$

Pressure:

$$P = \psi_P \times P_c \text{ (see Table 4)}$$

Table 4 Impulse and pressure values of the targeted component using normalization approach

Impulse [psi-ms]	Pressure [psi]	Impulse [psi-ms]	Pressure [psi]	Impulse [psi-ms]	Pressure [psi]
122.49	859.50	133.06	14.65	636.90	4.56
126.57	546.71	151.04	9.32	793.64	4.44
127.31	347.75	170.12	7.72	988.96	4.34
127.31	221.19	211.99	6.33	1232.34	4.27
127.87	140.69	236.14	5.93	1913.54	4.17
127.12	89.49	264.16	5.64	2384.46	4.13
125.64	56.92	329.16	5.22	7163.99	4.03
125.08	36.21	410.17	4.93	n.d.	n.d.
126.94	23.03	511.11	4.71	n.d.	n.d.

Note: 1 psi = 6.8948 kPa

Solution: Part (b) – the curve fitting approach

Step 1 to Step 4: Same solution as Step 2 to Step 5 in part (a).

Step 5. Determine impulse asymptote modification factor

Natural period:
$$T_n = 2 \times \pi \times \sqrt{K_{LM} \times M/k}$$

$$= 2 \times \pi \times \sqrt{0.66 \times 1799/16.34} = 53.56 \; ms$$

Modification factor (from Table 3): $\qquad\qquad\qquad \gamma = 1$

Step 6. Develop the impulse and pressure curve of the targeted component

By assuming values of impulse, use Equation 15 to calculate pressure:
$$P = \frac{a(P_0 + \gamma I_0)}{(I - \gamma I_0)^b} + P_0$$

$$P = \frac{0.35 \times (3.95 + 1 \times 108.57)}{(I - 1 \times 108.57)^{0.8}} + 3.95$$

(The solution is shown in Table 5)

Table 5 Impulse and pressure values of the targeted component using curve fitting approach

Impulse [psi-ms]	Pressure [psi]	Impulse [psi-ms]	Pressure [psi]	Impulse [psi-ms]	Pressure [psi]
122.48	500.00	170.12	7.33	1109.62	4.28
125.18	334.09	205.21	6.21	1338.49	4.23
125.58	223.23	216.18	5.93	1614.57	4.19
125.88	149.15	247.53	5.61	1947.60	4.16
126.18	99.66	298.59	5.23	2349.31	4.13
126.58	66.59	360.18	4.96	2833.89	4.12
126.98	44.49	434.47	4.77	3418.42	4.10
126.98	29.73	524.09	4.62	4123.51	4.08
128.18	19.86	632.19	4.50	4974.04	4.07
133.08	13.27	762.58	4.41	6000.00	4.06
148.18	8.87	919.88	4.34	n.d.	n.d.

Note: 1 psi = 6.8948 kPa

Summary: The *P-I* curves that were obtained for the targeted component via the normalization and curve fitting approaches are compared against a *P-I* curve obtained from SDOF analysis of the same component (Figure 14).
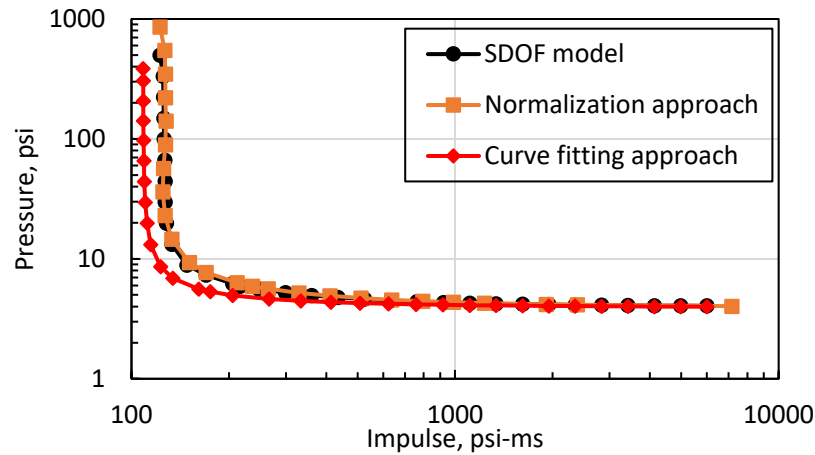
Figure 14 Targeted component *P-I* curves, obtained via the normalization and curve fitting approaches as well as SDOF analysis. Note: 1 psi = 6.8948 kPa

2.7.   Simplified *P-I* generating tool

To better facilitate the implementation of the proposed methods into conventional engineering practices, a spreadsheet-based tool was developed to enable users to easily generate the *P-I* curves based on a set of input parameters that correspond to the wall panel of interest. Due to its overall lower error distribution, the normalization approach was selected as the featured method for this tool. The main purpose of this tool is to provide a rapid evaluation of component damage when subjected to a blast load. To use this tool, the user must first obtain the blast pressure and impulse demands (i.e. the design-basis threat) and select the desired response limit. The constitutive properties of the component of interest can then be input to the spreadsheet, after which the tool determines whether the component is able to satisfy the desired LOP for the given blast demands. If the initial design does not satisfy the response limit (i.e. the blast demand point falls above and to the right of the *P-I* curve), the designer can easily change the design parameters until the component meets the desired LOP. The tool also provides the plastic moment capacity of the wall and the reaction forces, which allows the designer to rationally estimate the connection types

29

needed to satisfy the given blast demands. A screenshot of the simplified tool is shown in Figure 15. It should be noted that this tool is intended only for preliminary design and should not be used for final design evaluation.
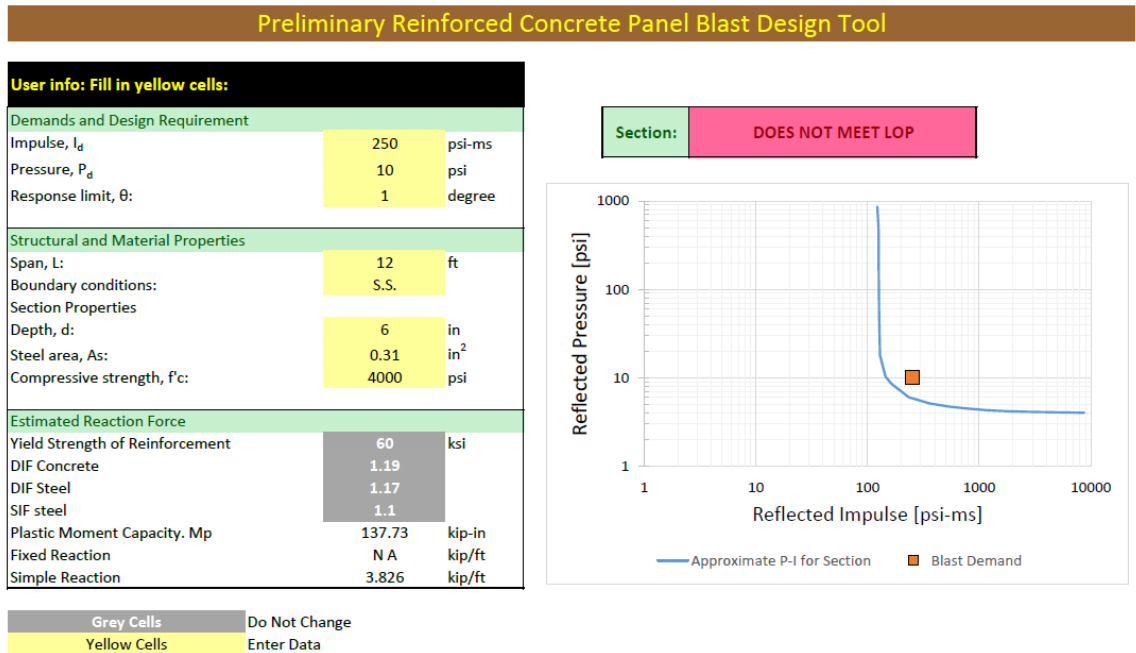
Figure 15 Screenshot of the spreadsheet-based tool for simplified *P-I* calculation via the normalization method

3. FLEXURAL RESISTANCE OF NON-LOADBEARING PRECAST CONCRETE FAÇADE PANELS WITH DISCRETE CONNECTIONS SUBJECT TO BLAST LOADING

3.1. Introduction

A building façade provides the first line of defense in protecting occupants against exterior blast threats. Blast hazards are typically bifurcated into two classifications: near-field, to which a façade panel responds via breach and spalling; or far-field, for which a panel response is characterized by flexure and shear. This paper addresses the response to far-field blast hazards, which constitutes a majority of intentional or accidental hazards that are addressed by current blast resistant design standards for buildings [1,2]. Concrete panels are often chosen for blast resistant building applications due to their mass and customizable strength and ductility. Precast panels possess several advantages over cast-in-place concrete, including high quality control via plant fabrication and rapid erection and enclosure of the building. Unlike cast-in-place concrete construction, precast concrete panels are attached to the main structural system, typically at the floor diaphragms, using discretely welded or bolted connections. During the blast design process, discrete connections are often idealized as continuous line supports along the panel edge at the floor diaphragms. The panels are thereby designed to span vertically to resist the blast load while the horizontal (i.e. transverse) direction is often detailed with only minimal (i.e. temperature and shrinkage) requirements for reinforcement [13,14]. Depending upon the connection spacing, boundary condition assumptions and cross-section properties, the realistic flexural response of the component may not be constrained to one direction only. Formation of two-way flexural behavior may lead to significant discrepancies in both strength and ductility relative to the one-way design assumptions. In some cases, the transverse direction, designed for only minimum reinforcement

requirements, may govern the response mechanism and exhibit significantly less flexural resistance than expected.

The goal of this paper is to investigate the influence of discrete connections and the ratio of vertical-to-horizontal ultimate resistance, calculated following the current approach, on the flexural performance of solid (i.e. single wythe, not insulated) non-loadbearing precast concrete cladding panels under uniform lateral pressure due to blast. The study utilizes a validated finite element (FE) model to compare the load-deflection response of panels with realistic connection layouts with the assumed one-way flexural response commonly used in current design practice. The outcomes of this study provide guidance regarding the appropriate selection of modeling parameters and limit states when conducting blast resistant design of precast façade panels with discrete connections. Note that this study does not address the response of precast panels with openings for windows, doors, and ventilation or insulated wall panels. These topics will be the focus of future work.

3.2. Background

Precast cladding wall panels are designed with a variety of geometric shapes and connection arrangements. The panel geometry and connection layout are determined based on architectural design (e.g. the layout of corners, windows, doors, and other openings in the façade), shipping or erection limitations, and the location of available supports at floor slabs and other framing. A generic solid precast wall panel is shown in Figure 16a with a one-story vertical span between floor diaphragms and an approximate aspect ratio of 2. The panel is shown with a common layout of six discrete connections that are capable of resisting lateral displacement. Since most non-load bearing façade panels are hung from the building, the top row of connections would also be designed to carry the panel self-weight.
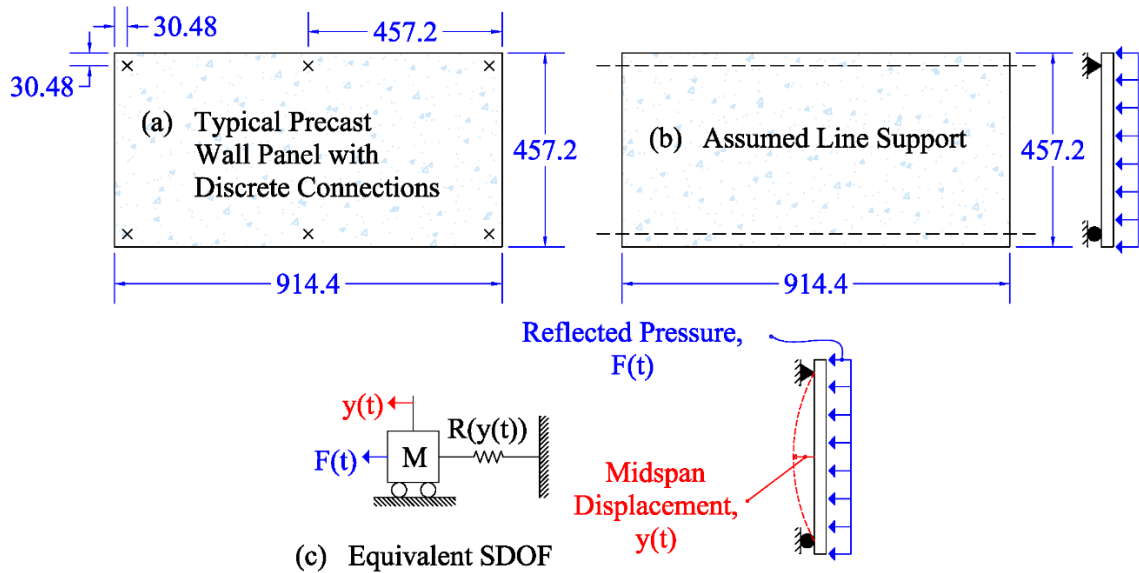
Figure 16. Current practice design process

In current practice, blast resistant design is typically initiated after a conventional design of the wall panel for shipping, handling, and service loads is completed. Though some panels are commonly designed using prestressing strands to control cracking, most of the conventional design is typically achieved using mild steel reinforcement (either rebar or welded-wire reinforcement). This study will focus on panels that are reinforced with steel rebar (i.e. not prestressed). For blast resistant design, the precast panel is typically modeled assuming one-way response and idealized continuous boundary conditions as shown in Figure 16b [15]. It is generally assumed that the presence of multiple connections along the top and bottom of the panel will minimize flexure in the horizontal direction and provide an equivalent "line" support to vertical flexure. Using these assumptions, it is standard practice to utilize an equivalent single degree of freedom (SDOF) system [2], as shown in Figure 16c, to assess the blast performance of the component.

As shown in Figure 17, two types of discrete connections are typically used to support non-loadbearing precast cladding components in US practice: bearing and tieback. Bearing connections are designed to resist gravity loads without significant restraint to out-of-plane demands. Tieback connections are used to resist out-of-plane lateral loading conditions such as wind and blast demands. Some tieback connections are designed to accommodate temperature changes by

allowing movement in one or more directions in the plane of the panel. For example, the slotted

tieback connection in the lower right corner of Figure 17 allows translation in the vertical direction.
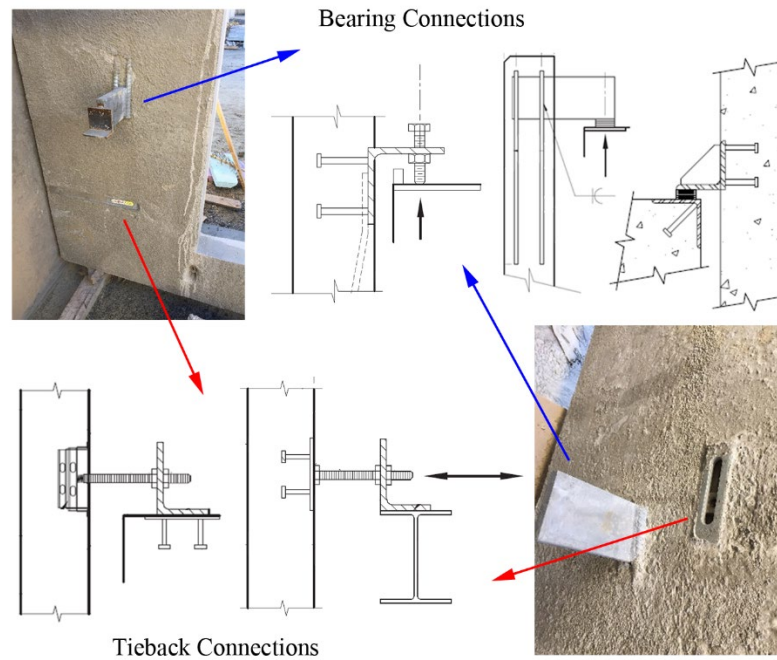
Figure 17. Typical cladding connections

Despite the widespread use of these and other similar connection details, non-loadbearing

precast concrete façade panels are typically designed as spanning one-way between the floor

diaphragms [15]. Most recent blast tests of non-loadbearing precast panels have adopted this

assumption by providing full edge bearing support to induce one-way bending [16] [17] [18] [13].

Large scale blast tests of non-loadbearing precast wall panels with discrete connections have been

performed in several recent studies [19],[20]. However, these studies were still primarily focused

on the one-way response of panels, and the spacing of the discrete connections was much smaller

than the primary panel span. Despite this, the resulting crack patterns indicated that some bi-

directional response still can occur due to the presence of discrete connections. Note the cracking

pattern near bottom connections of blast loaded panels shown in Figure 18a - such behavior is also

observed in other experimentally tested panels with point supports [21],[22] when subjected to out-

of-plane loading. To date, bi-directional response for realistic discrete connection spacing in full-

scale façade panels has not been directly examined. Blast testing on concrete panels to examine two-way flexural response has predominantly provided continuous support to all four edges [23] [24] rather than using discrete connections.

In addition to showing some evidence of bi-directional response, the previous tests by Cramsey and Naito [19] and Naito et al. [20] showed that discrete connections designed for conventional design loads do not perform well when subjected to blast demands. Fracture of welds used for connection of tiebacks, buckling of tieback plates, and punching shear failure of steel stud plates embedded in the concrete panels can occur when these connections are not properly detailed for blast design requirements as shown in Naito et al. [25] (Figure 18b-e). The reaction loads to which these connections will be subjected during a blast event will be heavily influenced by the governing flexural mechanics and capacity in either one-way (vertical or horizontal) or two-way bending due to the presence of discrete connections and varying bi-directional reinforcement. The numerical modeling undertaken in this study will (1) improve understanding of the fundamental flexural response of realistically supported and reinforced precast façade panels, (2) provide guidance to designers regarding the governing mechanics of these systems, and (3) inform the development of future experimental test programs on this topic.
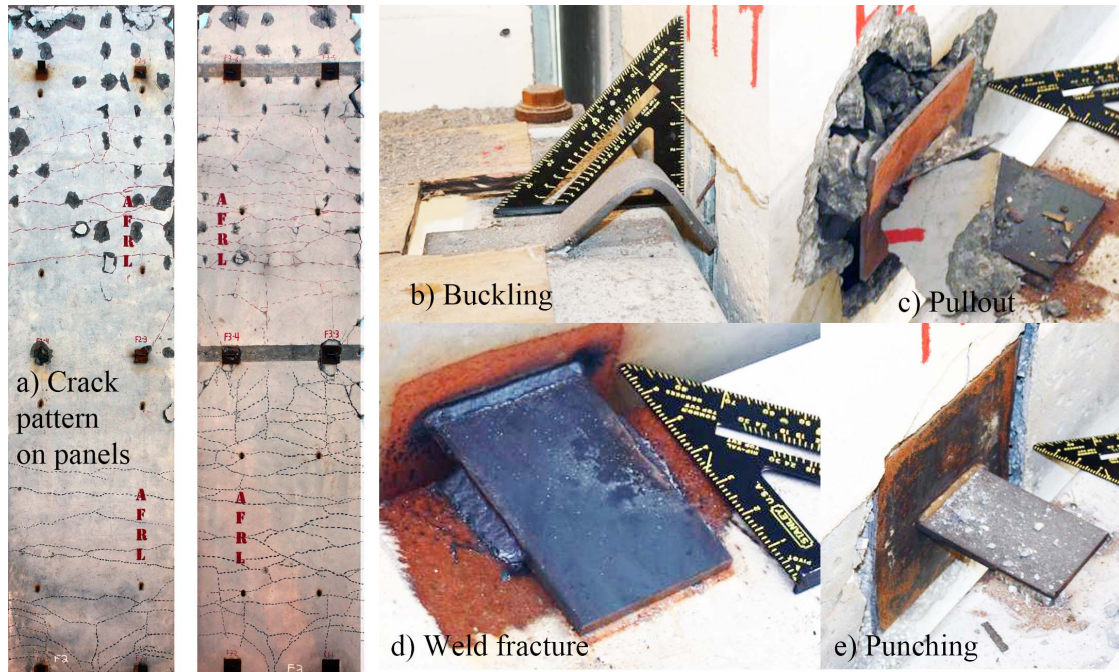
Figure 18. Bi-directional cracking around base connections on blast loaded panel (adopted from [25])

3.2.1. *Standard Practice for Blast Resistant Design*

For blast resistant applications, non-loadbearing precast panels are typically equated to a SDOF system by transforming spatial variations of loads and distributed mass via a load-mass factor, K_{LM}, based on the normalized deflected shape. Typical SDOF approaches for blast resistant design assume that the flexural response of the element under blast loading will follow a static deflected shape using conservatively idealized boundary conditions [2]. The SDOF equation of motion can be solved considering the mass, M, resistance function, $R(y(t))$ and the applied pressure-time history, $F(t)$. The resistance function can be determined based on material properties, cross-section geometry, span length, and boundary conditions. Via iterative analysis, the panel is then reinforced to achieve a specified level of allowable damage when subjected to the design-basis blast load. To absorb energy, the panels are often designed to experience permanent deformations under the short-duration (i.e. typically 5-30 msec) blast load. Subsequent design of the connections is based on either the equivalent static reaction force at the panel's ultimate capacity or the peak dynamic reaction force [15]. When precast wall panels with multiple discrete connections are

designed for vertical flexure assuming a line support at the floor diaphragms, the resulting ultimate capacity or peak dynamic reaction force of the idealized SDOF model is typically distributed to the discrete connections according to tributary area.

3.2.2. Response and Performance Metrics

Most US Government design standards [26] have adopted response criteria for anti-terrorism and force protection that were developed by the US Army Corps of Engineers [10] to assess the performance of a structural component to intentional blast demands. Five damage levels ranging from superficial (i.e. element with no permanent visible damage) to blowout (i.e. the element is completely overwhelmed) are correlated to empirically prescribed component deformation limits. As discussed by Gombeda et al. [27], these response limits do not directly capture material limit states and were developed based on visual observations from a series of blast tests. To account for the utilization of material capacity in response to blast loading, Gombeda et al. [27] proposed alternative performance-based definitions of response limits based on mechanical and material behavior milestones. The recommended response milestones, based on similar milestones for permanent deformation under seismic loading [28], correspond to first yield, half peak, three-quarters peak, and peak flexural capacity along the load-deformation resistance of the panel as a whole.

Gombeda et al. [27] introduced these milestones for a one-way spanning non-loadbearing precast panel using the line support boundary condition assumption shown previously in Figure 16b. Due to the idealized simple supports, such a panel exhibits an approximately bilinear resistance to lateral blast pressure in which peak capacity occurs at peak displacement. Panels with discrete connections, however, may form an initial mechanism earlier in the load-deformation history followed by a stable secondary mechanism. For example, the ultimate strength of a panel can be reached due to initial two-way engagement of the panel, after which peak displacement is reached at a lower capacity once the weaker of the two flexural directions progresses toward

material failure. For this study, the peak displacement of the panel is used to represent the peak milestone. Comparisons of response limits for reinforced concrete flexural members according to the US Army Corps [10] and Gombeda et al. [27] are shown in Table 6. Both sets of response criteria will be used to assess the flexural performance of panels with discrete connections later in this paper.

Both sets of response limits are compatible with the SDOF analysis approach. Calculation of the resistance function, which inherently quantifies flexural strength, stiffness and deformation capacity, is needed for this methodology and heavily influences the dynamic response of the component. In current practice, the SDOF approach is traditionally conducted using simplified assumptions, including an elastic-perfectly plastic (EPP) resistance function for simply supported boundary conditions. Utilizing either the simplified EPP approach with the one-way spanning assumption may lead to inaccurate prediction of performance when discrete connections are used. As discussed, the presence of discrete connections may complicate the actual deformation response of the component if unexpected bi-direction deformation occurs. For example, a panel with minimal reinforcement in the transverse direction may result in a weaker mechanism orthogonal to the assumed one-way span leading to reduced overall resistance for the panel. Another example is where bi-directional behavior dominates the response resulting in less deformation but higher reaction forces that may overcome the design capacity of the connections. This study therefore relies on fundamental mechanics (via finite element modeling) to develop panel resistance functions that capture realistic response mechanisms and milestones for a panel with discrete connections. These load-displacement relationships can ultimately be used as input for the SDOF analysis methodology. This so-called "enhanced" SDOF approach can be performed using the methodology proposed previously by Gombeda et al. [27] but is outside the scope of this paper.

Table 6. Comparison of flexural response limits for non-loadbearing concrete panels

Member description	B1		B2		B3		B4	
	[10]	[27]	[10]	[27]	[10]	[27]	[10]	[27]
Reinforced concrete flexural members with no shear reinforcing and tension membrane	μ=1	yield of rebar	Ө=2º	1/2 *peak	Ө=5º	3/4 *peak	Ө=10º	*Peak

* Peak panel deformation

3.3. Validation of Finite Element (FE) Models

The out-of-plane flexural performance of non-loadbearing precast concrete wall panels with discrete connections is examined through nonlinear numerical modeling. Before a parametric study could be conducted, the modeling approach was experimentally validated using load-deformation data from previous tests of both one-way and two-way spanning non-loadbearing concrete panels.

3.3.1. FE Model Development

The nonlinear resistance function for a wall panel was determined using a finite element model developed in ABAQUS version 2017 [29]. The ABAQUS/Explicit analysis module was used to facilitate numerical stability with non-linear material models for concrete and mild steel reinforcement. Quasi-static analyses were conducted using a relatively slow rate of loading to allow for a gradual ramping of applied loads with negligible inertial effects. The quasi-static behavior was verified by insuring that a ratio of kinetic energy to strain energy of 10% is maintained throughout the analysis [29]. The panel is modeled using a three-dimensional homogenous shell element (type S4) which allows for transverse shear deformation. The S4 element automatically assigns the type of shell as either thick or thin. Thick shell theory is considered when the panel

thickness to its length ratio is larger than 1/15, and Kirchoff thin shell theory is used for other situations [29]. Steel reinforcement is defined as a smeared uniaxial layer at a user-defined depth in the shell element. The nonlinear behavior through the thickness of a component is defined by introducing integration points to calculate section properties [29]. Simpson's rule is used for the shell section integration with 2.75 integration points per centimeter (7 per inch), through the thickness of the section, to represent non-linear behavior [29]. The shell elements were meshed with an approximately square discretization of 10.16 cm (4 in). Both the number of integration points and the mesh size were determined to be sufficient via a preliminary convergence study using several of the validation cases.

Concrete behavior is modeled using a concrete damage plasticity (CDP) model with dilation angle of 36º and eccentricity of 0.1 [29]. The ratio of biaxial, σ_{b0}, to uniaxial compressive strength, σ_{c0}, is taken as 1.16 [29]. A yield function is used to account for the different tension and compression response. The ratio of the tensile to compression meridian that defines the yield function in the deviatory plane, K_c, was assumed as 2/3 [29]. The uniaxial stress-strain for concrete in tension is defined as linear elastic up to the modulus of rupture. After rupture, a smooth descending branch is used to account for the progression of micro-cracking and to avoid numerical instability. This softening model is populated using Equation 16 per Belarbi and Hsu [30] where f_t , ε_t are the tensile stress and strain; f_{cr}, ε_{cr} are the modulus of rupture and the corresponding strain; and n represents the rate of weakening, taken as 0.6. Unless the value is provided in the experimental data, modulus of rupture was calculated using Equation 17 [31], where f'_c is the concrete compressive strength (in MPa) and λ is a the aggregate modification factor, taken as 1.0. Popovics concrete numerical model [32] is used to define the uniaxial stress-strain for concrete in compression. Modulus of elasticity, E_c, for concrete (in MPa) was calculated using Equation 18 [31], where γ_c is the unit weight for concrete, assumed as 22.78 kN/m^3 (145 pcf) across all panel cases. Where needed, the elastic stiffness of the finite element model is calibrated to the initial

stiffness of the experimental test specimen by multiplying the elastic modulus by an adjustment factor α. The value of α is bounded by the limits of the realistic data scatter [33] upon which the elastic modulus coefficient specified in ACI 318 [31] is based. The ACI 318 prescribed design equation [31] (Equation 18) will be used for parametric study later in this paper.

$$f_t = f_{cr} \left(\frac{\varepsilon_{cr}}{\varepsilon_t} \right)^n$$
Equation 16

$$f_{cr} = 0.7\lambda\sqrt{f'c} \text{ (in MPa)}$$
Equation 17

$$E_c = \alpha \cdot 0.043 \, \gamma_c^{1.5}\sqrt{f'c} \text{ (in MPa)}$$
Equation 18

3.3.2. Experimental Validation

The finite modeling approach is validated against four experimental studies: Gombeda et al.[34], Cashell et al.[35], McNeice [21] and Sakka and Gilbert [22]. Gombeda et al. [34] evaluated the behavior of one-way solid reinforced concrete panels with no in-plane loading and varying reinforcement subjected to a uniform out-of-plane pressure loading. Cashell et al. [35] examined the response of a two-way slab with continuous edge supports subjected to out-of-plane point loads that were uniformly spaced and of uniform magnitude. McNeice [21] and Sakka and Gilbert [22] examined the behavior of a two-way panel with point supports. Figure 19 illustrates the experimental setup and cross sections of each test specimen. Material properties for all tests are summarized in Table 7. The steel reinforcement stress-strain model used by Gombeda et al.[34] was determined from tensile tests of the mild steel rebar used throughout that test program. Since similar data is not available for the other three studies, the remaining reinforcement stress-strain were assumed to be bilinear with an elastic-hardening response. The steel elastic modulus is assumed to be 200 GPa (29000 ksi) for all cases. The properties for steel (such as yield stress, f_{sy}, and the tensile stress, f_{su}, and strain, ε_{su}) as well as the properties for concrete (such as compressive strength, f'_c, modulus of elasticity, E_c, and ultimate strain, ε_{cu}) are also summarized in Table 7. The concrete modulus of elasticity for Gombeda et al.[34], Cashell et al. [35], and McNeice [21] were initially calculated using Equation 18. To provide an accurate match of the experimentally

measured stiffness of the whole panel, the elastic moduli for the three cases were modified by an

α-factor of 2/3. The concrete elastic modulus for Sakka and Gilbert [22] was directly provided. The

ultimate strain for concrete is calculate as a function of the modulus of elasticity and ultimate

compressive strength per the Popovics model [32].

Table 7. Material properties of experiments

Experiment	E_c (GPa)	f'_c (MPa)	ε_{cu} (%)	f_{cr} (MPa)	f_{sy} (MPa)	f_{su} (MPa)	ε_{su} (%)
Gombeda et al.[34]	22.35*	49.11	0.30**	3.78*	476	969	10.8
Cashell et at. [35]	19.0*	35.52	0.28**	3.10	550	589	2.5
McNeice [21]	19.89*	38.92	0.28**	3.37*	345	517*	10.0*
Sakka and Gilbert [22]	29.20	44.30	0.29**	3.61	600	641	2.2

Assumed value based on ACI 318 [31]; not provided by the test team

**Assumed value based on the Popovics model [32]; not provided by the test team
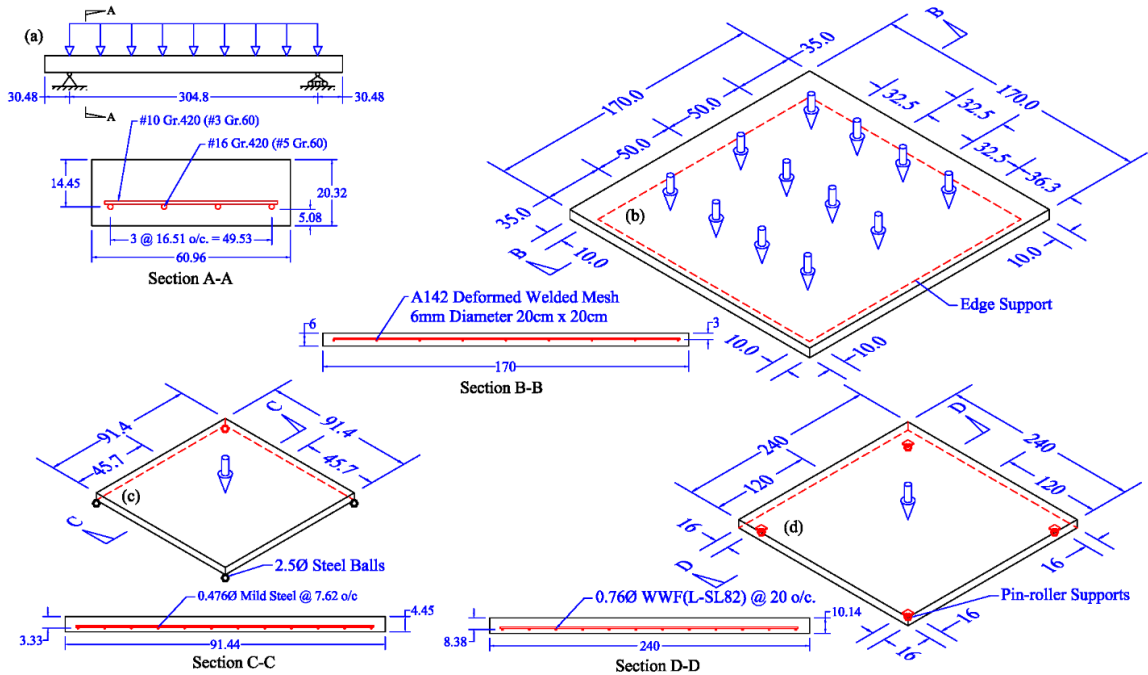
Figure 19. Schematic of experimental specimens (dimensions in cm) tested by (a) Gombeda et al.[34], (b) Cashell et al. [35], (c) McNeice [21] and (d) Sakka and Gilbert [22]

The FE results, experimental response, and component-specific milestones per [27] for the

four validation cases are shown in Figure 20a-d. The resistance is plotted as the applied pressure

on the panel versus the midpoint displacement of the panels. The FE model predictions show good agreement with the experimentally measured response. The peak displacement at flexural failure for the models of the Gombeda et al.[34] and Sakka and Gilbert [22] tests accurately match the experimental data. Marginal discrepancies are observed in the FE failure displacements for Cashell et al. [35] and McNeice [21], most likely due to the unavoidable use of several assumed material properties. The resistance at peak is generally conservative for all cases. The FE deflected shapes for the four experimental studies in Figure 21 also showed good agreement with the observations reported in each test. These results establish confidence for using this modeling approach in a parametric study to examine variations in discrete connection layouts and directional nominal moment capacity.
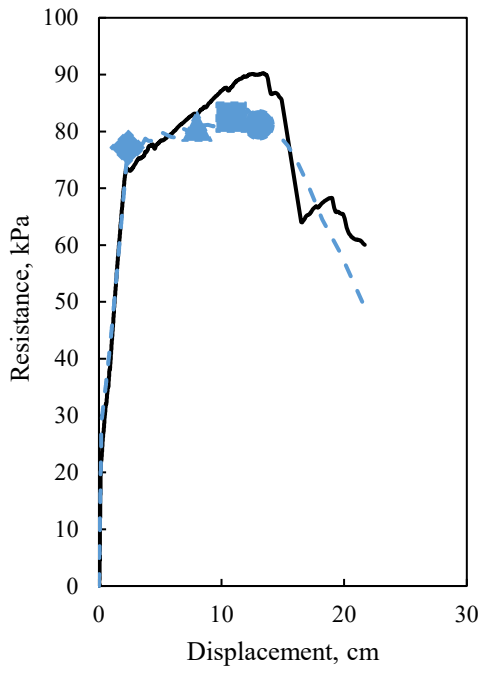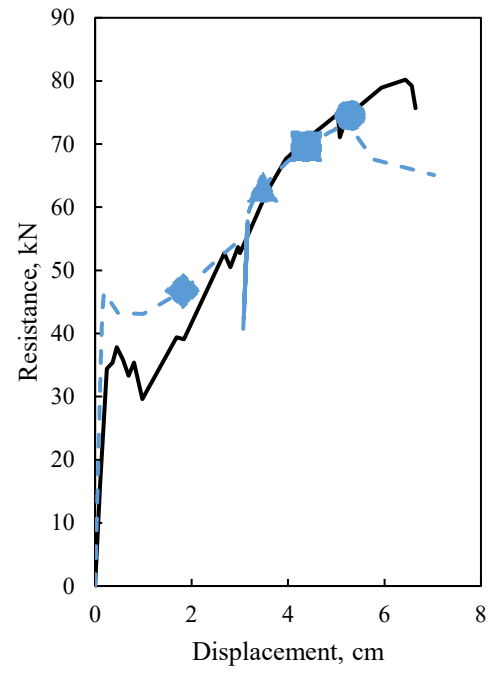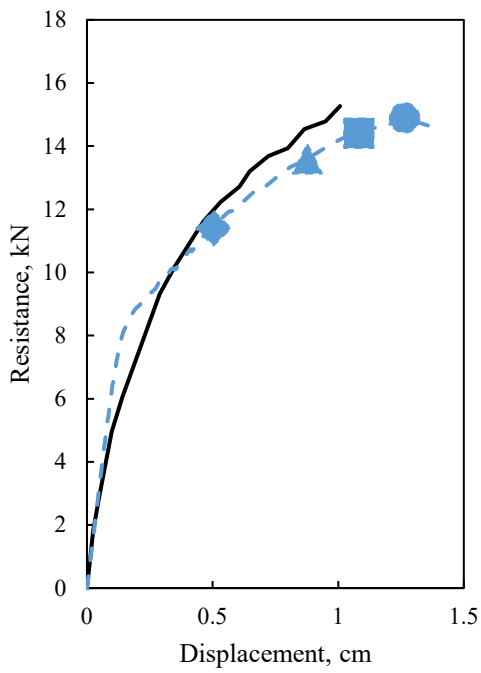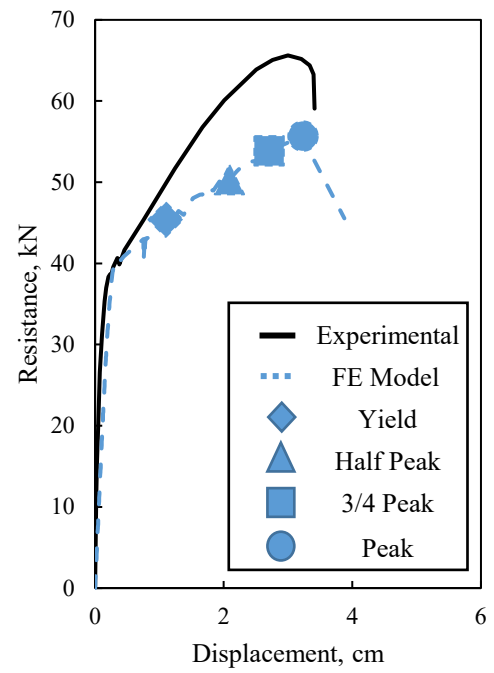
Figure 20. Comparison of FE resistance functions and experimental test data for (a) Gombeda et al.[34], (b) Cashell et al. [35], (c) McNeice [21], and (d) Sakka and Gilbert [22]
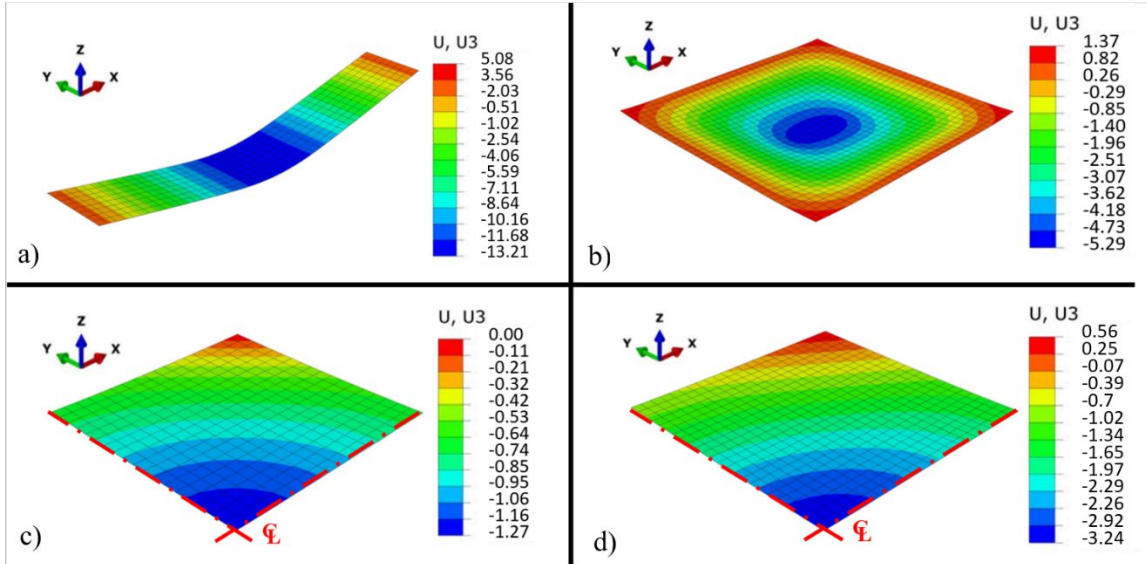
Figure 21. Deflected shapes (all dimensions in cm) of FE models representing (a) Gombeda et al. [34], (b) Cashell et al. [35], (c) McNeice [21] and (d) Sakka and Gilbert [22]

3.4.   Parametric Study

The validated FE model is used to examine the influence of varying connection spacing and the primary-ultimate flexural strength on the flexural resistance functions and limit states of blast-resistant cladding panels. The parametric study is based on a generic prototype wall panel geometry measuring 9.14 m (30 ft.) long and 4.57 m (15 ft.) tall with a thickness of 15.24 cm (6 in.). The wall panel is designed for conventional loads including wind, stripping, shipping and handling, and erection in accordance with the PCI Design Handbook [15]. The geometries and cross-section details of the panel are shown in Figure 22. The vertical bar size in Figure 22 is not labeled because the amount of reinforcement, used within the ultimate resistance calculation, in that direction is varied as part of the parametric study. The vertical reinforcement of the baseline prototype panel, designed for conventional loads, consists of #13 (#4 US) bars at 39.37 cm (15.5 in.) on center on each face. Horizontal reinforcement is designed only for shrinkage and temperature requirements and consists of #10 (#3 US) bars at 45.7 cm (18.0 in.) on center.

Material properties used for the FE model in the parametric study are summarized in Table 8, and stress-strain models for concrete and steel are plotted in Figure 23. The same concrete

material model presented in Section 3 is again used for the parametric study. The stress-strain response for steel reinforcement is based on tensile test data from Gombeda et al. [34] and is scaled to match the minimum requirements for yield strength, tensile strength, and ultimate tensile strain in ASTM A615 [36]. The EPP stress-strain model that is used in the UFC approach for steel reinforcement is also shown in Figure 23b for comparison.
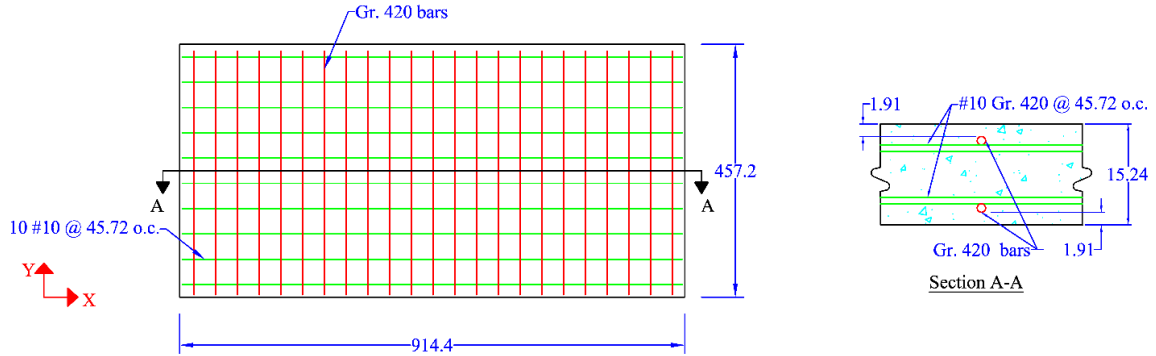
Figure 22. Generic precast panel configuration (all dimensions in cm) for parametric evaluation

Table 8. Material properties of the parametric FE models,

E_c (GPa)	f'_c (MPa)	ε_{cu} (%)	f_{cr} (MPa)	f_{sy} (MPa)	f_{su} (MPa)	ε_{su} (%)
28.09	34.47	0.18	3.66	413.69	620.53	9.0

(a)   (b)
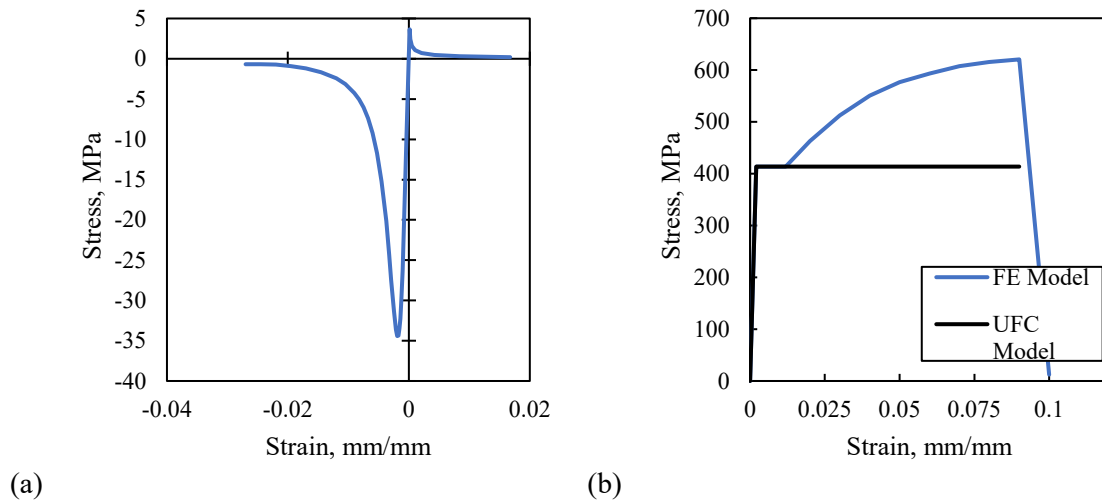
Figure 23. Stress-strain relationships for (a) concrete and (b) reinforcing steel in the parametric FE models

3.4.1. Variation in Connection Spacing

Spacing of discrete connections along the panel edges at the floor diaphragms is examined. The panels are analyzed with six (6DC) and eight (8DC) discrete connections. Figure 24 shows

arrangements of discrete connections and their locations on the panel. Also shown are the idealized spans and boundary conditions between each connection that would be used for one-way SDOF calculations of the panel's blast resistance in the primary and transverse flexural directions per current design guidelines [37]. Similar to Figure 16b, the idealized boundary conditions in Figure 24 are assumed to be line supports that run through all connections in the same vertical or horizontal line (i.e. the connections are assumed to provide adequate stiffness across these lines such that the idealized boundary condition can be reasonably applied). Figure 24 shows graphical descriptions for the primary, w_1, and transverse, w_2, pressure demands that would be required to achieve the ultimate strength for each case. The results of the validated finite element models will be compared to the simplified one-way strength assumptions for the primary and transverse axis directions to evaluate the applicability of the idealized component-based approach.
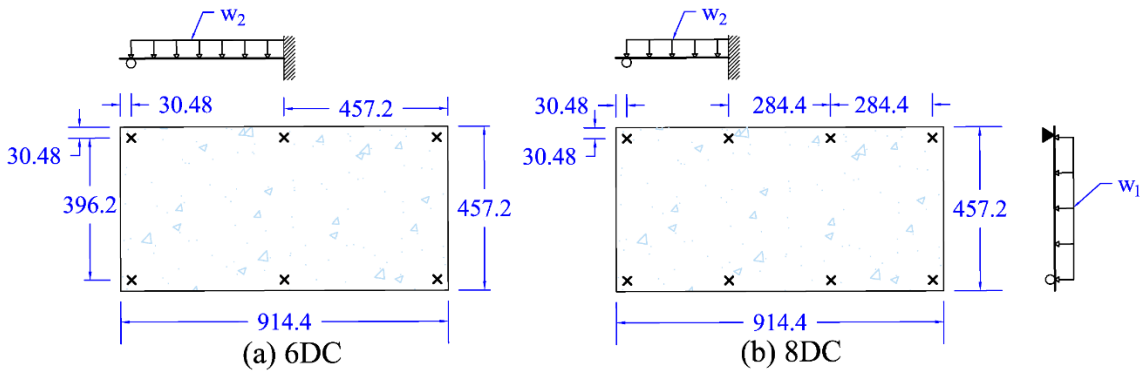
Figure 24. Variation in discrete connection spacing (units in cm) for parametric study

3.4.2. *Varying the Primary Ultimate Flexural Resistance*

The performance of the panel is examined relative to the control panel. The ultimate flexural resistance, w_1, of the panel in the primary flexural direction is 9.89 kPa (1.43 psi). Using the prototype panel as a baseline, the ultimate resistance, w_1, is increased while the transverse ultimate resistance, w_2, is kept constant, as a result of using the minimum reinforcement, at 6.26 kPa (0.91 psi) for the cases with 6DC and 14.13 kPa (2.09 psi) for the cases with 8DC. Table 9 shows the range for the ratio of primary to transverse ultimate resistance used in this study. It is

interesting to note that these ratios indicate that the transverse w_2 ultimate capacity would control the design of most panel configurations. Reinforcement ratio, also shown in Table 9, is calculated using Equation 19 where A_s corresponds to the steel area of the extreme tension reinforcing bar (i.e., the bar closer to the compression face is not included in the reinforcement ratio calculation as is common in current U.S. practice); d is the distance from the extreme compression concrete fiber to center of the extreme tensile steel reinforcement; and b is the bar spacing. Table 9 summarizes the reinforcement configurations considered in this study. As shown in Figure 22, the doubly reinforced cross-section utilizes the same rebar arrangements for the top and bottom layers. It is assumed that the precast concrete walls in this study are exposed to weather and manufactured under controlled plant conditions, and thus the clear cover for all rebar is set at 1.91 cm (0.75 in.) in accordance with ACI 318-14 [31].

As shown in Table 9, the range of primary (vertical) ultimate resistance is varied from 7.61 kPa to 52.31 kPa, representing an increase in lateral resistance per the idealized vertical span assumption in Figure 16b with line supports at the floor diaphragms. The nominal moment capacity and net tensile strain are calculated via strain compatibility analysis considering both layers of reinforcement. For simplicity, the reinforcement ratio is computed using only the extreme tension steel, though it is important to note that the reinforcement near the compression face is subjected to tension at nominal and is included in the flexural strength calculations. The lowest primary ultimate resistance is chosen such that the ratio of the nominal, M_n, to cracking moment, M_{cr}, calculated using gross section properties is slightly greater than 1. The largest primary ultimate resistance is chosen such that the net tensile strain, ε_t, is 0.005 (i.e. the lower limit for tension controlled sections in accordance with ACI 318-14 [31]) in the extreme tension reinforcement at the nominal flexural capacity.

Table 9. Matrix for the range of primary ultimate flexural resistance used in parametric study

Bar size	#10 (#3)	#13 (#4)	#13 (#4)	#16 (#5)	#16 (#5)
d (cm)	12.86	12.7	12.7	12.54	12.54
b (cm)	28.58	39.37	30.48	15.24	7.62
ρ (%)	0.19	0.25	0.33	1.04	2.09
ρ_T (%)	0.13	0.13	0.13	0.13	0.13
ε_t	0.04	0.03	0.023	0.007	0.005
M_n (kN-m)	136.61	177.45	225.0	522.94	938.4
M_n/M_{cr}	1.05	1.36	1.74	4.0	7.25
w_1 (kPa)	7.61	9.89	12.53	29.14	52.31
w_1/w_2 (6DC)	1.22	1.58	2.00	4.66	8.36
w_1/w_2 (8DC)	0.54	0.70	0.89	2.07	3.71

$$\rho = \frac{A_s}{b \cdot d}$$ Equation 19

3.4.3. Varying the Connection Restraint

As shown previously in Figure 17, several different types of connections are used to attach the cladding panels to the main structure, and these connections can be arranged to create a variety of boundary conditions for the panel. For example, tieback connections can be arranged to act as roller (i.e., no translational restraint) connections in either the vertical or horizontal direction. The orthogonal direction could be idealized as either a pin or stiff translational spring. The parametric study examines three possible boundary condition variations for the six connection (6DC) panel. BC1 is shown in Figure 25a where tieback connections are arranged to allow thermal expansion in the transverse direction and resist translation in the primary (vertical) direction. This case provides an idealized representation of the typical tieback orientation used in practice. In Figure 25b, BC2 shows a tieback orientation that allows expansion along the primary axis. In Figure 25c, BC3 shows an idealized case where tieback connections would allow translation in both the vertical and horizontal directions (i.e. resembling a true simple supported panel). Note that for all assumed boundary condition schemes, additional bearing connections along the top of the panel would be used to support the gravity loads. It is commonly assumed that the bearing connections act only in the vertical directions and would not influence the response of the panel to lateral loading.
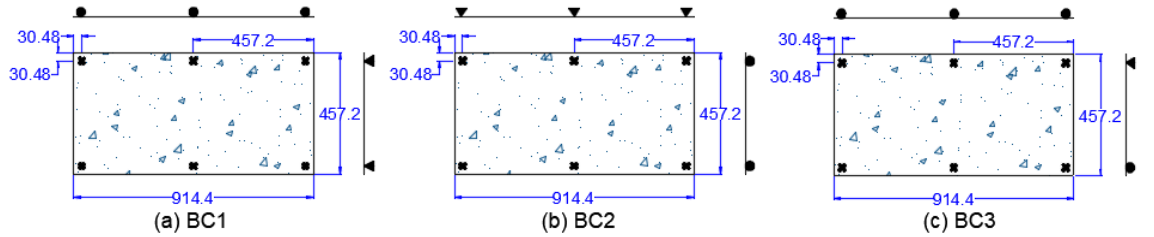
Figure 25. Idealized support conditions for parametric FE models panels with 6 discrete connections (units in cm)

3.5. Analysis Results

The results of the parametric analyses are labeled as follows: the first parameter denotes the number of discrete connections in a panel (6DC and 8DC as shown in Figure 25); the second parameter shows the ratio of primary to transverse ultimate resistance (e.g. $R = w1/w2 = 1.58$ (for 6DC) as shown in Figure 24); and the third parameter denotes the type of boundary conditions (BC1, BC2 and BC3 as shown in Figure 25). The initial focus will evaluate the out-of-plane flexural performance of the 6DC panels, which represent a more typical connection configuration in practice. Following this, the analysis will evaluate the out-of-plane flexural performance of panels with 8DC.

3.5.1. Panels with Six Discrete Connections

3.5.1.1. Preliminary Evaluation of Connection Rotational Stiffness

Note that all lateral connections to this point have been represented in the FE model as a translational restraint at a single node. Connections in precast construction are conventionally fabricated by embedding plates in the precast wall element. To ensure adequate force transfer, these connections require the use of cast-in embeds plates with steel studs or other mechanical or post-installed anchorages. Consequently, while connections are often idealized as a point support in design models, the true physical size of the embedment may provide a small amount of localized rotational resistance in addition to lateral resistance. Preliminary analyses were performed prior to the parametric study to compare panel flexural performance with lateral connections represented as translational restraint at either one node or at four neighboring nodes (i.e. assuming a connection

50

size of 10.16 cm. by 10.16 cm (4 in by 4 in)). The idealized 4-node restraint was used to represent an upper bound for the development of localized moment resistance by eliminating connection rotation at the shell element surrounded by the four supported nodes (representing a plate embed). This numerical representation provides much higher rotational stiffness than a realistic embed connection, which would have low rotational stiffness at its interface with the bolts or welded plates that attach the embed to the structural system. The analysis is carried out only for the conventionally designed panel with 6DC and BC1 (Figure 25a) for preliminary evaluation. A fourth parameter is added to the reference labeling system for "large" boundary conditions (LBC) to identify cases in which the connections are represented with a 4-node lateral restraint instead of single node lateral restraint.

Figure 26a compares the plots of semi-static load-displacement obtained from FE analysis of the 6DC-w1/w2=2-BC1 prototype with single node and 4-node (LBC) connections). The plotted lateral displacement represents the maximum overall panel displacement measured approximately midway between the connections as shown in Figure 26b. The performance-based response limits per Gombeda et al. [34] are also plotted for each case. As expected, the presence of additional rotational restraint at the connections provides ~25% more out-of-plane flexural resistance and slightly greater deformation capacity. As noted previously, realistic connections will exhibit low rotational stiffness that more closely resembles the single supported node; therefore, the remaining analyses are conservatively conducted using the point support simplification.
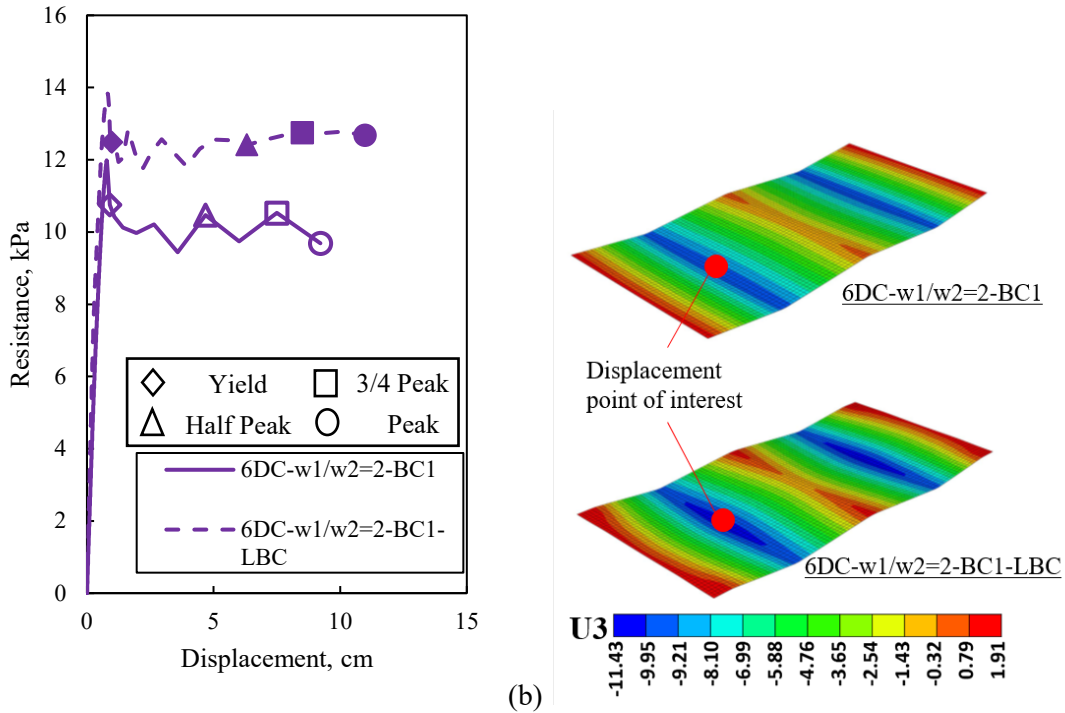
Figure 26. Preliminary evaluation of connection rotational stiffness: (a) resistance functions and (b) deflected panel shapes with single node and "large" 4-node supports (units in cm)

3.5.1.2. *Vertical and horizontal span design option*

As explained previously, the current approach assumes the discrete connections to behave as an idealized line support and the cladding panels are evaluated assuming one-way vertical behavior. The designer also has the option of designing the panel to span horizontally. This section examine the two spanning design options. Thus, the resistance functions based on 1) the current approach, 2) the FE model with idealized line supports and 3) the FE model with discrete connections are obtained and compared. The comparison between these results provides indication of the effect of realistic materials, discrete connections and performance-based response limits. The panel with 6DC and w1 to w2 equals 1.58, shown earlier in Table 9, is designed to span vertically. Table 10 shows information of the panel designed to span horizontally where the primary reinforcement will be the outside layer and the clear cover for the rebar is set at 1.91 cm (0.75 in.). The transverse (horizontal) direction for this panel consists of #10 (#3 US) bars at 45.7 cm (18.0 in.) on center which is designed for temperature and shrinkage requirements.

52

Table 10. Data of the panel designed to span horizontally

Bar size	d (cm)	b (cm)	ρ (%)	ρ_T (%)	ε_t	M_n (kN-m)	M_n/M_{cr}	w1 (kPa)	w1/w2
#13 (#4)	12.7	39.37	0.25	0.13	0.03	88.73	1.37	12.79	0.38

The FE deflected shapes at peak deformation for the panels with the idealized line supports, BC1 and BC2 are shown in Figure 27. The vertically spanned panel with 6DC and BC1, i.e. 6DC-w1/w2=1.58-BC1, reaches to a failure mechanism in the weaker (horizontal) direction which is equivalent to the panel with vertical line supports, i.e. Vertical LS-w1/w2=1.58. The deflected shape for the horizontally spanned panel with 6DC and BC1, i.e. 6DC-w1/w2=0.38-BC1, indicates failure mechanism in the weaker (vertical) direction and also shows bi-directional behavior. The results for panels with BC1 illustrates that the intended mechanism is not achieved and the failure mechanism will occur in the weaker direction for both design options. When the tieback connections are rotated (BC2) in the vertically spanned panel, the panel reaches to the intended mechanism, i.e. similar to the panel with horizontal line supports. The panel with BC2, designed to span horizontally, has a failure mechanism in the weak (vertical) direction similar to the panel with horizontal line supports.

The resistance functions as well as the limit states for the panels with the idealized line supports, BC1 and BC2 are shown in Figure 28. It should be noted that the PDC limit states are averaged for both span direction. The panels with idealized line supports shows higher resistance than the elastic-plastic resistance of the UFC current approach which illustrates the effect of using realistic materials in the FE model compared with approximation, such as elastic perfectly plastic for steel used in the UFC current approach. The resistance functions for the panels with discrete connections and BC1 illustrate significant reduction in ductility due to the unexpected failure mechanism. The vertically spanned panel with 6DC and BC2, i.e. 6DC-w1/w2=1.58-BC2, reaches to similar resistance as the panel with horizontal line supports, i.e. Horizontal LS-w1/w2=1.58, consistent with the deformed shape results as shown in Figure 27. The horizontally spanned panel

with 6DC and BC2, i.e. 6DC-w1/w2=0.38-BC2, shows similar resistance functions as the panel with horizontal line support, i.e. Horizontal LS-w1/w2=0.38, in agreement with the failure mechanism. It should be noted that both of horizontally spanned panel, i.e. Horizontal LS-w1/w2 =1.58, and vertically spanned panel, i.e. Vertical LS-w1/w2=0.38, reach to the intended mechanism, as shown in Figure 27, yet horizontal spanned panel with line support possesses higher ductility which indicates that designing the panel to span vertically is more preferable.
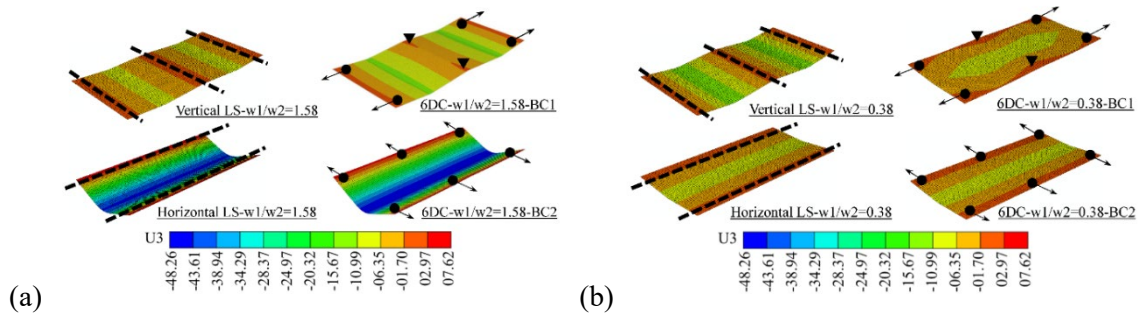
Figure 27. The FE deflected shape at peak for the designed panel to span (a) vertically and (b) horizontally

(a)

(b)
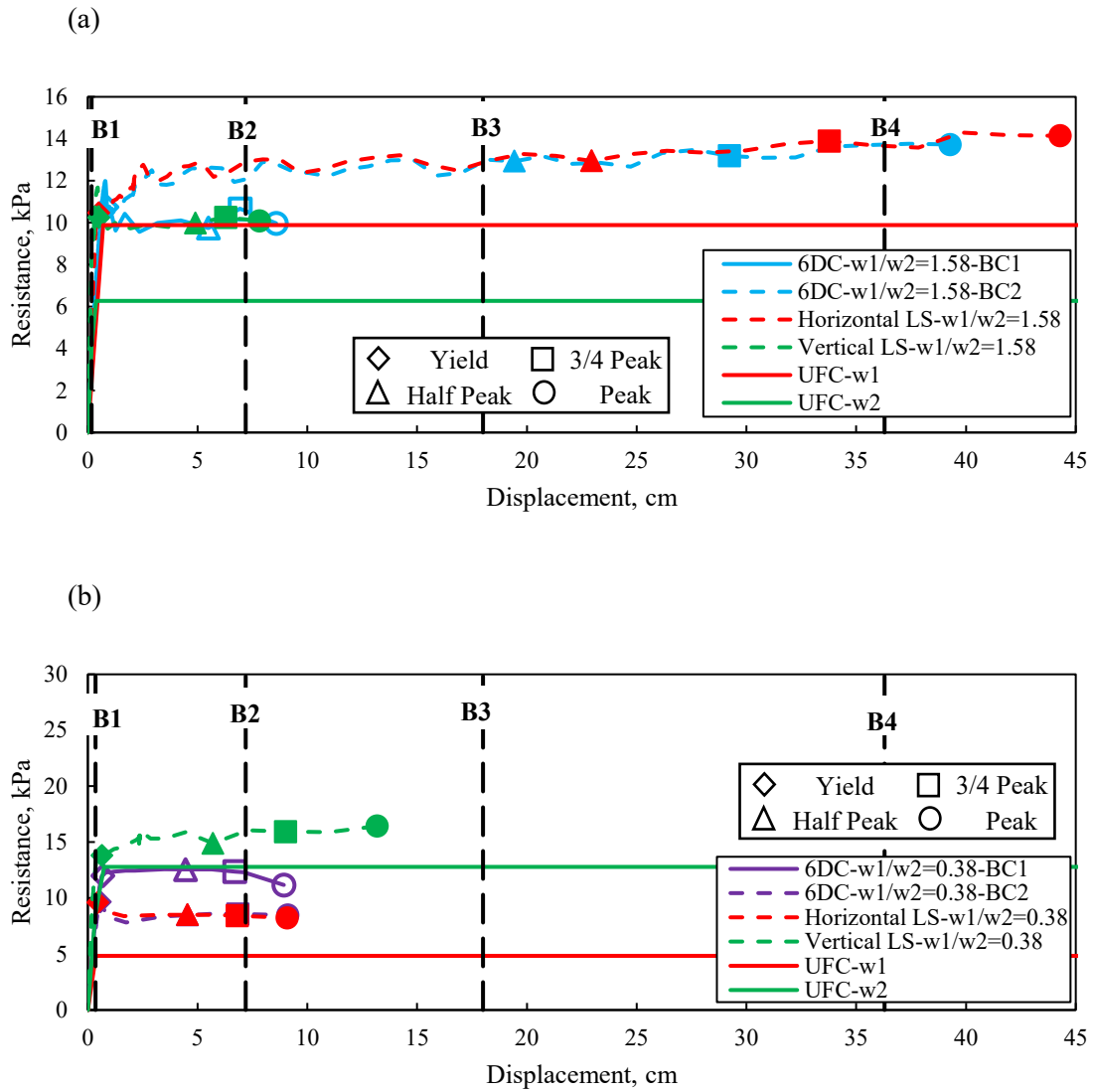
Figure 28. Resistance functions for the designed panel to span (a) vertically and (b) horizontally

Strain energy

Comparison of strain energy provides a means of assessing the dynamic resistance of a strucutral component. For wall panels strain energy is computed as the area under the resistance function up to the desired response limit. Figure 29 illustrates an example for the calculated area (strain energy) under the FE and the current UFC curve for w1/w2=1.58 panel up to the desired response limits, i.e. 3/4 peak and B3. The FE strain energy is compared relative to the UFC strain

energy of the governed mechanism. A comparison of the strain energy of the FE models and the UFC approach for 6DC with BC1 and BC2 are shown in Figure 30a. The vertically spanned panel with BC2, i.e. 6DC-w1/w2=1.58-BC2, which is the one reached to the intended mechanism possesses a FE strain energy higher than the UFC approach for all damage levels. The other cases for panels with 6DC achieve close results for the lower damage levels while majority of the FE strain energies are underestimated by the UFC approach for higher damage levels. This is related to the formation of the unexpected mechanism which also caused reduction in deformation capacity, as explained earlier. These results indicate that for the cases with the unexpected failure mechanism, the amount of damage will likely be higher than would be expected from the current practice.
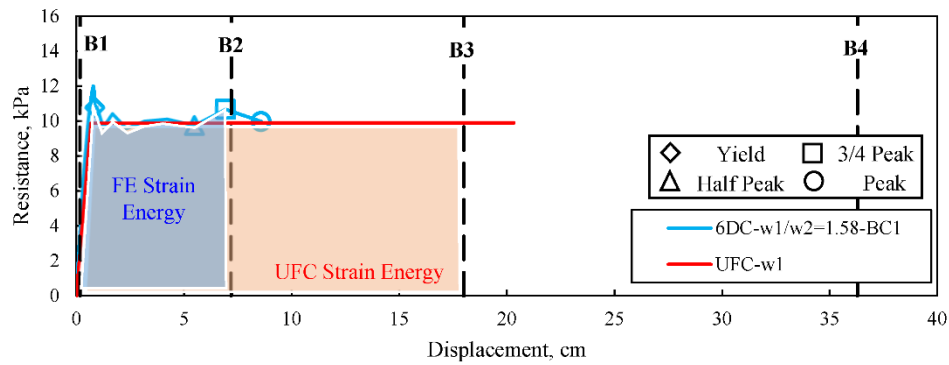
Figure 29. The UFC and FE strain energy
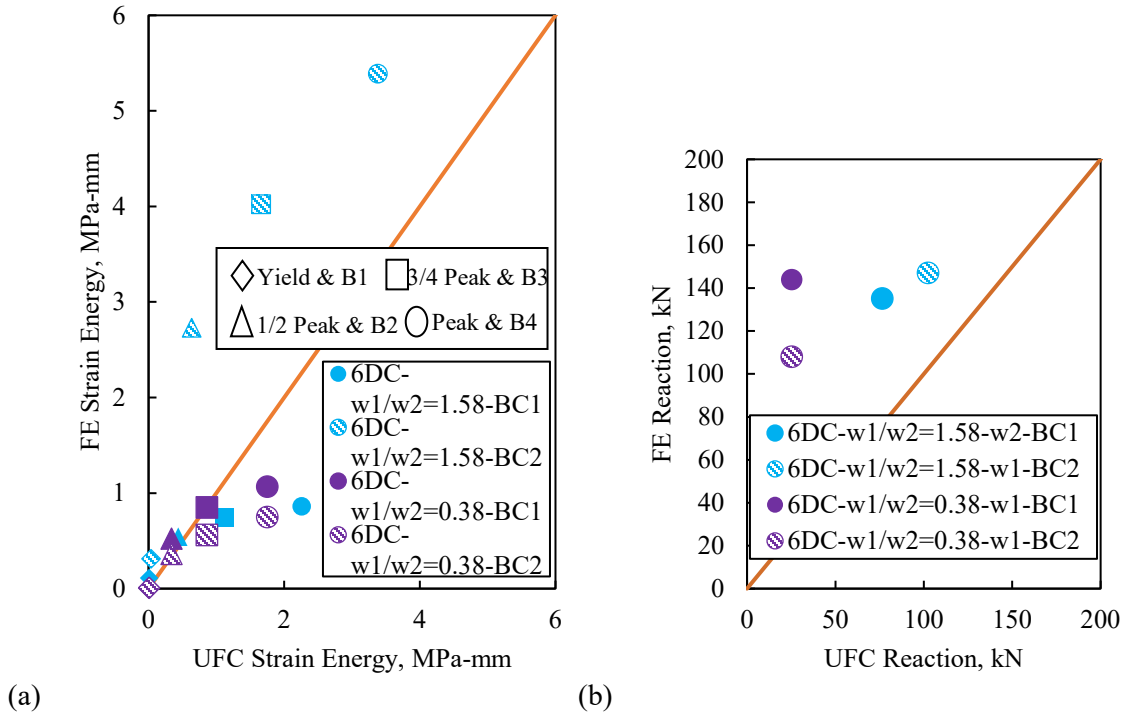
Figure 30. Linear correlation for (a) strain energy and (b) connections reaction

Connections reaction

The reaction demands for the panel connections are examined to determine the accuracy of the UFC approach. The reaction of the mid connection from the FE study is compared to the reaction calculated based on the current UFC approach. The reaction demands are based on the relative tributary area of each connection. The UFC reaction is found by multiplying the UFC ultimate flexural resistance relative to the governed failure mechanism in the FE model with the tributary area of the connection. The comparison between the UFC approach and the maximum FE reaction of the middle connection is performed using linear correlation as shown in Figure 30b. The results reveals that the UFC calculation underestimates the connection capacity of the FE model for all cases.

3.5.1.3. Resistance functions and deflected shapes

Designing the panel to span vertically leads to higher ductility compared with the designed panel to span horizontally. This confirms the prevailing assumptions as considered in the current

practice as well as the one assumed in the parametric study. Thus, the resistance functions and deflected shapes are obtained using the validated FE model to analyze the 6DC panel shown in Figure 24a for the ratios of primary to transverse ultimate resistance, shown in Table 9, and for all three boundary condition cases (BC1, BC2 and BC3). Figure 31 shows the deflected shape of each case at peak displacement (representing the maximum damage limit per Gombeda et al. [34]). For BC1 (i.e. the most common case in practice), flexural behavior at peak displacement was governed by the weaker transverse (horizontal) direction. As a result, all cases with BC1 possess similar deformation at peak since the transverse reinforcement remained unchanged. Peak displacements for BC3 (with no in-plane translational restraint at the connections) are almost identical to those for BC1, with only the smallest ratios of primary to transverse ultimate resistance showing minor indications of two-way bending.

When the tieback connections are rotated to behave as a roller in the primary direction and a pin in the transverse direction (BC2), the deformation increases due to in-plane translational restraint in the transvers direction which allows the panel's flexural capacity to become governed by the vertical reinforcement per current design assumptions at primary to transverse ultimate resistance ratios up to 2.0. Further increases in the primary reinforcement of BC2 allows the transverse reinforcement to once again control the peak response with lower maximum ductility, similar to BC1 and BC3.
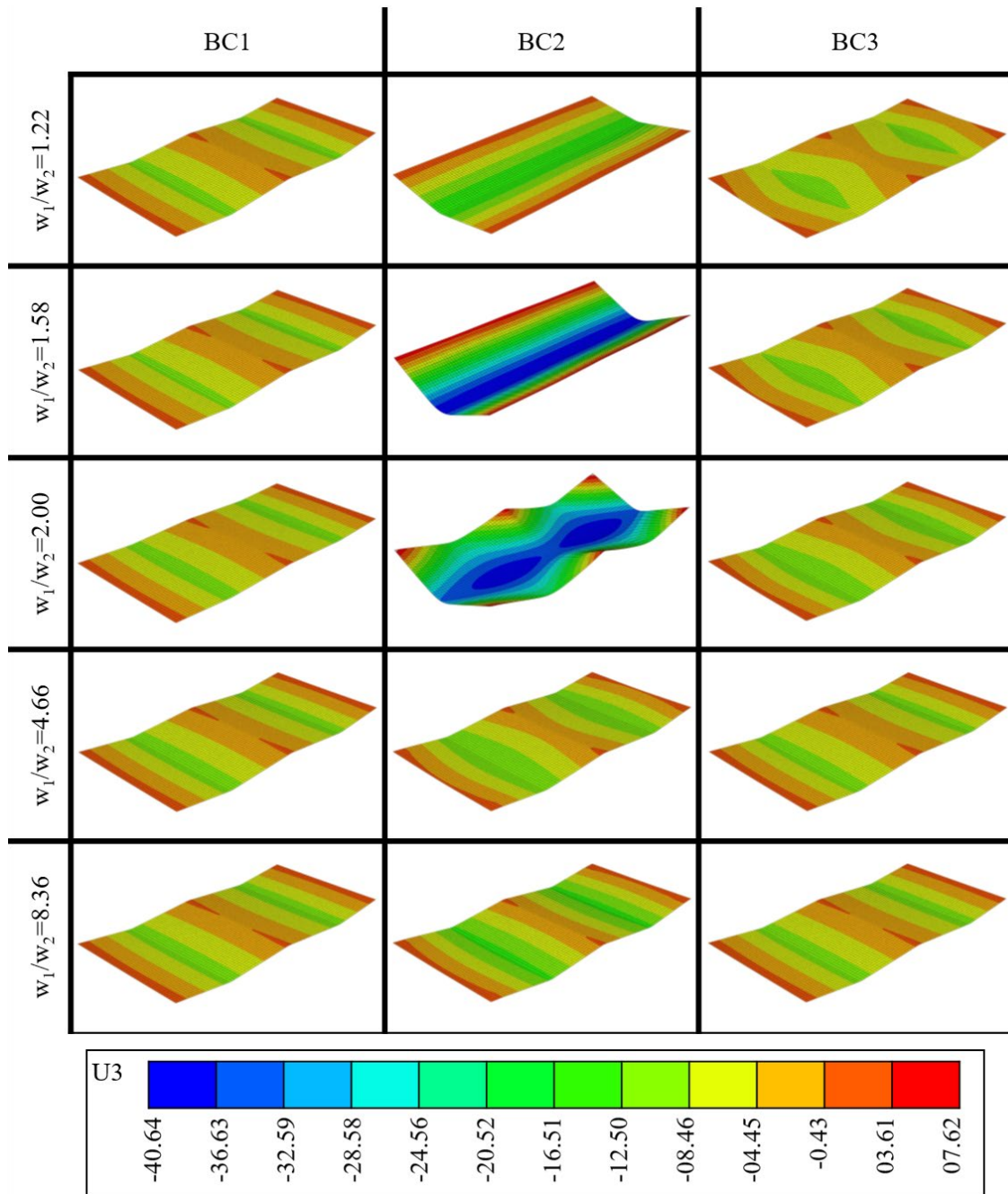
Figure 31. Peak FE deflected shapes for the 6DC panel (units in cm)

The FE model resistance functions of BC1 and BC2 are plotted in Figure 32a. The resistance is normalized relative to the flexural strength computed using idealized one-way assumptions and elastic perfectly plastic steel properties per the standard UFC approach [1]. The normalization (Figure 32b) is calculated relative to the one-way strength in the vertical direction

(w_I) via the boundary conditions in Figure 16b, as is often assumed in current practice. The plotted displacement is measured at the location of maximum displacement at peak response (i.e. at flexural failure), which is approximately the same as that shown in Figure 26b. Performance-based response limits per Gombeda et al. [34] (i.e. yield, half peak, three-quarter peak and peak deformation) and the prescriptive PDC response limits for a flexural reinforced concrete member with no shear reinforcement and without tension membrane [10] (plotted as vertical dashed lines B1 through B4) are also shown in Figure 32 for comparison.

(a)

(b)
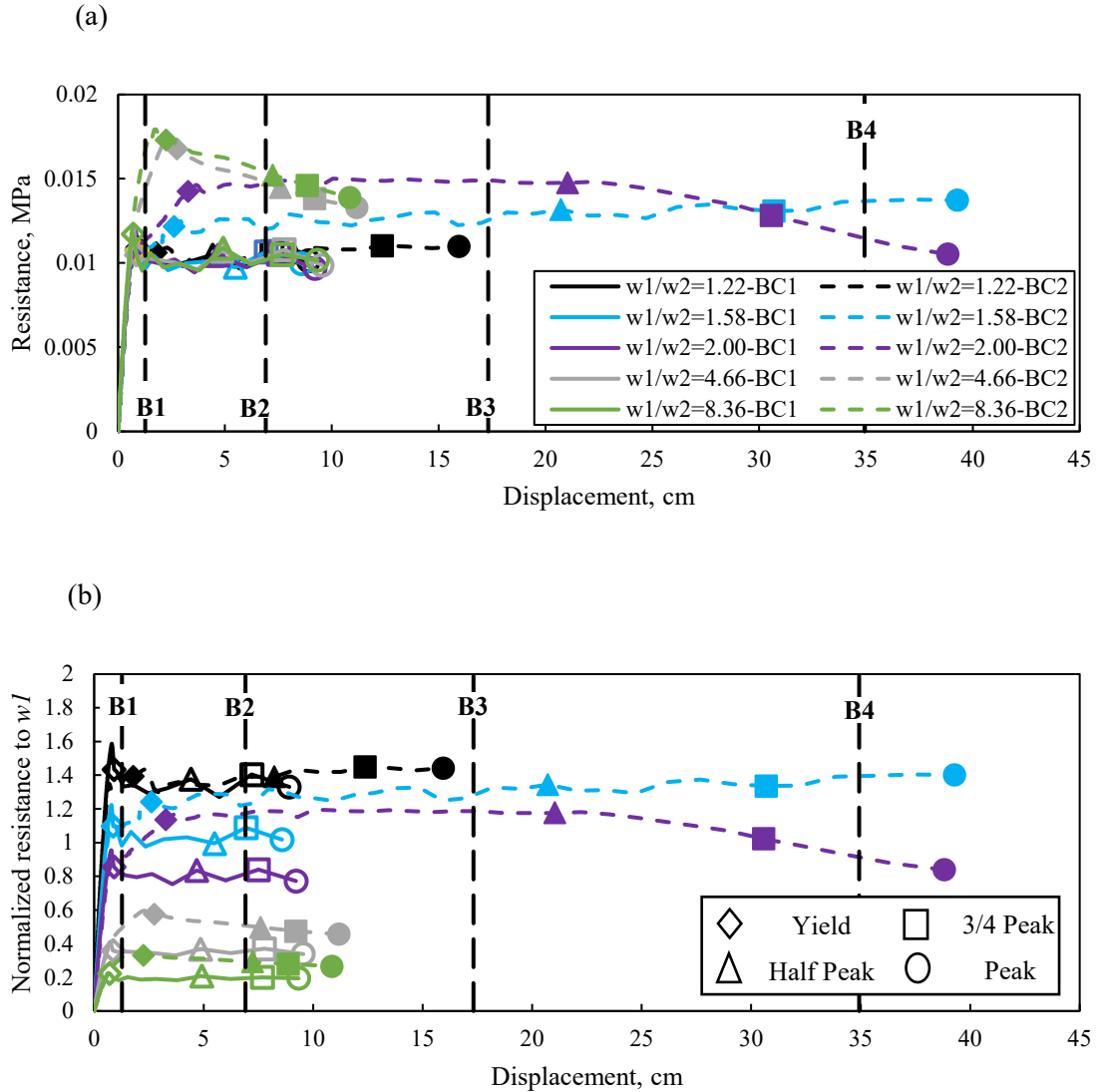
Figure 32. Out-of-plane flexural resistance of the 6DC panel: (a) load-displacement resistance functions and (b) normalized to w_1

Consistent with the deflected shapes in Figure 31, Figure 32a shows that all cases whose peak flexural response is governed by transverse bending reached a much smaller peak displacement than cases controlled by predominant flexural response in the primary direction (w_1/w_2 of 1.22, 1.58 and 2.0 for BC2). These BC2 cases achieved by far the largest peak ductility, with peak displacements extending conservatively past the PDC's B4 response limit to blowout for w_1/w_2 of 1.58 and 2.0. The remaining cases, governed by transverse bending, were only able to extend past the PDC B2 response limit to heavy damage at flexural failure. The transverse direction

61

not only has less reinforcement than the primary direction but also has stiffer boundary conditions due to its continuity at the vertical centerline between the two transverse spans (whereas the vertical span can rotate freely at both ends). Both of these differences contribute to reduced peak ductility versus the prescriptive PDC limit states. The failure in the transverse direction also significantly reduces the capacity of the panels. When the resistance is normalized by the conventionally assumed one-way capacity in the primary direction, Figure 32b shows that three panels are able to achieve the w_1 peak flexural capacity even when their expected flexural strength in the longitudinal direction is less than the transverse (w1/w2) see Figure 24.

Similar to the observations in Figure 31, Figure 33 confirms that the FE resistance functions for the 6DC panels with BC1 and BC3 boundary conditions are nearly identical. Since BC3 represents a hypothetical case that is not practical for realistic construction, it is therefore neglected for the remainder of this paper.
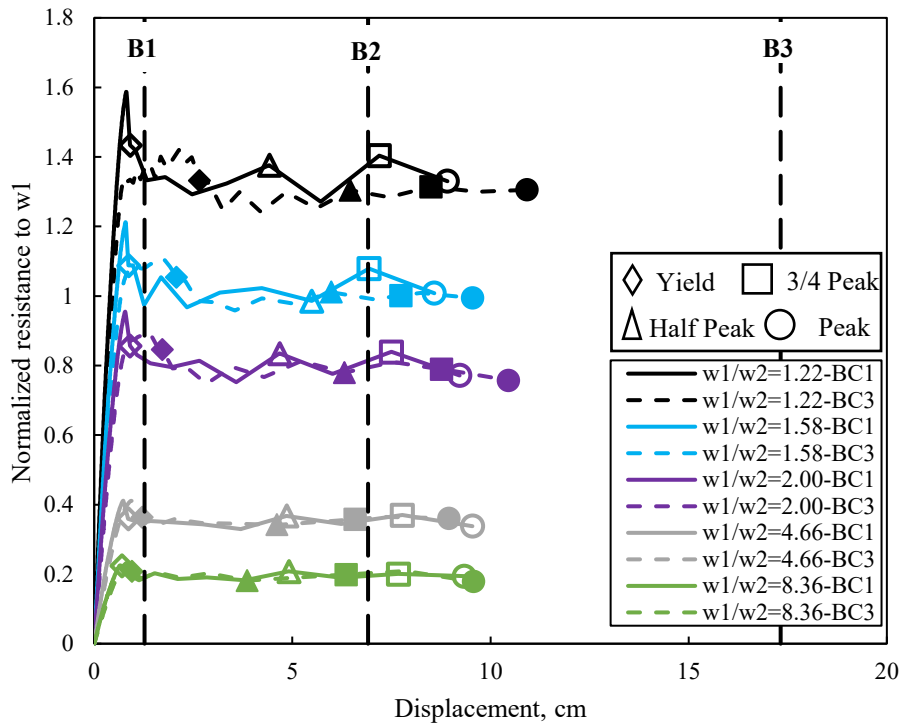
Figure 33. Normalized resistance functions of the 6DC panels with BC1 and BC3

3.5.1.4.   Strain energy.

A comparison of the strain energy of the FE models and the UFC approach for 6DC with

BC1 and BC2 are shown in Figure 34a and b. For BC1 panels, the study reveals that close results

are achieved for the yield milestone for cases with lower primary to transverse ultimate resistance

ratios. For higher damage levels and primary to transverse ultimate resistance ratios, the UFC

approach overestimates the amount of strain energy for all cases but that of BC2 with primary to

transverse ultimate resistance ratios of 1.22, 1.58 and 2.0. This is related to the formation of the

unexpected mechanism which also caused reduction in deformation capacity, as explained earlier.

These results indicate that for the majority of cases, the amount of damage will likely be higher

than would be expected from the current practice.

(a)   (b)

Figure 34. Linear correlation of the UFC approach and the FE strain energies for 6DC panels with (a) BC1 and (b) BC2

3.5.1.5.   Connection reactions

The reaction of the middle connection from the FE study for the panels with 6DC and BC2

are compared to the reaction calculated based on the current UFC approach. The reaction demands

are based on the relative tributary area of the connection. The capacity of a connection, *r*, is found

using Equation 20.

$$r = \min(w_1, w_2) \times Tributary\ Area \qquad\qquad \text{Equation 20}$$

Figure 35 illustrates the FE reaction for two different connection locations: edge and middle of the panel. The comparison between the UFC approach and the maximum FE reaction of the middle connection is shown in Figure 35b. Cases which fall above and to the left of the bisecting line demonstrate situations where the UFC approach under predicts the reaction. The panel reactions are under predicted by the UFC approach. Thus, designing the connections for the lower one-way flexural strength, as commonly done in the real practice, can result in an under prediction of the actual loads on the connection. This occurs due to the use of realistic material which is not the case with the UFC approach.

(a)   (b)
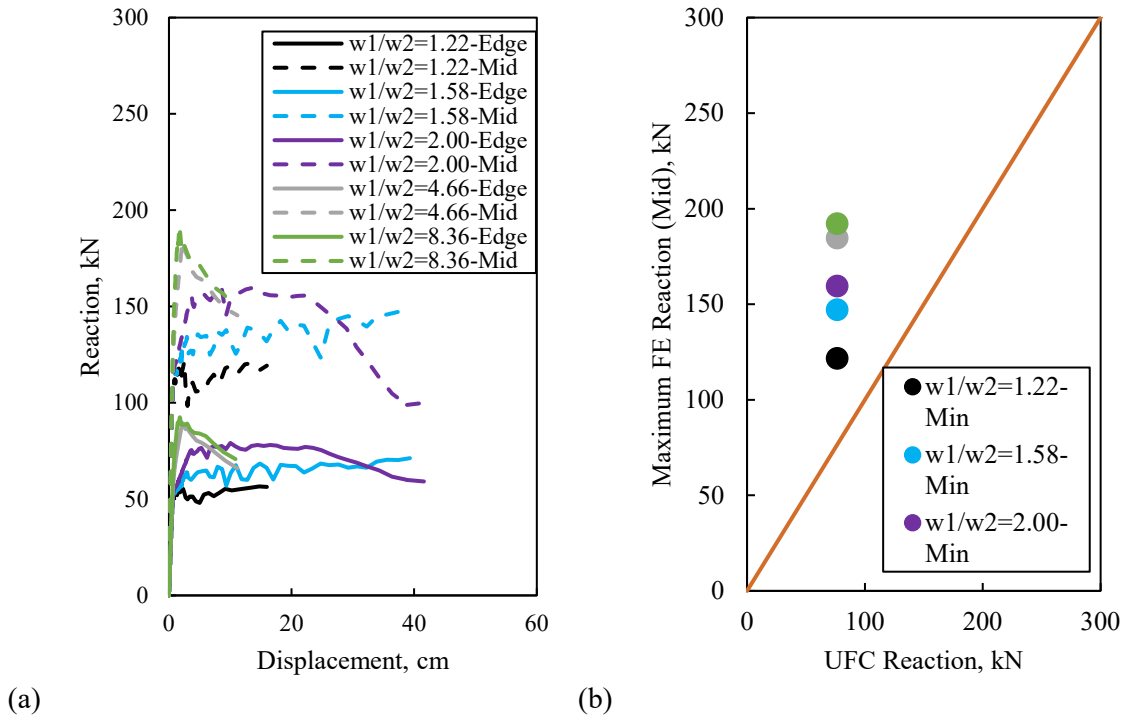
Figure 35. (a) reactions and (b) linear correlation (for mid BC) for 6DC panels with BC1

3.5.2. Dominant span sensitivity study

The parametric study assures that most of the panels with higher primary to transverse ultimate resistance reached to weaker (unexpected) mechanism. As a result, reduction in ductility which leads to the current practice to overestimates the strain energy of the panels and thus more

damage would occur. The study also shows that some panels reached to the intended mechanism which results in high ductility and good estimation for the UFC strain energy. Therefore, this section aims to investigate the ratio of primary to transverse ultimate resistance that will insure reaching the vertical mechanism, as assumed in the current practice. The study is performed for the 6DC panel with BC1 (the most realistic boundary conditions). To insure reaching the vertical mechanism, the transverse ultimate resistance in the prototype panel, i.e. 6DC-w1/w2=1.58-BC1, is increased by replacing the minimum reinforcement with larger amount of reinforcement and thus reduce the potential of having a weaker mechanism. Table 11 shows the new arrangement of reinforcement size and spacing that replaces the minimum reinforcement. The deflected shape at peak deformation is shown in Figure 36. The transition in the deformed shapes from weaker mechanism to bi-directional and then reaching to the intended mechanism are observed with the decrease in w_1 to w_2 ratio. The deformed shape illustrates that strengthen the transverse mechanism induces the one-way primary mechanism when the ratio of w_1 to w_2 equals 0.5. Consistent with the deformed shape, Figure 37 reveals improvement in resistance and ductility for the strengthen panel when the ratio of w1 to w2 decreases. The resistance function for the panel with w1 to w2 equals 0.5 shows reduction in strength prior to peak deformation milestone which results from a transition from bidirectional behavior to one-way direction. Thus, the study illustrates that prediction the dominant bending direction for the panel with realistic boundary conditions BC1 and 6DC is not as simple as ensuring w_1 to w_2 less than one.

Table 11 New arrangement of transverse reinforcement

Cases	6DC-w1/w2-0.9-BC1	6DC-w1/w2-0.77-BC1	6DC-w1/w2-0.5-BC1
Bar size and spacing	#10 @ 25.4 cm o.c.	#13 @ 39.37 cm o.c.	#13 @ 24.13 cm o.c.

6DC-w1/w2=1.58-BC1   6DC-w1/w2=0.9-BC1   6DC-w1/w2=0.77-BC1   6DC-w1/w2=0.5-BC1
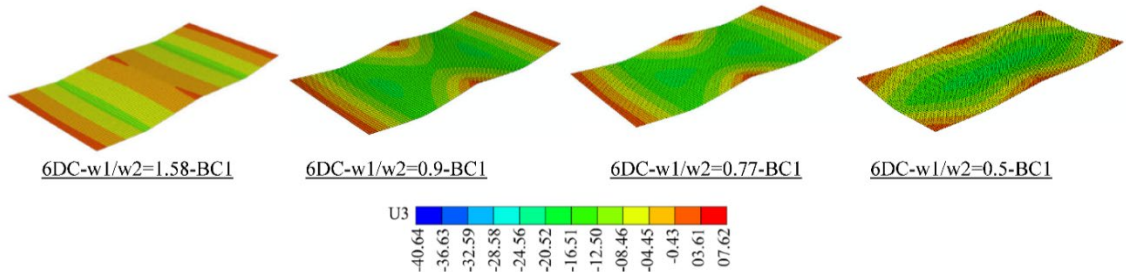
Figure 36. The FE deflected shape at peak deformation for the strengthen panel (units in cm)
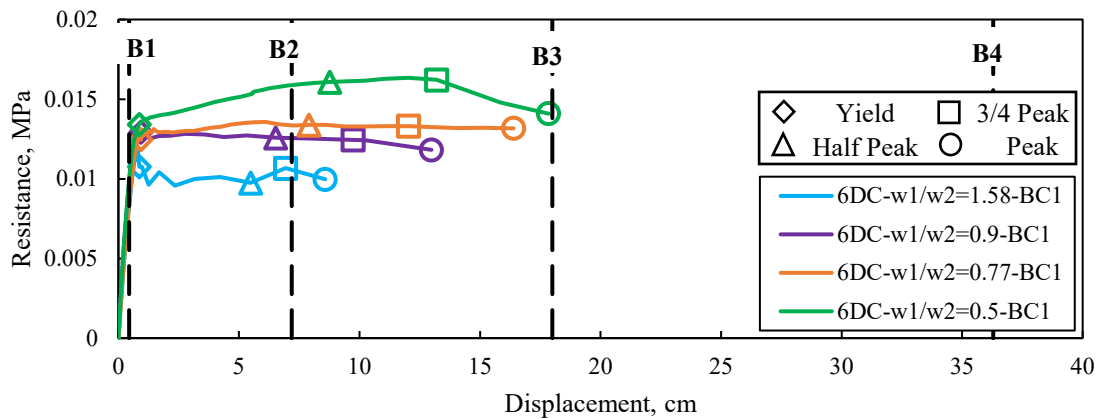
Figure 37. Out-of-plane flexural resistance of the strengthen panel

3.5.3. Panels with eight discrete connections

3.5.3.1. Resistance functions and deflected shapes

Increasing the number of connections from six (6DC) to eight (8DC) discrete connections leads to smaller ratios of w_1 to w_2 within the range of panels used in the parametric study, as shown in Table 9. Using BC1 (the realistic case), the prototype panel is examined and compared with the current practice design. The deformed shapes at peak milestone are presented in Figure 38. The panel with a ratio of w_1 to w_2 equals 3.71 is not shown since it reaches to the same conclusion as the panel with w_1 to w_2 equals 2.07. Panels that have higher ratios of w_1 to w_2 result in failure modes

in the non-primary direction. Lower ratios of w_1 to w_2, however, reveal failure modes similar to current practice prediction, i.e. one-way approach. The FE resistance functions, shown in Figure 39, are normalized to the UFC approach (w_1) and plotted against the displacement at the interested point. The interested point is measured at the location of maximum displacement at peak response (i.e. at flexural failure). The FE capacity is higher than the standard UFC estimations for the panels with lower primary to transverse ultimate resistance ratios. It should be noticed that the reduction in the resistance function after the yield milestone occurs due to the transition from a bi-directional mechanism to a one-way vertical mechanism. An example for this behavior is shown in Figure 40 for the panel of w_1 to w_2 equals 0.70. As the primary possesses higher ultimate resistance than the transverse direction, the measured capacity is less than the UFC estimations which results due to the unexpected mechanism, as illustrated in Figure 38. Discrepancy is observed between component-specific and current practice response limits in general, yet the panels reach to the intended mechanism show higher ductility than the panels fails in the transverse direction. The study shows that the panel with 8DC and BC1 reaches to the intended mechanism at ratio of w_1 to w_2 equals 0.89.
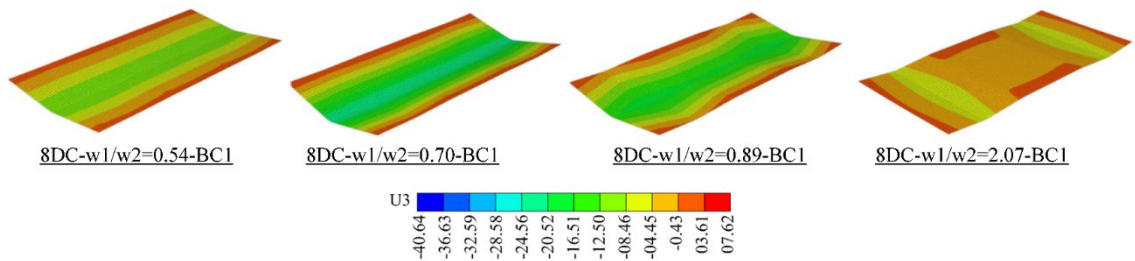
Figure 38. The FE model deflected shapes at peak for 8DC panels with BC1 (units in cm)
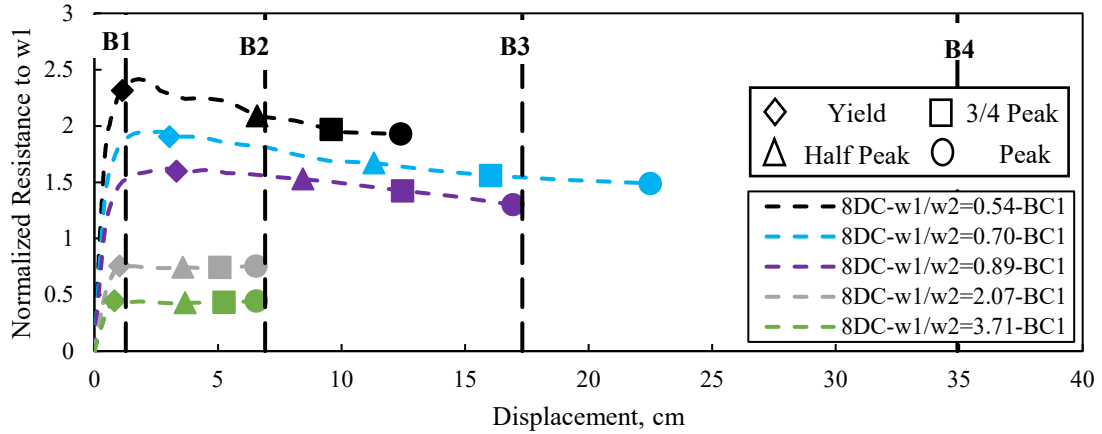
Figure 39. Normalized resistance functions to w1 for panels with BC1 and 8DC

8DC-w1/w2=0.70-BC1(Yield)   8DC-w1/w2=0.70-BC1(Half peak)
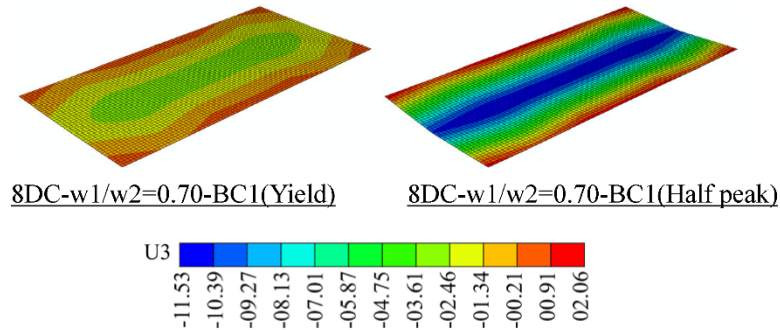
Figure 40. The FE model deflected shapes at yield and half peak for 8DC panels with BC1 (units in cm)

3.5.3.2.   Strain energy

Linear correlation of strain energies of the UFC current practice and the FE model for panels with 8DC and BC1 are shown in Figure 41. This is related to the formation of unexpected mechanism, as shown in Figure 38, which compromises the deformation capacity. The formation of the expected one-way mechanism, as shown in Figure 38, leads to conservative results for the cases of w_1 to w_2=0.54, 0.70 and 0.89. For higher ratios, however, the study shows unconservative results due to the unexpected mechanism which results in reduction in ductility and thus the FE strain energy.
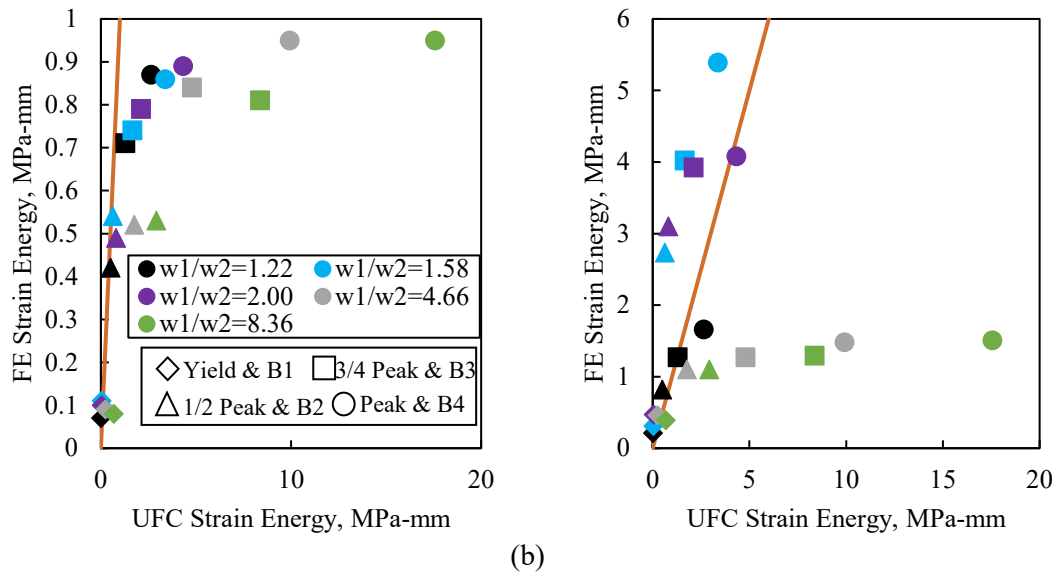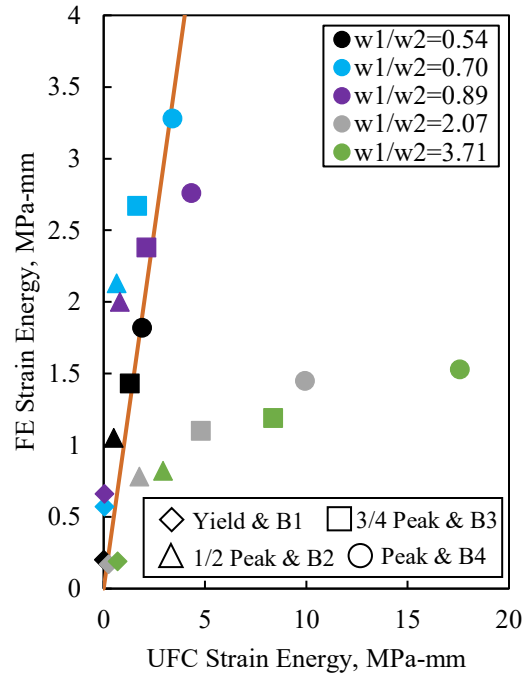
Figure 41. Linear correlations of the UFC approach and the FE strain energies 8DC panels with BC1.

3.5.3.3.   *Connection reactions*

The reactions for 8DC panels with BC1 are shown in Figure 42. The FE maximum reaction compared with the UFC reaction of either axis with minimum strength, as explained earlier. Reactions of edge and inner connections of the 8DC panel are shown in Figure 42a. Linear correlation analysis of the UFC current practice and the FE reactions is also developed and shown in Figure 42b. Similar conclusion as 6DC panel with BC1 is observed for 8DC panels. The linear correlation analysis reveals unconservative design for all cases when following the UFC approach based on the minimum strength in either direction due to the use of realistic material as well as the bi-directional behavior, explained earlier, which are not account by the current approach.
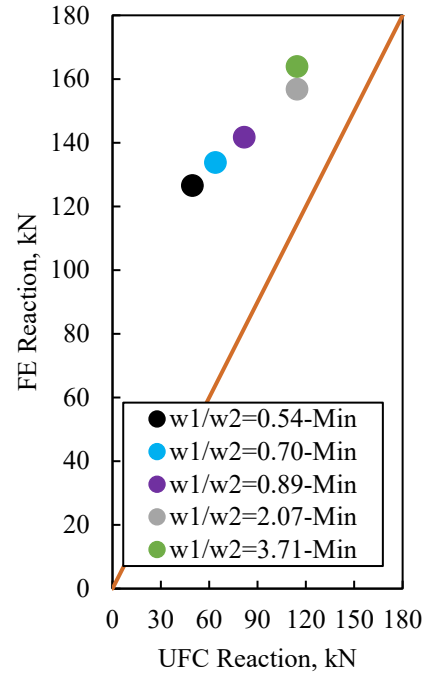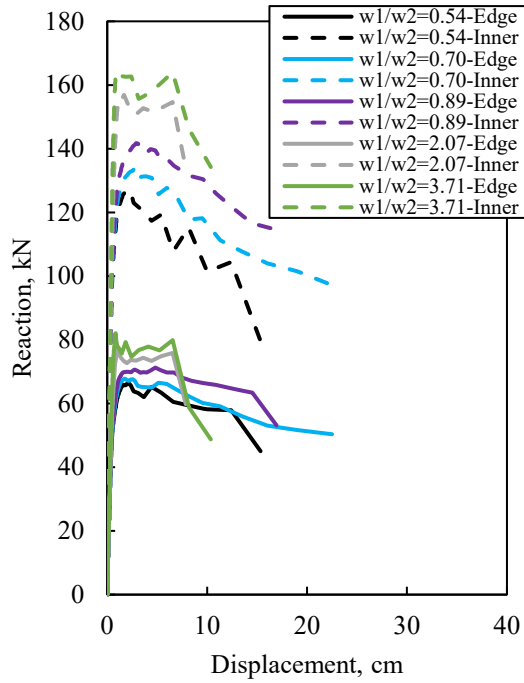
Figure 42. (a) Reactions and (b) linear correlation (only inner BC) for BC1 panels with 8DC

4. FLEXURAL RESISTANCE OF NON-LOADBEARING PRECAST CONCRETE FAÇADE PANELS WITH DISCRETE CONNECTIONS AND OPENINGS SUBJECT TO BLAST LOADING

4.1. Introduction

Precast concrete wall panels are often used as the building's first line of defense against external explosive threats. Current simplified blast design methods rely on the resistance function of the component to calculate the dynamic response and assess the extent of damage following a blast event. This resistance function is dependent upon cross-section geometry, material properties and boundary conditions. Unlike monolithic cast-in-place concrete construction, precast concrete components require discrete connections for attachment to the main structural system. Several different types of these connections are commercially available with varying allowable degrees of freedom, such as translational movement in one direction only or fully moment resisting. The number of connections needed also varies depending upon the geometry of the panel and the design loads resulting from conventional (e.g., wind) or blast demands. Many conventional blast design assumptions idealize these discrete connection points as uniform line supports along the edge of the panel [1]. This assumption implies one-way flexural behavior and neglects the influence of realistic discrete connections on the bi-directional response of the panel. Without thorough consideration of all possible response mechanisms resulting from the presence of discrete connections, conventional blast design methods may not be able to recognize a realistic premature failure of the component. The effect of discrete connections on the performance of solid precast concrete panels (without openings) was previously examined by the author, as shown previously. The results of that study showed significant discrepancies when evaluating resistance functions generated using a validated FE model versus conventional design assumptions. A major focus of that study was to determine which primary and transverse direction ultimate resistance ratios

facilitated unexpected failure mechanisms and significant loss of ductility. These concepts will be extended for panels with both discrete connections and openings in this paper.

Some high risk facilities may require façades with blast-resistant windows or doors. The presence of these openings requires additional blast design considerations for precast concrete wall panels. These include (1) characterizing the load transfer interaction between the supporting edges of the window or door and the adjacent concrete surfaces and (2) compensating for the opening when calculating the static resistance function of the component. Current practice neglects resistance provided by regions above and below the openings for one-way vertical spanning components and thus assumes that the dominant flexural mechanism also occurs in that direction [37]. A major focus of this paper is to examine the combined effect of discrete connections and openings on the realistic performance of precast concrete wall panels. The study compares resistance functions generated using nonlinear finite element (FE) models versus conventional one-way flexural design assumptions. This study also considers component-specific response limits, previously proposed [27], which are developed as a function of the constitutive properties of the panel in comparison to currently prescribed antiterrorism response criteria [10]. A comprehensive parametric study examines the sensitivity of primary to transverse ultimate resistance ratio and number of openings, in conjunction with discrete connections, on the resistance functions of these panels. The results indicate that conventional design assumptions may lead to unexpected premature response mechanisms which may compromise both flexural capacity and ductility.

4.2.   Background

4.2.1. Glazing Systems for Precast Concrete Panels

While precast concrete panels may be designed with openings for doors or windows, the focus of this paper will be limited to examine openings with windows. Conventional glazing systems for windows are often assumed to provide insignificant resistance to blast loading. However, hardened versions of these systems can be designed to resist varying levels of blast-

induced damage. Seven hazard levels, ranging from "no break" (i.e,. no visible damage) to "high hazard", and correspond to progressively severe descriptions of glazing damage [38]. This study solely focuses on the behavior of the reinforced concrete section of the panel and does not consider the detailed performance of the glazing system. While the glazing used as part of the components herein is not assigned a specific hazard rating, the analyses conducted later in the paper assume that the windows either maintain sufficient structural integrity to continue transmitting blast pressure demands to the attached concrete panel or are completely blown out. In the former case, this study assumes that the glazing system does not provide additional flexural capacity to the reinforced concrete elements. Furthermore, it is also assumed that none of the reflected blast pressure will clear through a newly formed opening resulting from a heavily damaged or perforated glazing pane.

Although the windows must be properly sealed on all sides for weather protection and energy consumption considerations, their structural connection to the adjacent concrete panel may be idealized along either two or all four edges. The assumption of only two edge supports, on opposite sides of the glazing, is commonly used to coincide with the assumed one-way flexural behavior in current blast-resistant design practices. This study characterizes the load transfer interaction between windows and surrounding concrete regions using three different assumptions: (1) glazing is completely blown out and does not transmit any blast pressure loading to the surrounding concrete, (2) the glazing transmits the blast pressure over the entire opening area through two uniform line supports (Figure 43a) and thus spans the same primary direction as the idealized one-way panel and (3) the glazing transfer the blast pressures over the opening area through triangular line supports on all four edges (Figure 43b). The effect of these assumed boundary conditions will be thoroughly examined later in this paper.
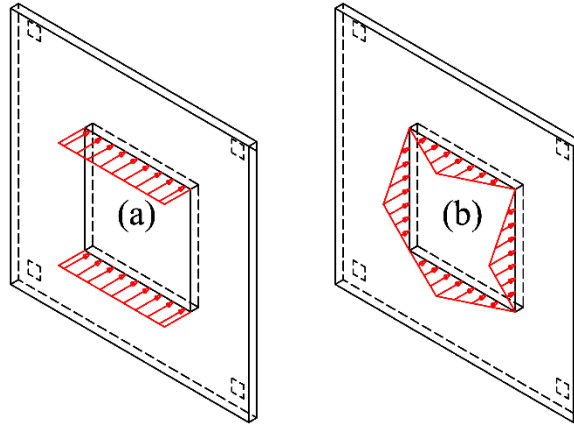
Figure 43. Windows blast resistance equivlant loading: (a) Line and (b) Triangular loads

4.2.2. *Current Practice Design*

A generic precast wall panel with openings is shown in Figure 44a. As mentioned previously, conventional design practice assumes that all one-way flexural resistance is provided by continuous (i.e., no breaks for openings) vertically spanning regions of the panel adjacent to the opening(s). This represents a conservative estimate in component capacity as the resistance of all regions above or below the openings (in a vertically spanning panel) is neglected in this assumption. As a conservative estimate, reflected pressure demands are applied over the entire surface area of the panel (i.e., full tributary) as shown in Figure 44b [37]. Clearing effects are commonly neglected which assumes that the blast pressure wave does not infiltrate any openings or seams between the damaged glazing and panel or through significant cracks developed in the glazing.

If a blast design requirement is prescribed for the component, it is first designed to withstand conventional loads, such as lifting, handling, wind, and self-weight. Following the initial static design, the component is equated to a generalized single-degree-of-freedom (SDOF) system [39] to estimate its blast-induced dynamic response as shown in Figure 44c. Consistent with the one-way flexure assumption, each continuous vertically spanning region adjacent to the openings is modeled as a beam element with simply supported boundary conditions to determine its resistance function. The resistance function is calculated as a function of the constitutive properties of the component, cross-section geometry, span length and boundary conditions. The panel is

equated to a SDOF system by normalizing spatially distributed loads and mass using a load-mass transformation factor, K_{LM}, calculated as a function of the deflected shape of the component normalized to the maximum displacement. The SDOF equation of motion can be solved considering the mass, M, resistance function, $R(y(t))$, and the applied pressure history, $F(t)$, using any compatible numerical method.
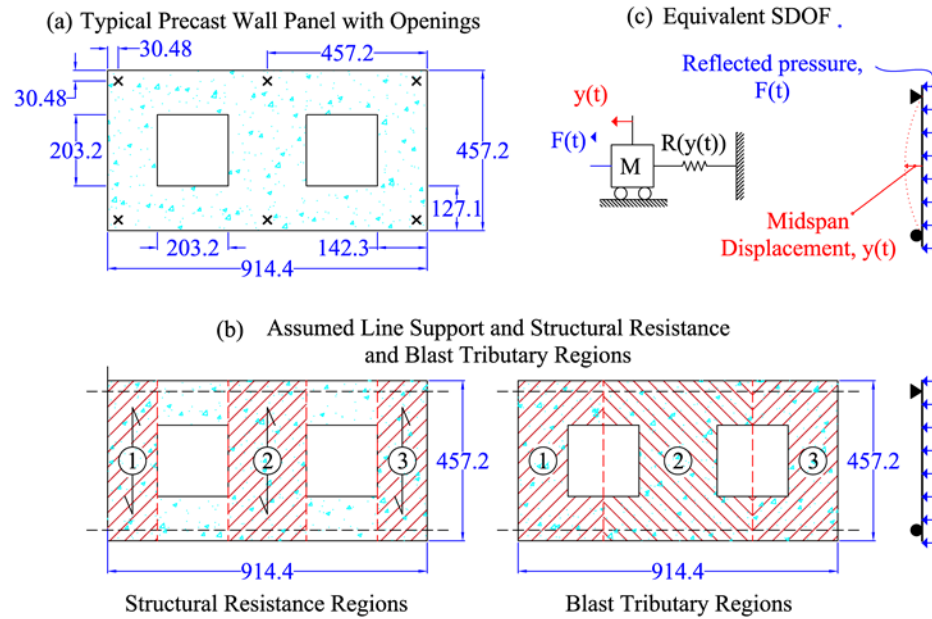
Figure 44. Current practice design process

The extent of blast-induced damage evaluated by comparing the maximum displacement response of the component to a set of prescribed response criteria. These criteria vary depending upon component type and the intended use of the component. This paper will focus on response criteria for anti-terrorism and force protection [10], which are commonly used in blast design practices. Five levels of damage range from *superficial* (i.e., no permanent visible damage) to *blowout* (i.e., component is completely overwhelmed). Component-specific response limits are developed which correlate damage levels to critical milestones along the resistance function of the component [27]. This facilitates a direct comparison between constitutive properties and realistic response mechanisms based on first principles of structural mechanics. The recommended response milestones based on Gombeda et al. [27] correspond to yield, half peak, three-quarter peak and

peak flexural strength. A summary of current response limits provided by the US Army Corps [10] and component-specific (CS) milestones for reinforced concrete flexural members are shown in Table 6. Both sets of response limits will be examined in this study to determine limitations where conventional design assumptions may not facilitate realistic estimations of component response, depending upon openings and discrete connections. A major focus of this paper is to evaluate the sensitivity of resistance functions for these panels considering variations in opening geometry in conjunction with varying numbers of discrete connections. These studies will be performed using a performance-based design framework incorporating finite element modeling and will be compared with conventional design assumptions.

4.2.3. Discrete Boundary Conditions

Precast concrete wall panels are connected to the building through discrete connections. As mentioned previously, current practice idealize these discrete connections as a uniform line support and consistent with one-way flexural response assumptions. Design of the transverse direction (i.e., orthogonal to the assumed primary span direction) is often limited to temperature and shrinkage reinforcement requirements and thus may not be properly detailed to resist a realistic two-way flexural response mechanism. The realistic implications of this assumption was examined for solid wall panels (i.e., non-insulated and without openings), shown previously. The paper examined variety of number of discrete connections and nominal moments of solid wall panels. This previous study compared resistance functions of wall panels with discrete connections calculated using a performance-based approach which was also compared with conventional design assumptions. This study revealed that current assumptions and prescriptive response criteria often lead to significant overestimations of deformation capacity when compared to the component-specific, first-principles based approach. In many cases, panels designed for one-way flexural response realistically exhibited an unexpected failure in the transverse direction. The study also demonstrated that the unexpected failure mechanisms occurred due to increasing the primary

ultimate resistance while weakening the orthogonal direction by maintaining its ultimate resistance to the temperature and shrinkage requirements.

This paper serves as an extension of the previous study, i.e. solid panels, to include precast concrete wall panels with openings. The studies presented herein examine the impact of discrete boundary conditions, conventional reinforcement strategies and presence of openings on the load-deformation resistance of blast-resistance precast cladding panels. The panels are modeled using a nonlinear finite element framework, the results of which are compared with standard one-way response elastic-perfectly plastic (EPP) assumption and conventional anti-terrorism response criteria. This paper focuses on developing the nonlinear resistance function considering the non-one-way behavior and assessing the component-specific response limits and in comparison with the current practice approach.

4.3. Validation of Finite Element (FE) Modeling

The performance of precast concrete wall panels with discrete connections and openings are examined through nonlinear finite element modeling. To ensure the accuracy of the predictions, the modeling approach is first validated through comparisons with two experimental tests.

4.3.1. Finite Element Model Development

The finite element modeling approach used in this paper was derived from the framework previously used for solid (i.e., no openings) wall panels with discrete connections. Several modifications were added to this existing framework to facilitate modeling of panels with discrete connections and openings. Similar to the previous study, the resistance function of the panel was quantified using a quasi-static analysis to determine the entire load-displacement relationship. The concrete regions are modeled with three-dimensional homogenous shell element (ABAQUS element S4). Concrete constitutive properties are modeled using a concrete damage plasticity model (CDP) with dilation angle of 36º and eccentricity of 0.1 [29]. The ratio of biaxial, σ_{b0}, to uniaxial compressive strength, σ_{c0}, is taken as 1.16 [29]. A yield function is used to account for the different

tension and compression response. The ratio of the tensile to compression meridian that defines the yield function in the deviatory plane, K_c, was assumed as 2/3 [29]. The uniaxial stress-strain for concrete in tension is defined as linear elastic up to the modulus of rupture. After rupture, a smooth descending branch is used to account for the progression of micro-cracking and to mitigate numerical instabilities. Softening was modeled using Equation 16 which was developed by Wang and Hsu [40]; where f_t, ε_t are the tensile stress and strain, f_{cr}, ε_{cr} are the modulus of rupture and the corresponding strain; n represents the rate of weakening taken as 0.6. Modulus of rupture was calculated using Equation 17 [31], where f'_c is the ultimate concrete compressive strength (in MPa) and λ is a the aggregate modification factor taken as 1.0. Popovics concrete numerical model is used to define the uniaxial stress-strain for concrete in compression [32]. Reinforcement is included as a smeared uniaxial layer within the shell element. The constitutive properties for steel reinforcement will be discussed in detail for each validation case.

4.3.2. Validation Study

The modeling approach is validated against two experimental studies: Smith and Kim [41] and Enochsson et al. [42]. Smith and Kim [41] describes the behavior of a one-way panel with a central opening and Enochsson et al. [42] examined the response of a two-way slab with an opening and idealized line supports subjected to a uniformly distributed load. Figure 19 shows the loading diagrams and cross section configurations for each case. Quarter symmetry is utilized for the model in both cases to increase computational efficiency. Enochsson et al. [42] used steel frames (HEA 200 beams) to provide the line supports for the slab, which was restrained against downward movement while permitting horizontal and upward translations. Upward movements were noticed at slab corners which indicated that the slab cannot be modeled using the simple prescribed boundary conditions, i.e. pin or roller support. Enochsson et al. [42] assessed the stiffness of the support system and found out that the elastic support system showed good agreement with experimental results. Therefore, the steel frames (i.e. HEA 200 beams), used to support the slab are

modeled as an elastic system support in this study. A coupling constraint is used along the line support between the HEA 200 beams and the slab to restrict the movement in the Z direction only. The constraints are not used within 52 cm of the corner to allow for the corner uplifting as observed during the Enochsson et al. [42] test. Figure 46 shows a schematic of the support system used in this particular case. The steel reinforcement stress-strain for Smith and Kim [41] was assumed as bi-linear with elastic-hardening response. The steel elastic modulus is assumed to be 200 GPa. Steel reinforcement stress-strain for the Enochsson et al. [42] test was adopted from a tensile test of the bars used in the experiment [43]. The properties for steel, such as yield stress, f_{sy}, and the tensile stress, f_{su}, and strain, ε_{su}, as well as the properties for concrete, such as compressive strength, f'_c, modulus of elasticity, E_c, and ultimate strain, ε_{cu}, are summarized in Table 12. Material properties of experiments. The ultimate concrete compressive strain is calculated as function of modulus of elasticity and ultimate compressive strength in accordance with Popovics's approach [32].

Table 12. Material properties of experiments

Experiment	E_c (GPa)	f'_c (MPa)	ε_{cu} (%)	f_{cr} (MPa)	f_{sy} (MPa)	f_{su} (MPa)	ε_{su} (%)
Smith and Kim [41]	28.10	42.00	0.21*	3.30	557.00	648.00	9.60
Enochsson et al. [42]	34.00	46.5	0.20*	3.10	510.00**	630.40	3.93

* The data was assumed

** 0.2% yield strength
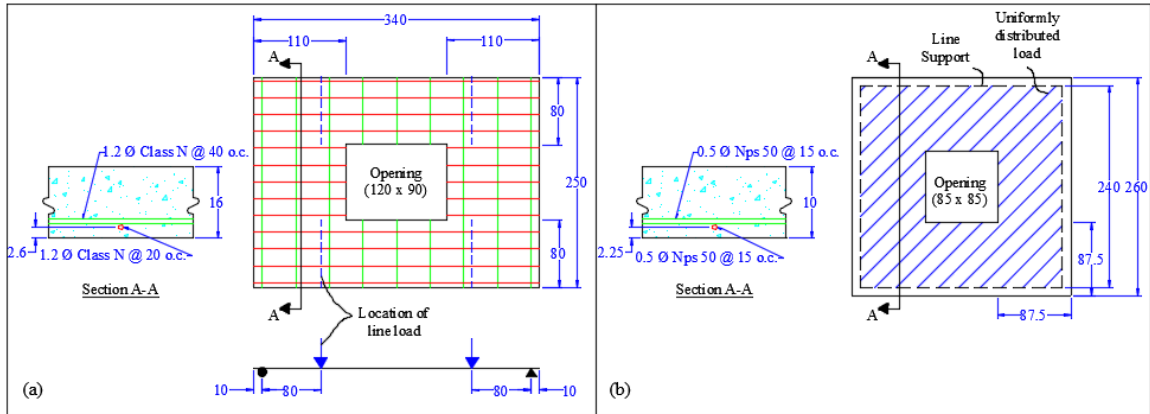
Figure 45. Schematic of experiments (dimensions in cm) tested by (a) Smith and Kim [41] and (b) Enochsson et al. [42]
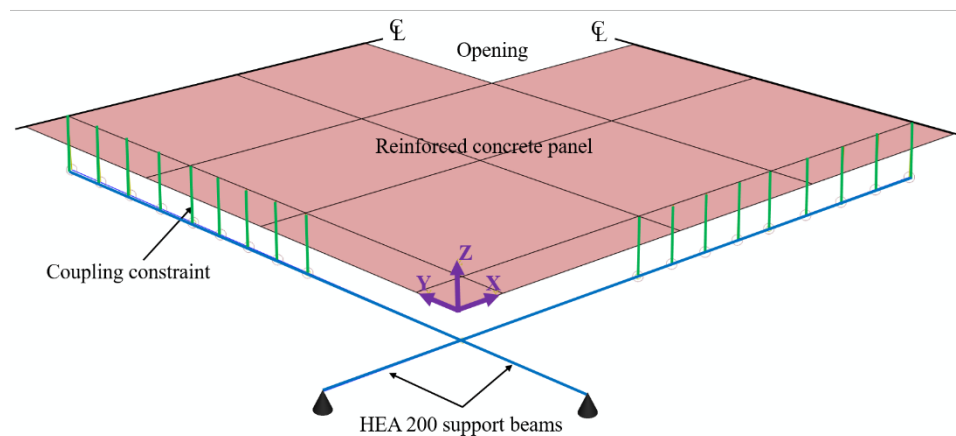
Figure 46. The FE details for Enochsson et al. [42]

The FE results, in comparison with experimental results for Smith and Kim [41] and Enochsson et al. [42], are shown in Figure 20a-b. The resistance is plotted versus the displacement at the point of interest. The acquired displacement for Smith and Kim [41] is located at mid-span near to the opining. The displacement point of interest for Enochsson et al. [42] is at the midpoint closed to the opening. The displacement history for Smith and Kim [41] was truncated at 100 mm due to an extension limitation of the actuator. The FE model predictions compare reasonably well with the measured experimental response for both cases. The final cracking pattern for Smith and Kim [41] indicated that flexural cracks propagated along opening length parallel to the line loading. Also, diagonal cracks propagate from corners and then forced to form parallel to the line loading.

80

Enochsson et al. [42] test shows two diagonal cracks propagates from the corner of the opening and then split in a symmetrical manner to arrive adjacent to the slab corner. Principal of plastic strains for the tension concrete fiber in the FE model demonstrate good agreement with cracking patterns of Smith and Kim [41] and Enochsson et al. [42] as shown in Figure 21.

The FE modeling approach provides an adequate level of accuracy for a variety of solid panels with discrete connections in previous study for solid panels without openings. The FE modeling approach also reaches to an acceptable level of accuracy for panels with openings as seen earlier. Therefore, the FE modeling approach is used to examine the precast panels with discrete connections for a variation of primary to transverse ultimate resistance ratios and number of openings as shown next in the parametric study section.

(a)　　　　　　　　　　　　　　　　　(b)
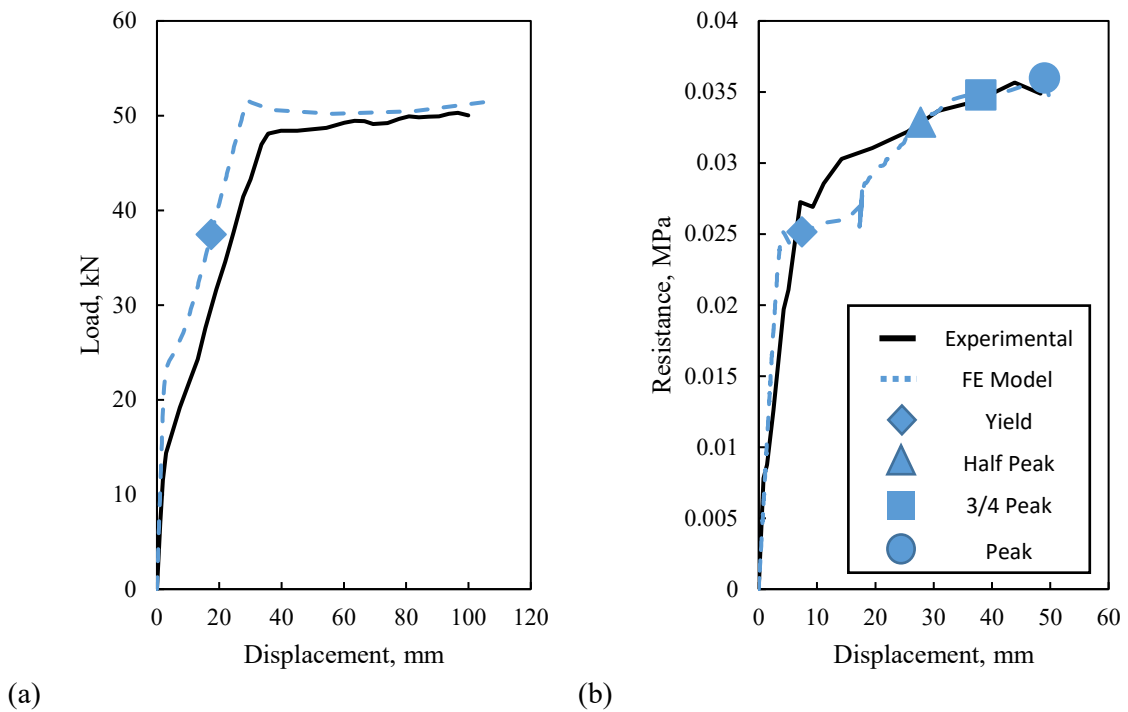
Figure 47. Finite element resistance function and experimental test data for (a) Smith and Kim [41] and (b) Enochsson et al. [42]
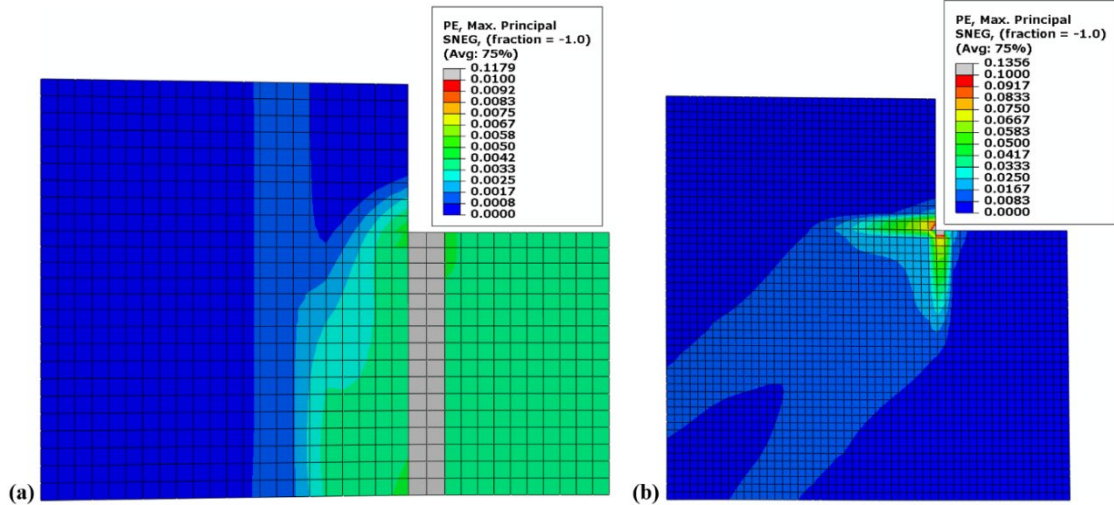
Figure 48. The plastic strain (PE) contours for (a) Smith and Kim [41] and (b) Enochsson et al. [42]

4.4.   Parametric Study

A parametric study is conducted to examine variations of ultimate resistance and number of openings on the resistance functions and limit states of blast-resistant cladding wall panels with discrete connections. The parametric study is based on a prototype panel measuring 9.14 m (30 ft) long, 4.57 m (15 ft) tall and a thickness of 15.24 cm (6 in) with six discrete connections as illustrated in Figure 22. The boundary conditions in the study consist of rollers along the x-axis and pin supports along the y-axis as indicated in Figure 22. This configuration represents a practical case where the tieback connections, used to resist lateral loads, are set to allow thermal expansion in the transverse direction and resist movement in the primary (y-axis). This study was limited to panels with square openings to avoid introducing additional complexities caused by variations in opening aspect ratio in these initial examinations. Panels with a single and two openings were considered with the area of each opening corresponding to 10% of the total panel area. The geometries and cross-section details of the base panel design are shown in Figure 22. The vertical bar size in Figure 22 is not labeled because reinforcement ratio, and thus bar size, is varied as part of the parametric study. Specific details for the openings, such as dimensions and locations within the panel, are discussed later in this study. It should be noted that the vertical bars (running along the y-axis) are

typically detailed as the primary flexural reinforcement in accordance with current design practice. Horizontal (along x-axis) reinforcement is included only to resist shrinkage and temperature demands in accordance with ACI 318 [31].
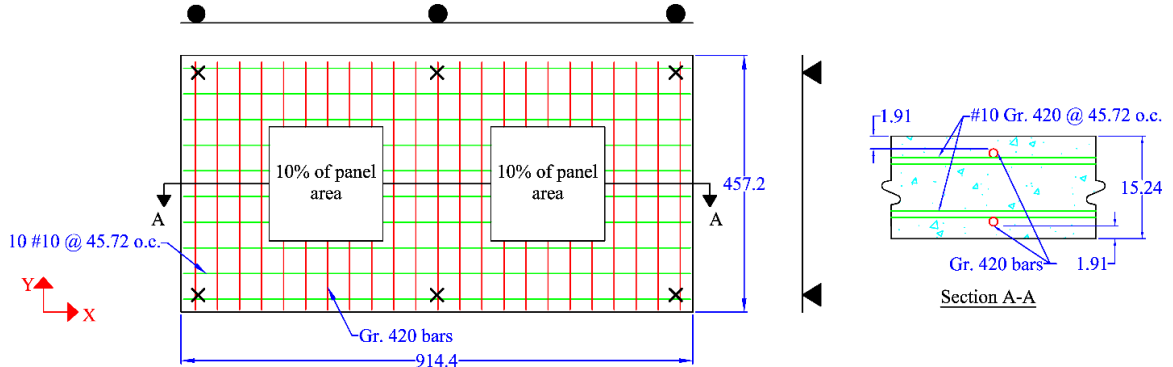
Figure 49. Configurations of precast panel and its boundary conditions (all dimensions in cm)

Like the validated FE model, the parametric study is modeled in ABAQUS using shell elements (S4) with a uniform mesh size of 10.16 cm (4 in). The parametric study also uses the concrete material model discussed previously in section 3. A summary of all material properties used in the study is shown in Table 8. Material properties of the parametric FE models,. To facilitate more accurate comprison of the model with realstic panel response, an expected rebar stress-strain curve is obtained from Gombeda et al. [34]. For the purpose of this paper, the curve is scaled to match the minimum yield, tensile strengths and ultimate tensile strain values prescribed by ASTM A615 [44]. Plots of constitutive properties for concrete and steel reinforcement are shown in Figure 23a and b, respectively. The elastic-perfectly-plastic stress-strain behavior used in the conventional design approach is also shown for comparison in Figure 23.

4.4.1. Variation in Number of Openings

Panels with a single (Op1) and two openings (Op2) are examined in this study. The results of the finite element model are compared with the resistance that is calculated using the one-way assumption. Figure 50 shows the geometries of the panels with a single and two openings and their corresponding locations. Figure 50 also shows the support conditions and loading diagrams to calculate the current practice flexural resistance (one-way assumption) for each case. The one-way

ultimate resistance for each cases is calculated considering the primary, w_1, and transverse axis, w_2 [37]. As mentioned previously, the current practice assumes one-way behavior and considers the flexural resistance of the primary (vertical spanning) direction only. To evaluate this assumption, the response of the FE model is compared with the ultimate resistance in the primary direction of the panel. The comparison is mainly focused on resistance function, response limits and strain energy.

The interaction of windows designed to sustain blast loading and the adjacent concrete regions are represented in the FE model by idealizing the load transfer to the boundary conditions at the perimeter of the opening. As mentioned earlier, glass windows are typically connected to two or four sides of the edges as shown in Figure 43. The geometric pattern of reactions is represented by either triangularly or uniformly distributed line loads. The triangular pattern is applied on all four sides (4S) of the opening and simulates bi-directional response of the intact glazing whereas the uniform line load is only applied on two opposing sides (2S), which simulates a purely one-way response of the window. Either of these assumptions may be implemented for a given case depending upon the properties of the glazing and the connections to the surrounding concrete regions.
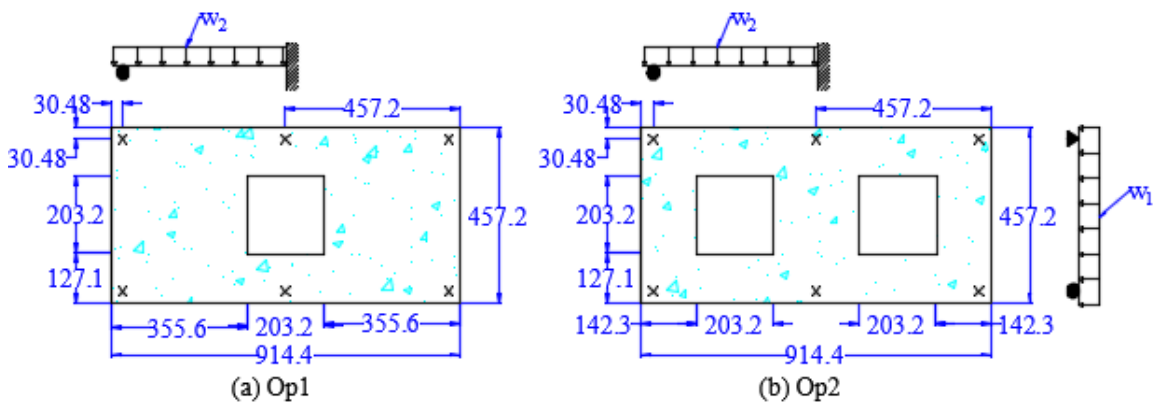
Figure 50. Variation in opinings and current practice support conditions (units in cm)

4.4.2. Varying the Primary Ultimate Flexural Resistance

The primary ultimate resistance, w_1, of the prototype panel is varied while orthogonal (transverse) ultimate resistance capacity, w_2, is kept constant for the minimum shrinkage and temperature requirements. Table 9 shows the primary, w_1, and transverse, w_2, ultimate resistance for each case. The transverse (along x-axis) reinforcement consists of #10 (#3) bars spaced at 45.7 cm (18.0 in.) on center for all cases. Table 9 summarizes all panel design case studies analyzed in this study. Using the strip method, reinforcement ratio is calculated using Equation 19 where A_s corresponds the area of steel of the extreme tension reinforcing bar (i.e., the bar closer to the compression face is not included in the reinforcement ratio calculation); d corresponds to distance from extreme compression fiber to centroid of the extreme tensile reinforcement; b corresponds to the tributary spacing of the bars. A detailed schematic of the cross-section configuration is shown in Figure 22. The doubly reinforced cross-section utilizes the exact same reinforcement layout in the top and bottom layers. It is assumed that the precast concrete walls in this study are exposed to weather, and thus the minimum clear cover for each bar is 1.91 cm (0.75 in.), in accordance with ACI 318-14 [31].

The ratio of primary to transverse ulrimate resistance is varied from 1.69 to 6.57 (for Op1) and 1.2 to 4.57 (Op2). The lower bound ultimate resistance was selected to ensure that the ratio of nominal moment capacity, M_n, to cracking moment, M_{cr}, remains greater than 1. This ensures that the nominal moment capacity will occur on the cracked section and thus mitigates any brittle failure mechanisms or significant discrepancies when applying the component-specific limit states. The upper bound ultimate resistance corresponds to net tensile strain, ε_t, of 0.007 which is approaching the lower bound limit of 0.005 for tension controlled sections in accordance with ACI 318-14 [31]. The nominal moment for the structural resistance regions as well as net tensile strain is calculated using strain compatibility and considering both top and bottom steel reinforcement layers.

Table 13. Range of primary to transverse ultimate resistance ratios for case studies

Bar size	#10 (#3)	#13 (#4)	#16 (#5)
d (cm)	12.86	12.7	12.54
b (cm)	28.58	39.37	15.24
ρ (%)	0.19	0.25	1.04
ρ_T (%)	0.13	0.13	0.13
ε_t	0.04	0.03	0.007
M_n (kN-m/m)	14.94	19.41	57.22
M_n/M_{cr}	1.05	1.36	4.0
w_1 (Op1) (kPa)	5.9	7.7	23.0
w_1/w_2 (Op1)	1.69	2.2	6.57
w_1 (Op2) (kPa)	4.2	5.5	16.0
w_1/w_2 (Op2)	1.2	1.56	4.57

4.5. Analysis Results

This section highlights the analysis results for panels with six discrete connections and openings. The analyses include combinations of three different primary to transverse ultimate resistance ratios for the single and two window openings. Both conventional (i.e., non-blast resistant) windows and blast-resistant windows are also considered in this study. The analysis aims to identify the impact of considering discrete connections when determining resistance functions for blast-resistant precast cladding panels with openings. The case study results are discussed in more detail below.

The following nomenclature is used label the parametric study cases: the first parameter denotes the ratio of primary to transverse nominal moment ratios, e.g. $w_1/w_2=1.69$; the second parameter shows number of openings (Op1 or Op2); the third parameters is added when blast-resistant windows (WBR) are used; lastly, the fourth parameter is used to indicate the load transfer pattern between the galzing and concrete (2S or 4S). All other labelings will be explained within the related section.

4.5.1. *Idealized line support and discrete connections*

This section is developed to examine and compare the resistance function based on the idealized line support as considered in the current practice with the discrete connection. This is performed in the panel with w_1 to w_2 equals 1.56 and two openings (Op2). The deflected shape at peak deformation milestone is shown in Figure 51. The panel with horizontal line support, i.e. Horizontal LS-w1/w2=1.56, reaches to the intended mechanism as expected. The panel with the discrete connections, i.e. 6DC-w1/w2=1.56-Op2, possesses unexpected failure mechanism which is equivalent to the formed mechanism for the panel with vertical line support, i.e. Vertical LS-w1/w2=1.56. The resistance functions for these panels are shown in Figure 52. The PDC limit states are included, for comparison with component specific milestone, and averaged for both span directions [10]. The response limits of B2, B3 and B4 are converted from support rotations to displacement in these analyses. The formation of the unexpected mechanism for the panel with discrete connections leads to reduction in ductility, i.e. near PDC B2. The panel with vertical line supports reaches to similar performance as the panel with discrete connection since both panels form transverse mechanism. If the intended mechanism is achieved as in the panel with horizontal line support, the resistance function reveals higher ductility, i.e. higher than PDC B4, compared with the panels with transverse mechanism. The effect of the realistic material is also observed in all cases where the capacity is higher than the UFC approach.
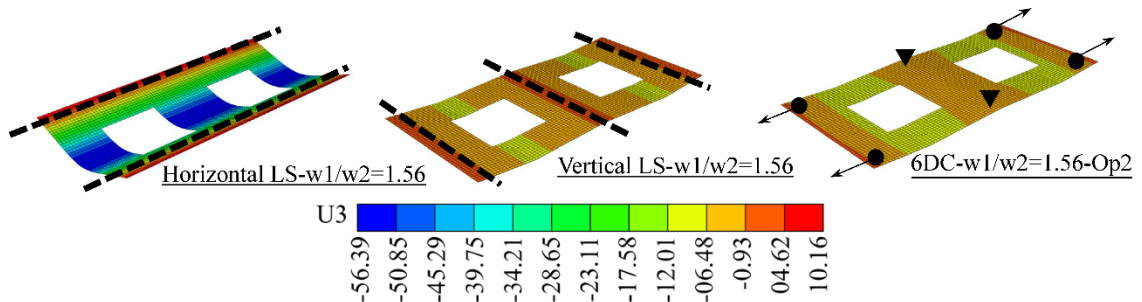
Figure 51. The FE deflected shape at peak for panels with idealized line support and discrete connections
(units in cm)
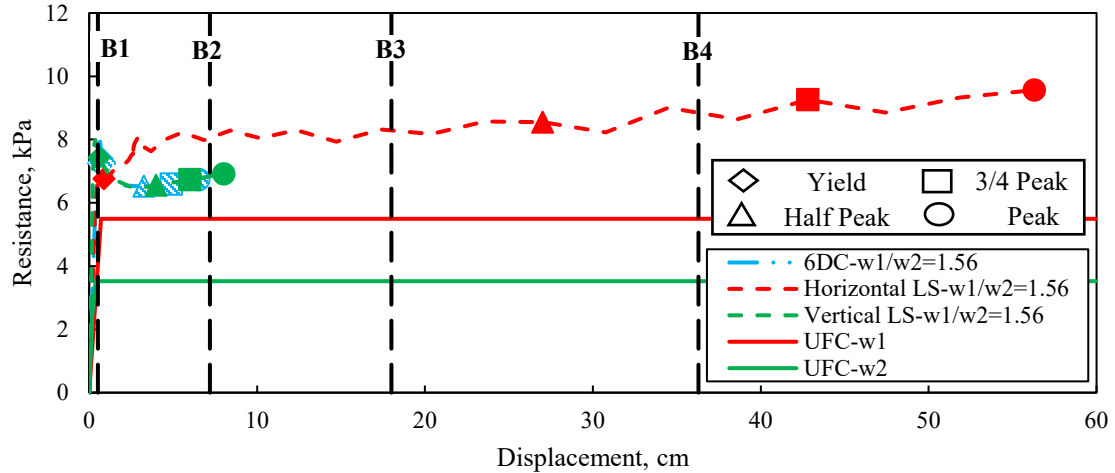
Figure 52. Resistance functions for the panels with idealized line support and discrete connections

4.5.2. Panels with a Single Opening

The parametric study results are separated in two sections for panels with a single and two openings. Variations in cross-section configurations and discrete connection layouts will be discussed in the subsections for each case.

4.5.2.1. Resistance functions and deflected shapes

Cladding panels measuring 9.14 m (30 ft) wide, 4.57 m (15 ft) tall with six discrete connections and a single opening are examined in this subsection. The analyses are performed for the range of primary to transverse ultimate resistance ratios shown in Table 9. The deflected shapes for all cases show the formation of flexural mechanisms in the direction opposite of the assumed response direction as illustrated in Figure 53. The unexpected mechanism is caused by the presence of the opening as well as the assigned minimum reinforcement which result in a localized reduction for strength above and below the opening. As a result, all cases fail in the top reinforcement layer along the middle support span. The FE model resistance functions (i.e., applied pressure versus displacement) for panels with non WBR, WBR-4S and WBR-2S are shown in Figure 32a. The resistance is also normalized relative to the ultimate resistance, w_1, which is computed using conventional one-way design assumptions in primary spanning direction (Figure 32b). The displacement, plotted on the x-axis, is taken at the location of the maximum displacement at the

peak response milestone as shown in Figure 55. Conventional response limits for a flexural member with no shear reinforcing and without tension membrane are also included for comparison [10]. The response limits of B3 and B4, not shown in Figure 32a and b, are equivalent to 17.32 cm and 34.93 cm, respectively. Component specific milestones, i.e. yield, half peak, three-quarter peak and peak, are also shown in Figure 32a and b.

Figure 32a shows that varying ratios of primary to transverse ultimate resistance has minimal implications for all examined cases due to the formation of the transverse mechanism which has minimum reinforcement for all cases. Additionally, both assumed window boundary conditions (2S or 4S) reach approximately the same peak capacity as indicated in Figure 32a. The reduction in capacity that is observed after yield milestone is caused by the transition behavior from a bi-directional resistance to the one-way resistance in the transverse direction. An example illustrating this behavior is shown in Figure 56. As illustrated, all panels fail near the expected B2 response level. The non-WBR cases result in higher resistance than the WBR cases which indicates that the additional loading around the opening induces the weaker mechanism earlier. Normalizing the strength by the assumed one-way capacity in Figure 32b shows that the responses fail to achieve the conventional strength, w_l, where the primary ultimate resistance design capacity is greater than 2.2 that of the transverse nominal moment capacity. The unexpected mechanism significantly compromises the deformation capacity of the panel as shown in Figure 32a.

The component specific milestones for all cases show discrepancies when compared with the current antiterrorism response limits. All panels examined in this subsection reach their ultimate flexural capacity at a displacement slightly larger than the than prescriptive B2 limit. This implies that current prescriptive response criteria for the assumed one-way flexural response, may lack the ability to capture unexpected response mechanisms captured in the results of this study. This emphasizes the significance of using component-specific response criteria in these cases, since the limit states are calculated as a function of the component's resistance function.

89
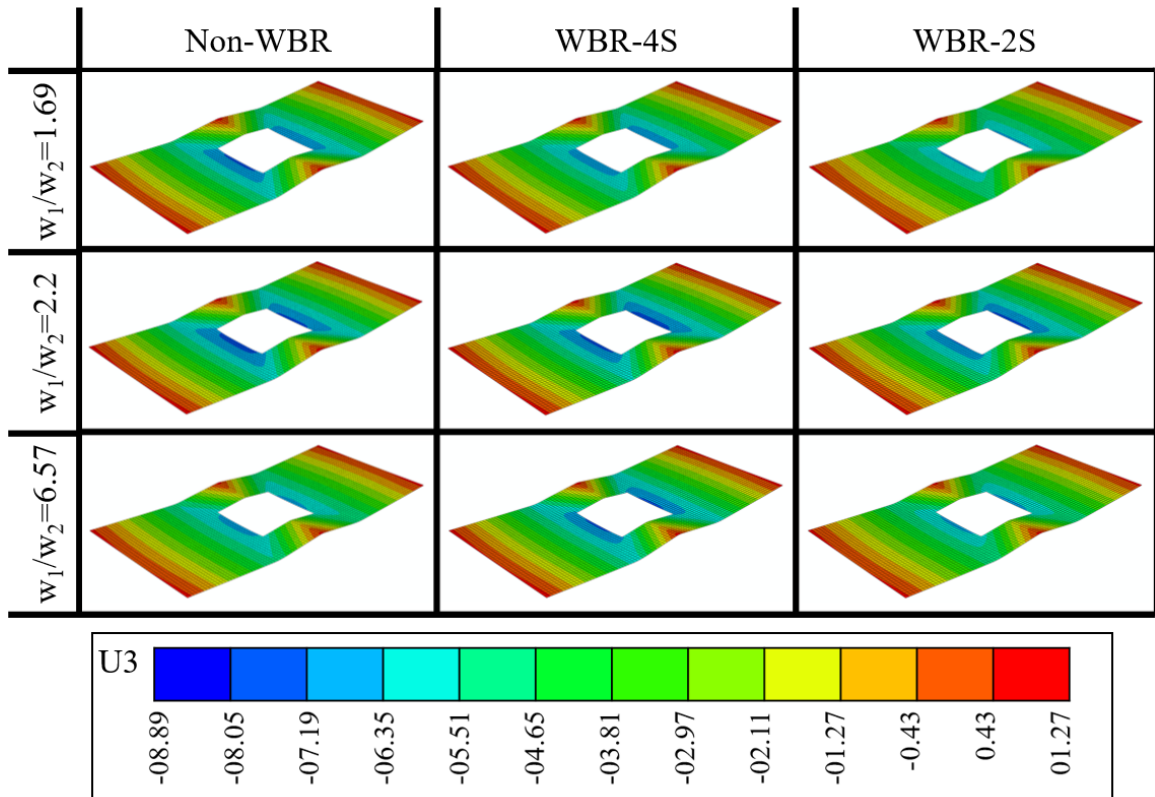
Figure 53. The FE deflected shapes at peak deformation for panels with a single opening (units in cm)
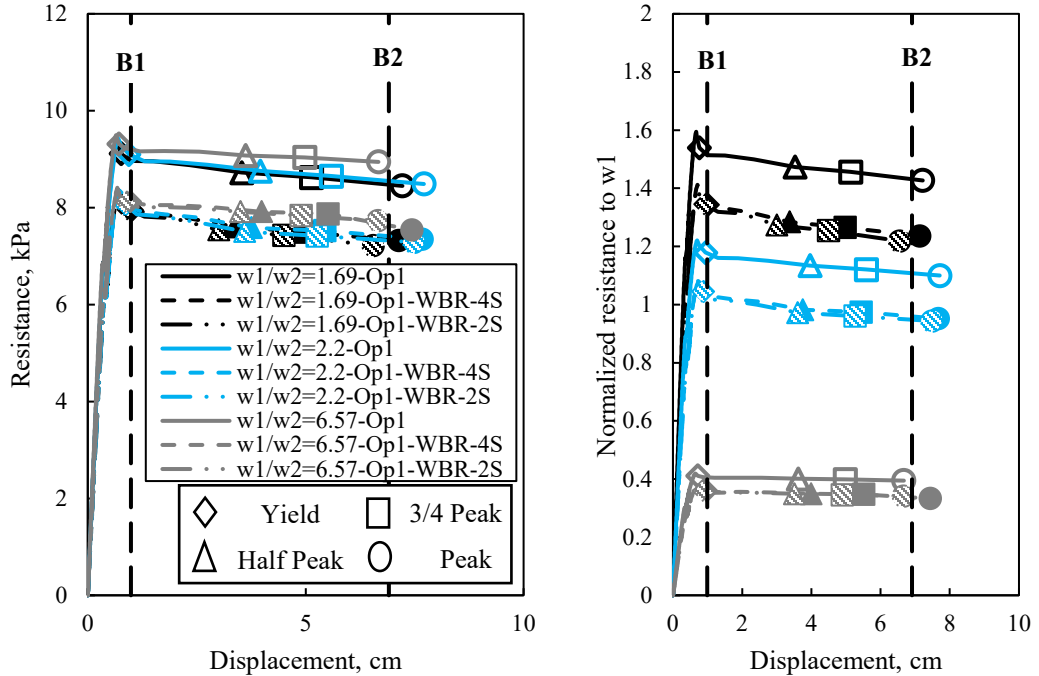
(a)   (b)

Figure 54. Out-of-plane flexural resistance of the panel with a single opening: (a) load-displacement resistance functions and (b) normalized to w_1
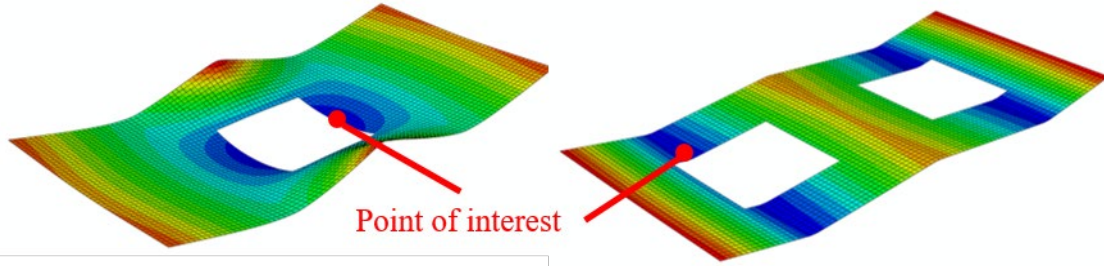
Figure 55. The FE deflected shape as an example for the location of the displacement interest point

w1/w2=2.2-Op1-WBR-4S(Yield)   w1/w2=2.2-WBR-4S(Half peak)

U3

-03.76 -03.40 -03.07 -02.72 -02.36 -02.01 -01.66 -01.31 -00.96 -00.61 -00.26 00.09 00.43
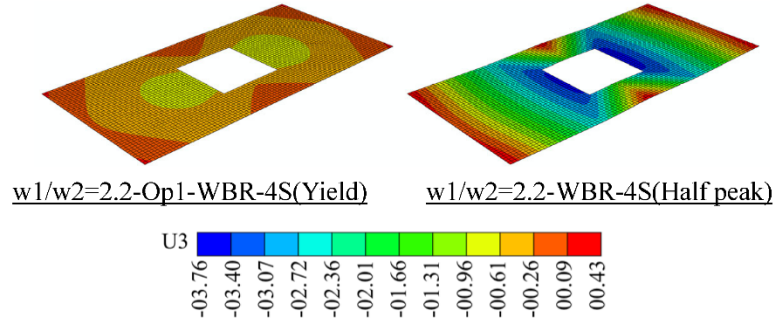
Figure 56. The FE deflected shapes at peak deformation for panels with Op1 and WBR-4S at yield and half peak milestones

4.5.2.2.   Connection reactions

Connections for precast wall panels are designed to resist the equivalent static reaction force, calculated from the ultimate one-way resistance of the component. Current design practices assume the connection will develop the governing flexural capacity of the panels without withstanding any damage itself. To assess the validity of this assumption for the panels examined in this study, the maximum reactions of the FE model for panels with a single opening and discrete connections are compared with the minimum UFC reaction (i.e., from either axis). For the FE model, the reactions are extracted directly from the boundary condition of interest, whereas the relative contribution of each connection in the UFC approach is calculated based on the flexural capacity and the tributary area for each connection.

Since the the cases examined above reach to similar performance, the FE connection reactions of cladding panel for single opening with WBR-4S are shown in Figure 35. Because of symmetry, Figure 35 reveals the results of only two out of six connections, located at edge and

middle of panels. Figure 35a shows reaction forces for WBR-4S, plotted against the displacement. As expected, middle connections result in higher reactions than edge connections. The linear correlation analysis of the middle connection for the UFC and FE reactions are shown in Figure 35b. Cases falling below and to the right of the linear line demonstrate that the UFC approach predicts higher reaction force than the FE model and thus the connection integrity assumption is satisfied. The opposite is true when cases fall above and to the left of the linear line which demonstrates that the expected panel response facilitates higher connection demands relative to the current UFC approach. The majority of panels fall into the latter classification as shown in Figure 35b. Calculating the governing UFC reaction based on the minimum capacity of either axis will always facilitate an underestimation of the connection's integrity. Since it was determined that the middle and edge connections reached the same conclusion, edge connection correlation results are not plotted.

(a)   (b)
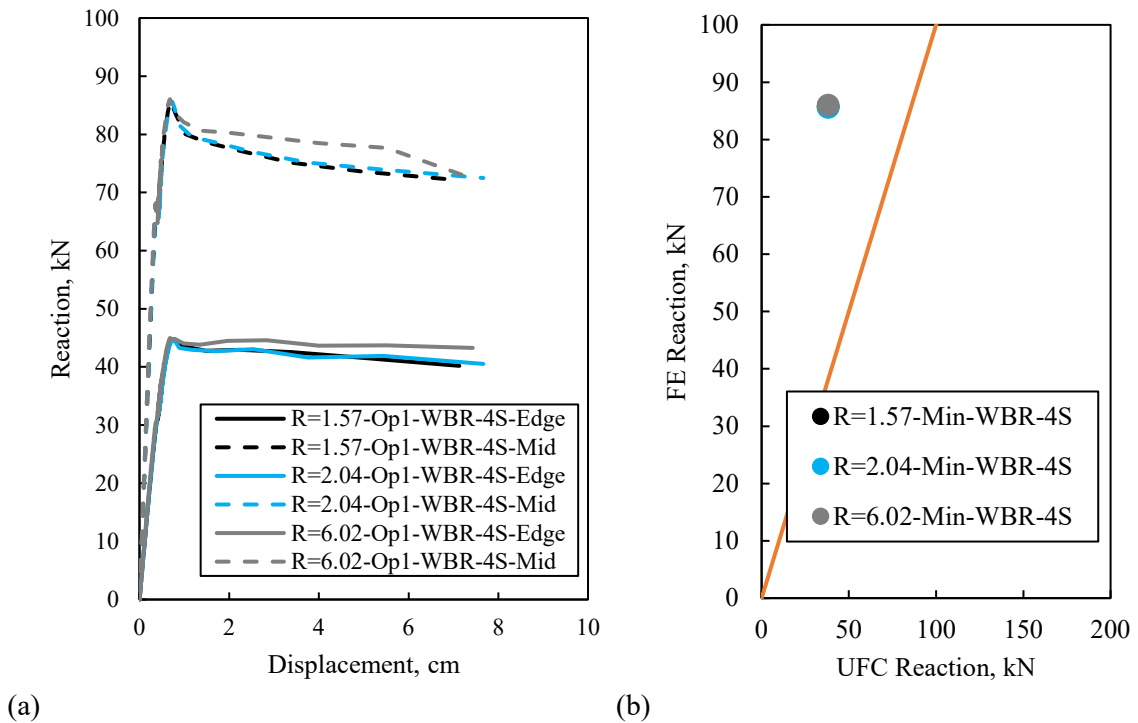
Figure 57. (a) reactions and (b) linear correlation for panels with a single opening and WBR-4S

92

4.5.2.3. Strain energy

Estimations of component performance and the extent of damage are often calculated using work-energy considerations during preliminary stages of blast design. Strain energy, defined as the area under the resistance function up to the desired response limit, is used to calculate minimum impulse and pressure for a given component. The simplification of the one-way approach and its corresponding response limits may result in unrealistic approximations of component performance for the panels examined in this study. Comparisons of strain energies for both the FE model results and current design assumptions for panels with WBR-4S and a single opening are calculated and plotted against each other using a linear correlation analysis as shown in Figure 58a and b. The cases fall below and to the right of the linear line illustrate higher UFC strain energy than the FE model and thus overestimate the actual behavior. The majority of cases fall within this classification, which indicates that the current approach often overestimates the expected strain energy when compares with the FE model response mechanism. The overestimated prediction is a result of the conventional design assumption failing to capture the unexpected premature failure mechanism in the weak flexural direction.
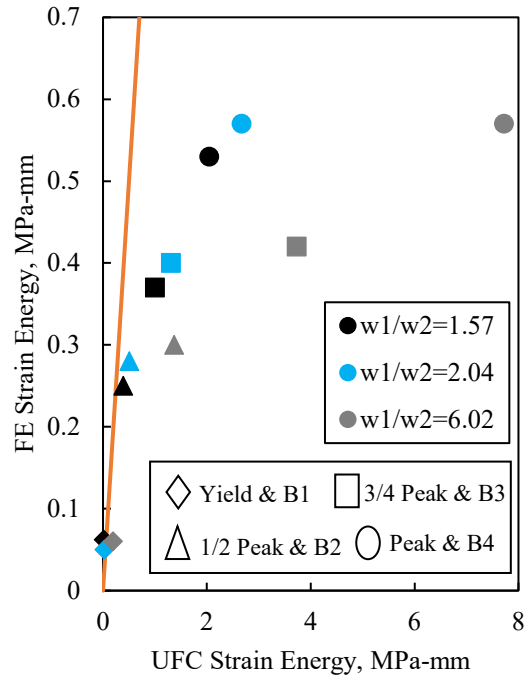
Figure 58. Strain energy linear correlation for panels with single opening WBR-4S

4.5.3. Panels with two openings

4.5.3.1. Resistance functions and deflected shapes

A similar study is performed for wall panels with two openings. The study is performed considering the range of primary to transverse ultimate resistance ratios, shown in Table 9. Figure 59 shows the deformed shapes at peak deformation. Similar to the single opening cases, all panels result in unexpected failure modes. The unexpected failure is caused by the weaker strength of the transverse axis due to the use of the minimum reinforcement. Figure 39a shows the FE resistance function plotted against the displacement of the interested point, as explained earlier, for the wall panels with two windows. Due to the failure of the weak axis, lower ductility of component specific limits is observed, compared with the current practice response limits. Figure 39b shows the normalized resistance function to the UFC ultimate resistance of the primary direction (w_1). The normalized resistance functions to w_1 show that the FE strength overestimates the UFC prediction for lower primary to transverse ultimate resistance ratios. The UFC over predict the strength of the FE model when primary to transverse ratio is increased, e.g. the w_1/w_2=4.57 case. While the non-

94

WBR cases result in higher resistance than the cases of WBR, no major difference in terms of the ductility and the deflected shape at peak. The WBR-4S cases possess slightly higher resistance than the WBR-2S cases. The comparison between component specific and current practice response limits shows discrepancy and unconservative results in general. However, yield component specific milestone and ductility of one response limit show close results.
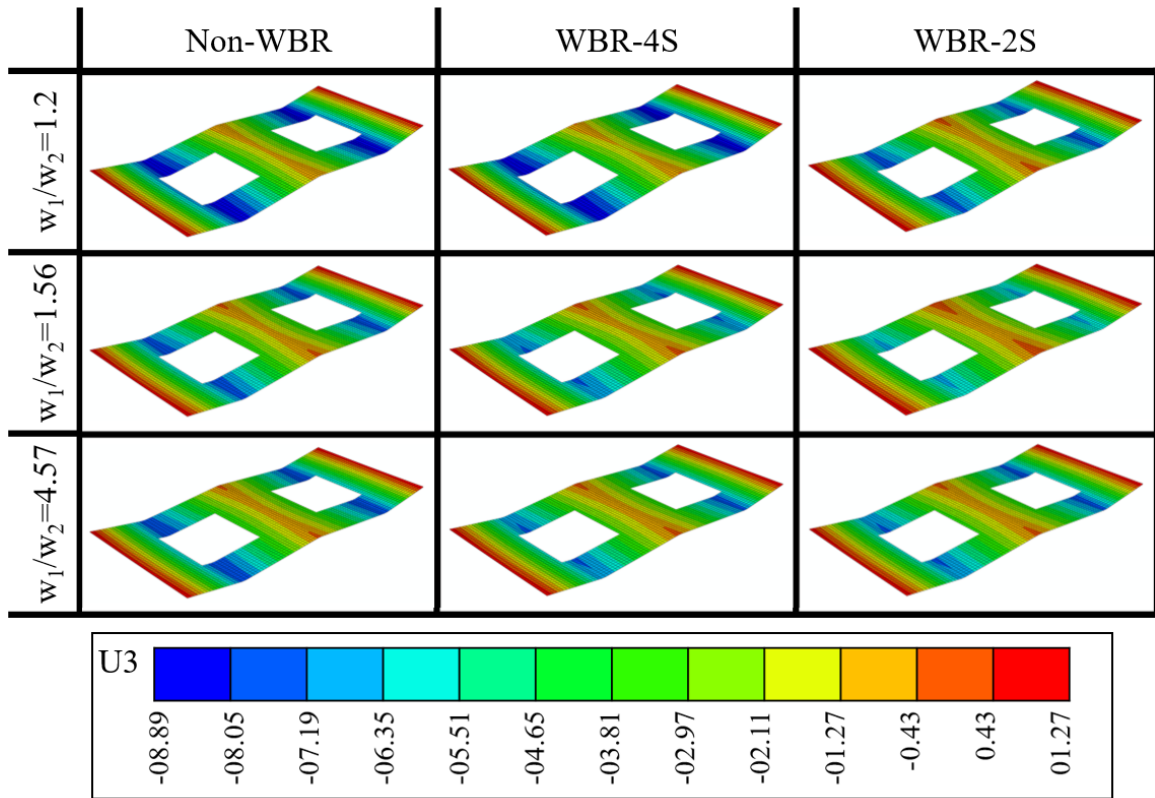
Figure 59. The FE deflected shapes for panels with two openings (units in cm)
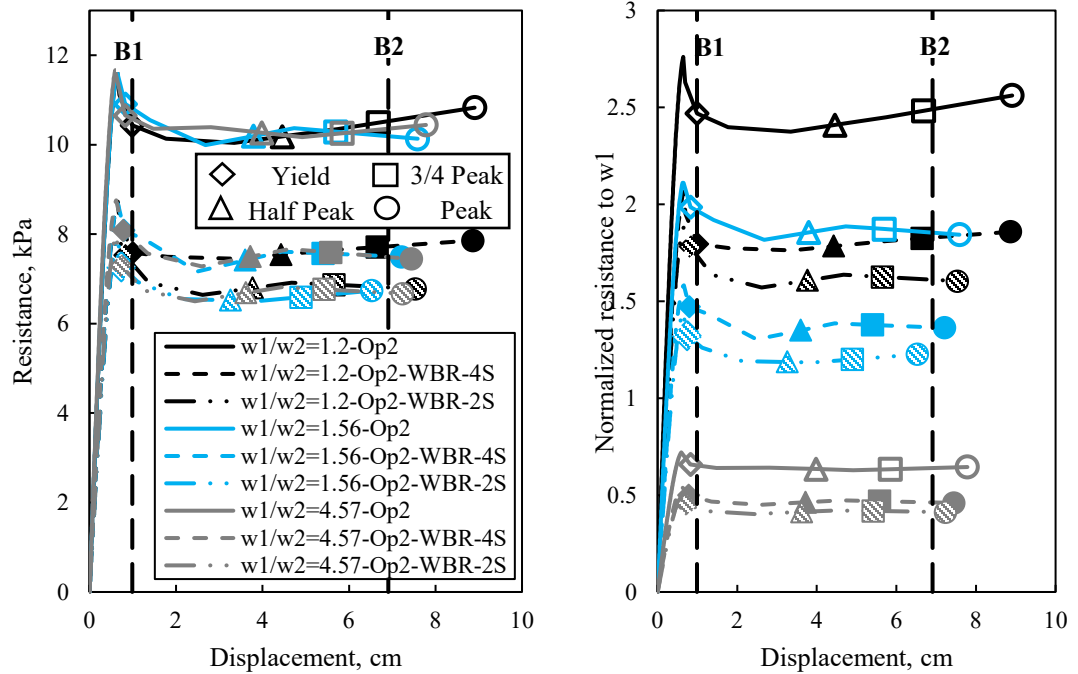
Figure 60. Resistance of panels with two openings (a) resistance functions and (b) normalized to w_1

4.5.3.2. *Connection reactions*

The assessment for the assumption of connection integrity is examined for wall panels with discrete connections and two openings. Since all panels reach to similar performance, reactions of edge and middle connections for the panels with WBR-4S are only shown in Figure 42a. As expected, the middle connection reaches to higher reaction than the edge connections. Linear correlation analysis of the UFC, calculated based on $\min(w_1, w_2)$, and the FE reactions for the middle connection are shown in Figure 42b. Majority of cases fall above and to the left of the linear line which indicates that the current UFC approach underestimates the actual connection demands. It was found that the middle and edge connections reach to the same conclusion for the linear correlation study and thus edge connections correlation results are not shown.

(a) (b)
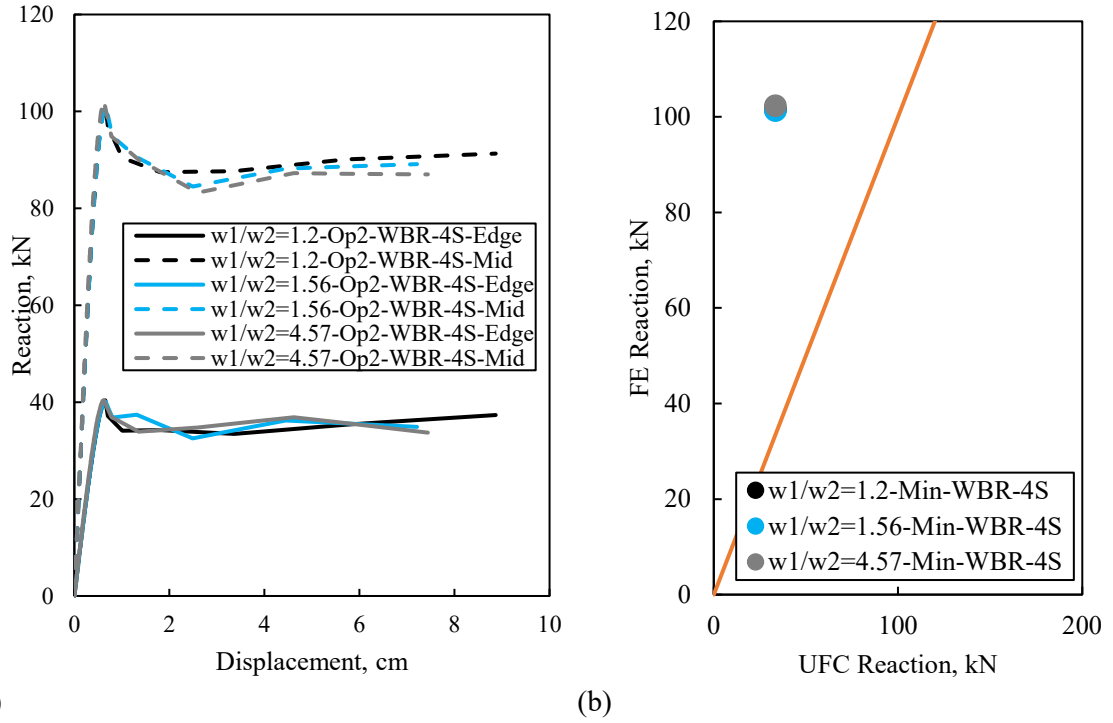
Figure 61. Reactions and normalized reaction for panels with two WBR-4S openings

4.5.3.3.   *Strain energy*

Strain energies for both the FE models and UFC current practice panels with two WBR-4S

openings are computed. Comparisons of the results are illustrated using the linear correlation plots

shown in Figure 62. The analysis shows that majority of cases, especially cases with high damage

levels, fall below and to the right of the linear line which indicates that the current approach

overestimates the actual strain energy. The energy overestimation occurs because of the weak axis

failure as shown in Figure 59 which results in ductility reduction as explained earlier. Therefore,

following the energy approach based on current practice may lead to unconservative prediction.
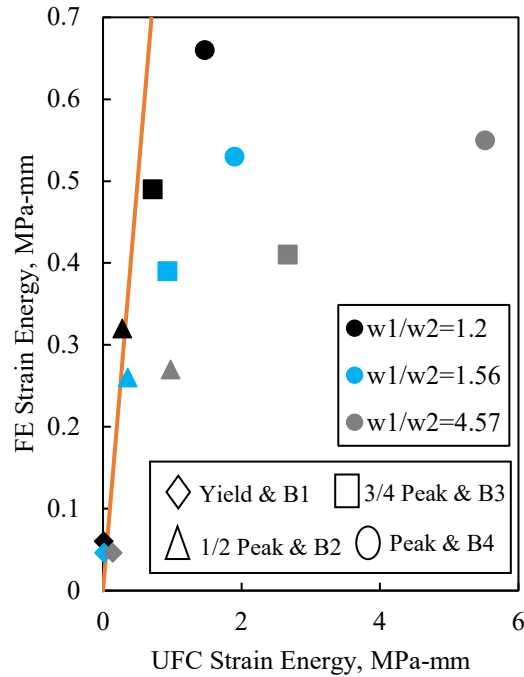
Figure 62. Strain energy linear correlation for panels with two WBR-4S openings

4.6. Dominant span sensitivity study

As observed from the parametric, all cases form transverse mechanism due to the use of minimum reinforcement which leads to a weaker strength compared with the primary directions, i.e. ratio of w_1 to w_2 bigger than 1. Thus, a dominant span sensitivity study is performed to illustrate when the ratio of w_1 to w_2 achieves the intended mechanism. This is done by strengthen the transverse direction for the panel with two WBR-2S openings and w_1 to w_2 equals 1.56 by replacing the minimum reinforcement with higher amount of reinforcement. The new arrangements of reinforcement that replace the minimum steel in the transverse direction are as follow: #13 @ 39.37 cm o.c. for w1/w2=0.87, #13 @ 25.65 cm o.c. for w1/w2=0.5 and #13 @ 12.07 cm o.c. for w1/w2=0.25. The deflected shape at peak deformation for the strengthen panels are shown in Figure 63 and revels that the intended mechanism is achieved at ratio of w_1 to w_2 equals 0.25. Prior to reaching the intended mechanism, bi-directional deformed shape, i.e. w1/w2=0.87 and w1/w2=0.5, is observed as shown in Figure 63. The resistance function for the strengthen panel is shown in Figure 64 and compared with the panel with minimum reinforcement, i.e. w_1 to w_2 equals 1.56.

98

Also, shown is the component specific and compared with current response limits. The strengthen panels show improvement in strength and ductility compared with the panel with minimum reinforcement. When the intended mechanism is reached, however, a decrease in the strength, after half peak milestone, is observed which leads to a reduction in the ductility as a result of altering from bi-directional to one-way response, i.e. the intended mechanism, shown in Figure 65.
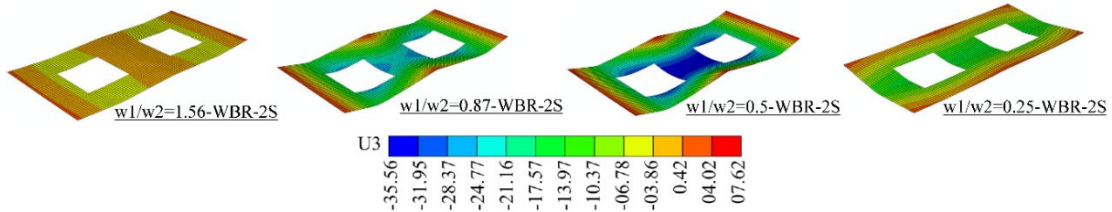
Figure 63. The FE deflected shape at peak deformation for strengthen panel (units in cm)
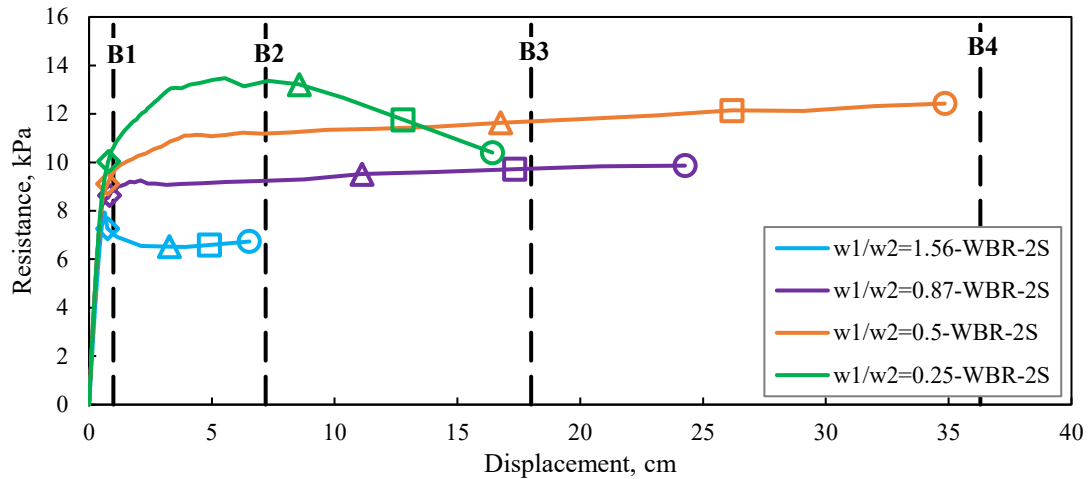
Figure 64. Resistance function for the strengthen panels

w1/w2=0.25-Op2-WBR-2S(Yield)   w1/w2=0.25-WBR-2S(Half peak)
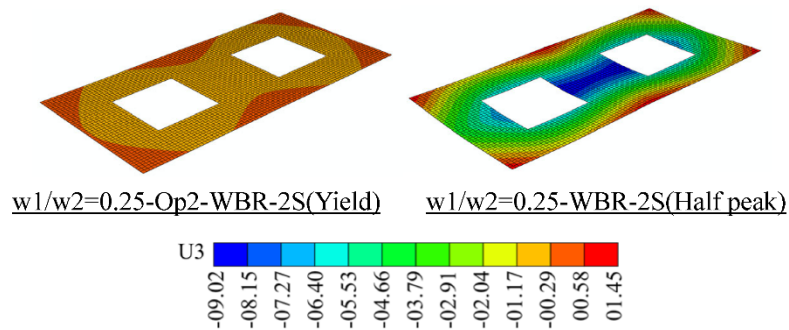
Figure 65. The FE model deflected shapes at yield and half peak for panels with two WBR-2S openings (units in cm)

5. FLEXURAL RESISTANCE OF NON-LOADBEARING PRECAST INSULATED CONCRETE FAÇADE PANELS WITH DISCRETE CONNECTIONS SUBJECT TO BLAST LOADING

5.1. Introduction

Significant improvement in constructions has been done recently to accommodate energy efficiency through the use of components that possess less thermal conductivity. Despite the high strength and rapid production that can be provided using concrete panels, they have a high thermal conductivity which results in inefficient energy saving elements. To overcome this issue, foam insulation is sandwiched between two layers of concrete, i.e. denotes as insulated wall panels, to achieve energy saving benefits. The effect of insulation in the flexural performance for insulated wall panels was first investigated by Pfiefer and Hanson [45]. Shear ties, connect the two layers of concrete, are used to insure the composite flexural behavior for insulated panels components. Thermally resistive shear ties, such as carbon fiber-reinforced polymers (CFRP) or glass fiber-reinforced polymers (GFRP) are developed to maintain the energy saving and to provide the required flexural resistance [46] [47].

Insulated precast concrete wall panels are connected to the main structural system using discrete connections. Current practice for blast-resistant precast components assumes the discrete connection to behave as a line support along the panel edge at the floor diaphragms [15]. Consequently, the primary (vertical) direction is designed to resist the blast load and shear ties are assigned to provide the one-way flexural composite behavior. The transverse (horizontal) direction is designed for temperature and shrinkage requirements and non-composite behavior [15]. These assumptions may complicate the response of insulted panels and unexpected failure mechanisms may be developed. The implication of these assumptions on the insulated non-load bearing precast concrete wall panels are not examined. Previous research investigated the effect of the discrete

connections in the blast-resistant solid non-load bearing concrete panels without and with opening(s), shown previously. The study for solid panels without openings examined the implication of using discrete connection on non-load bearing solid precast concrete panels. The results for the study showed significant discrepancies when evaluating resistance functions generated using a performance-based methodology versus conventional design assumptions. A major focus of that study was to investigate when primary to transverse ultimate resistance ratios facilitate unexpected failure mechanisms and significant loss of ductility. The concept of this study also extended to examine non-load bearing solid precast panels with opening(s), as shown previously. The study revealed that conventionally design panels fails in the transverse direction (unexpected failure mechanism) due to the existing of window(s) and the minimum reinforcement in the transverse direction which leads to significant reduction in ductility.

The goal for this paper is to extend the concept of the previous studies, i.e. solid panels with and without openings, by investigating the effect of the current design assumptions on insulated non-loadbearing precast concrete panels with discrete connections when chosen as a blast resistance component for far-field threats, i.e. uniform pressure assumption. The ratio of primary to transverse ultimate resistance is varied via a comprehensive parametric study which resembles the current one-way assumption. The study utilizes a validated finite element (FE) model to examine the sensitivity of this variation on the load-deflection response of insulated panels with realistic connection layouts and compare it with the current approach flexural response. The outcomes of this study provide guidance regarding the appropriate selection of modeling parameters and limit states when conducting blast resistant design of insulated precast façade panels with discrete connections.

5.2. Background

Insulated precast wall panels have been widely used to enhance the thermal performance of the building envelope. The insulation is placed between the exterior and interior concretes

wythes. To maintain the integrity between the two wythes, a mechanism such as shear tie connectors are used. The shear tie connectors are used to resist the shear transfer forces between the two wythes that may generate during fabrication, shipping, erection and service life. Shear ties are available in varying configurations and may come as connected ties, such as C-grid ties, or discrete ties, such as X-series ties. The shear transfer is calculated using the strength concept as given in the PCI design handbook [15]. The shear transfer considers the lesser of either the maximum compressive strength of concrete, i.e. top wythe assumes in compression, or the maximum tensile strength of reinforcement, i.e. assumes tension wythe reinforcement. The number of shear ties, N, to resist the transfer shear between concrete wythes can be computed using Equation 21; where A_s is area of steel in tension wythe, f_y is yield stress for steel, f'_c is concrete compressive strength, b_w js the width of the wall panel, t_c is the thickness of compression wythe and V_{ti} is the strength of the tie in shear. For a simply supported member with a uniform load, the shear ties must be placed on one half of the clear span length. Following this approach, the computed number of shear ties is assumed to provide a fully composite behavior between the concrete wythes.

$$N \geq \frac{\min(A_s\,f_y,\,0.85\,f'_c\,b_w\,t_c)}{V_{tie}}$$
<div align="right">Equation 21</div>

A typical non-load bearing insulated wall panel with discrete connections and shear ties is shown in Figure 66a. The panels is a one story vertical span between floor diaphragms. The panel consist of typical six discrete connections used to resist the out of plane loads, such as wind or blast, while the top row connections are typically designed to carry the panel gravity load. For blast resistant design, the current practice assumes the discrete connections to behave as a line support and thus one-way flexural response in the vertical direction (the primary direction), shown in Figure 66b [15]. Also, the shear ties is assumed to resist the in-plane shear resulted from assumed one-way flexural demands and therefore provide a composite action behavior in the vertical direction [15]. To assess the blast performance of the component using these assumption, it is standard

practice to utilize an equivalent single degree of freedom (SDOF) system [39], as shown in Figure

66c, by transforming spatial variations of loads and distributed mass via a load-mass factor, K_{LM},

based on the normalized deflected shape. The SDOF equation of motion can be solved considering

the mass, M, resistance function, $R(y(t))$ and the applied pressure-time history, $F(t)$. The resistance

function can be determined based on material properties, cross-section geometry, span length, and

boundary conditions. Via iterative analysis, the panel is then reinforced to achieve a specified level

of allowable damage when subjected to the design-basis blast load.

The extent of blast-induced damage evaluated by comparing the maximum displacement

response of the component to a set of prescribed response criteria. These criteria vary depending

upon component type and the intended use of the component. This paper will focus on response

criteria for anti-terrorism and force protection [10], which are commonly used in blast design

practices. Five levels of damage range from superficial (i.e., no permanent visible damage) to

blowout (i.e., component is completely overwhelmed). Component-specific response limits are

developed which correlate damage levels to critical milestones along the resistance function of the

component [27]. The recommended response milestones based on Gombeda et al. [27] correspond

to yield, half peak, three-quarter peak and peak flexural strength. Comparisons of response limits

for reinforced concrete flexural members according to the US Army Corps [10] and Gombeda et

al. [27] are shown in Table 6. Both sets of response criteria will be used to assess the flexural

performance of insulated panels with discrete connections later in this paper.
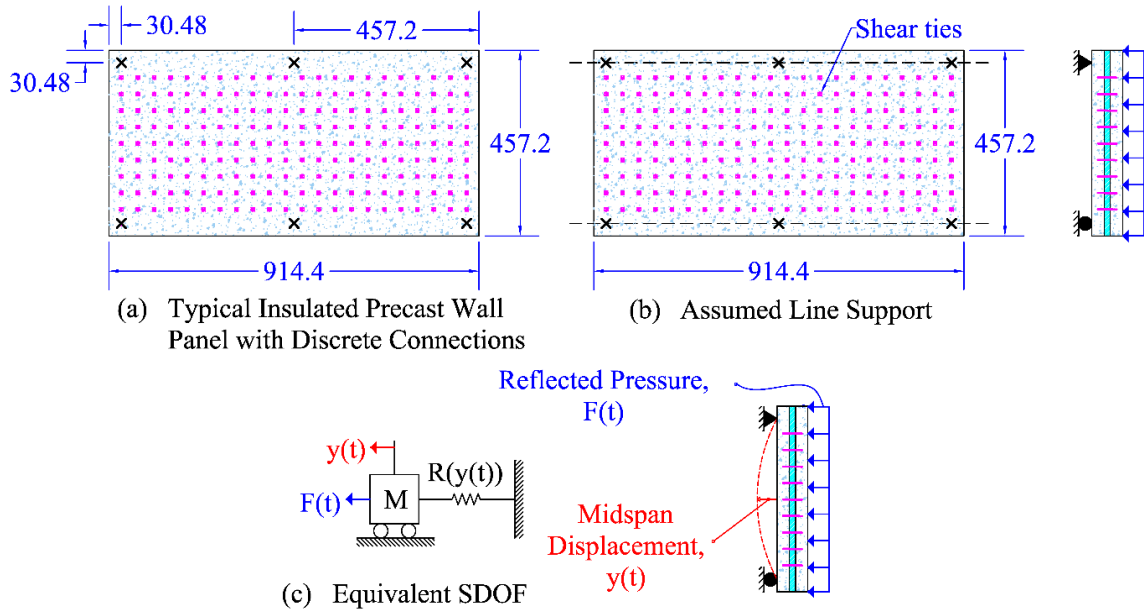
Figure 66. Current practice design process

Most of recent blast performance for the non-load bearing insulated precast concrete façade panels are performed considering the one-way assumption [19] [48] [49] [25]. This is done by either using full edge bearing supports or very large aspect ratio to insure the one-way bending. However, these studies were still focused on the one-way response of the panels. The performance of realistic boundary conditions and the effect of considering the shear ties in the primary directions only are not yet investigated. Solid panels with realistic boundary conditions examined variety of number of discrete connections and nominal moments of solid wall panels. The study compared resistance functions generated via a validated FE mode for solid precast concrete panels using discrete connections with simplified resistance function based on the current practice approach assuming elastic-perfectly plastic [15]. The results for this study showed that the current approach capacity significantly overestimates the FE model for higher primary to transverse ultimate resistance ratios. The study also revealed occurrence of weaker mechanisms in the transverse direction due to the use of minimum reinforcement which results in momentous loss in ductility. The concept of this study also extended to examine non-load bearing solid precast panels with opening(s), as seen previously. The results showed capacity overestimation for the current approach

104

compared with the FE model capacity for higher primary to transverse ultimate resistance ratios. Unexpected failure mechanism was also observed for the examined panels due to the existing of window(s) and minimum reinforcement in the transverse direction which leads to significant reduction in ductility.

The concept of the two previous studies for solid panels with and without openings will be extended for insulated precast concrete façade panels with discrete connections considering the current practice assumptions. The current practice, as mentioned previously, assumed the one-way primary direction assumption and thus shear ties to resist the flexural demands resulted from out-of-plane loadings. The assigned shear ties based on the current practice are assumed to provide a fully composite behavior between concrete wythes. The horizontal direction is designed for shrinkage and temperature requirements and assumed no shear ties required and thus non-composite action. These assumptions may complicate the insulated panel response and may results in non-one-way behavior.

5.3.   Validation of Finite Element (FE) Modeling

The performance of precast concrete insulated wall panels with discrete connections are developed using nonlinear finite element modeling. To ensure the accuracy for the predicted performance, the FE model, similar to the scheme used in this study, is validated previously in for solid panels with and without openings studies for assessing realistic discrete connection in non-loadbearing solid wall panels without and with opening(s). An extra validation through comparison with experimental tests is provided in this study to examine shear connectors used in the non-load bearing insulated concrete panels.

5.3.1.   FE Model Development

The finite element modeling approach used in this paper was derived from the framework previously used by the author for solid (i.e., no openings) wall panels with discrete connections and for wall panels with opening(s) and discrete connections. Several modifications were added to this

existing framework to facilitate modeling of insulated panels with discrete connections. The resistance function of insulated panels was quantified using ABAQUS version 2017/Explicit [29] quasi-static analysis to determine the entire load-displacement relationship. The concrete regions are modeled with three-dimensional homogenous shell element (ABAQUS element S4). Concrete constitutive properties are modeled using a concrete damage plasticity model (CDP) with dilation angle of 36° and eccentricity of 0.1 [29]. The ratio of biaxial, σ_{b0}, to uniaxial compressive strength, σ_{c0}, is taken as 1.16 [29]. A yield function is used to account for the different tension and compression response. The ratio of the tensile to compression meridian that defines the yield function in the deviatory plane, K_c, was assumed as 2/3 [29]. The uniaxial stress-strain for concrete in tension is defined as linear elastic up to the modulus of rupture. After rupture, a smooth descending branch is used to account for the progression of micro-cracking and to mitigate numerical instabilities. Softening was modeled using Equation 16 which was developed by Wang and Hsu [50] ; where f_t , ε_t are the tensile stress and strain, f_{cr}, ε_{cr} are the modulus of rupture and the corresponding strain; n represents the rate of weakening taken as 0.6. Modulus of rupture was calculated using Equation 17 , where f'_c is the ultimate concrete compressive strength (in MPa) and λ is the aggregate modification factor taken as 1.0. Popovics concrete numerical model is used to define the uniaxial stress-strain for concrete in compression [51]. Reinforcement is included as a smeared uniaxial layer within the shell element. The constitutive properties for steel reinforcement will be discussed in detail in the next section.

An additional feature is added in this study to the FE model to simulate the behavior of the shear tie used in the insulated panels. The shear tie and foam are modeled using cartesian connector which provides a connection between two nodes. The connection defines the three local connection directions in the first node and measures the change in location in the second node [29]. The second node follows the rotation of the first node [29]. The cartesian connector can accommodate linear and plastic material behaviors. More details will be explained in the next sections.

5.3.2. *Experimental Validations*

As illustrated previously, the FE model was already validated against the behavior of panels with discrete connections in for solid panels and for panels with openings, as shown previously. The validation here aims to insure the accurate modeling representation for the shear ties used in the test program. Thus, the modeling approach is validated against Naito et al. [49] and Trasborg [52] experimental study which describes the behavior of an insulated one-way panel. The panel was subjected to a uniform distributed load and possesses a simply supported boundary conditions. The shear ties used in the panel and their load-deflection functions are shown in Table 14 and Figure 67. Shear tie constitutive properties were adopted from experimental tests, i.e. CC ties, [53] and tie manufacturer specifications per Gombeda et al. [54]. The load-deflection in Figure 67 represents the resistance of the shear ties as well as 40.64 cm by 40.64 cm (16 in by 16 in) area of the foam. The behavior of the shear tie is represented using cartesian connector and acting in the longitudinal direction only. Figure 68 shows the loading diagrams, cross section configurations and locations of the shear ties in Naito et al. [49] and Trasborg [52] test. The steel reinforcement stress-strain for Naito et al. [49] and Trasborg [52] was assumed as bi-linear with elastic-hardening response. Trasborg [52] value of yield stress, f_{sy}, and the tensile stress, f_{su}, and strain, ε_{su} (shown in Table 15) assumed in accordance with ASTM A615 [44]. The steel elastic modulus is assumed to be 200 GPa. The properties for concrete, such as compressive strength, f'_c, modulus of elasticity, E_c, and ultimate strain, ε_{cu}, are summarized in Table 15. The ultimate concrete compressive strain is calculated as function of modulus of elasticity and ultimate compressive strength in accordance with Popovics's approach [51].

Table 14 Utilized shear ties information

Type	Source	Material	Size
Composite (CC)	Thermomass®	GFRP pin	CC 150-50-50-50
X-Series	Thermomass®	GFRP pin	X60-305
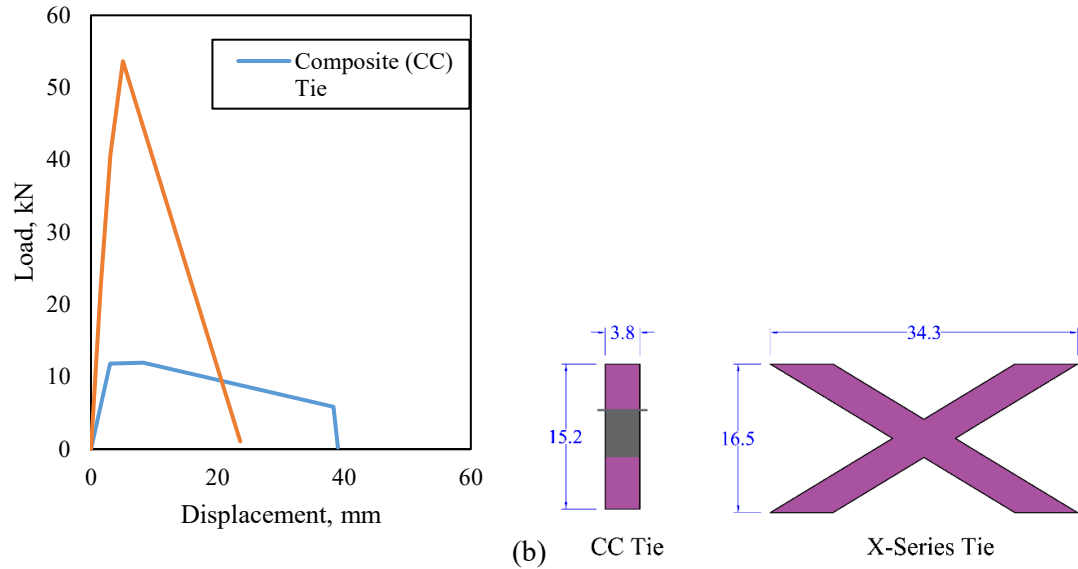
Figure 67. (a) Load-displacement for the used shear ties and (b) shear ties with dimensions

Table 15 Material properties of experiments

Experiment	E_c (GPa)	f'_c (MPa)	ε_{cu} (%)	f_{cr} (MPa)	f_{sy} (MPa)	f_{su} (MPa)	ε_{su} (%)
Naito et al. [49]	30.28*	36.06	0.18*	3.85	480.63	738.54	12.00
Trasborg [52]	30.35*	41.37	0.19*	3.77*	413.69*	620.53*	9.00*

* The data was assumed
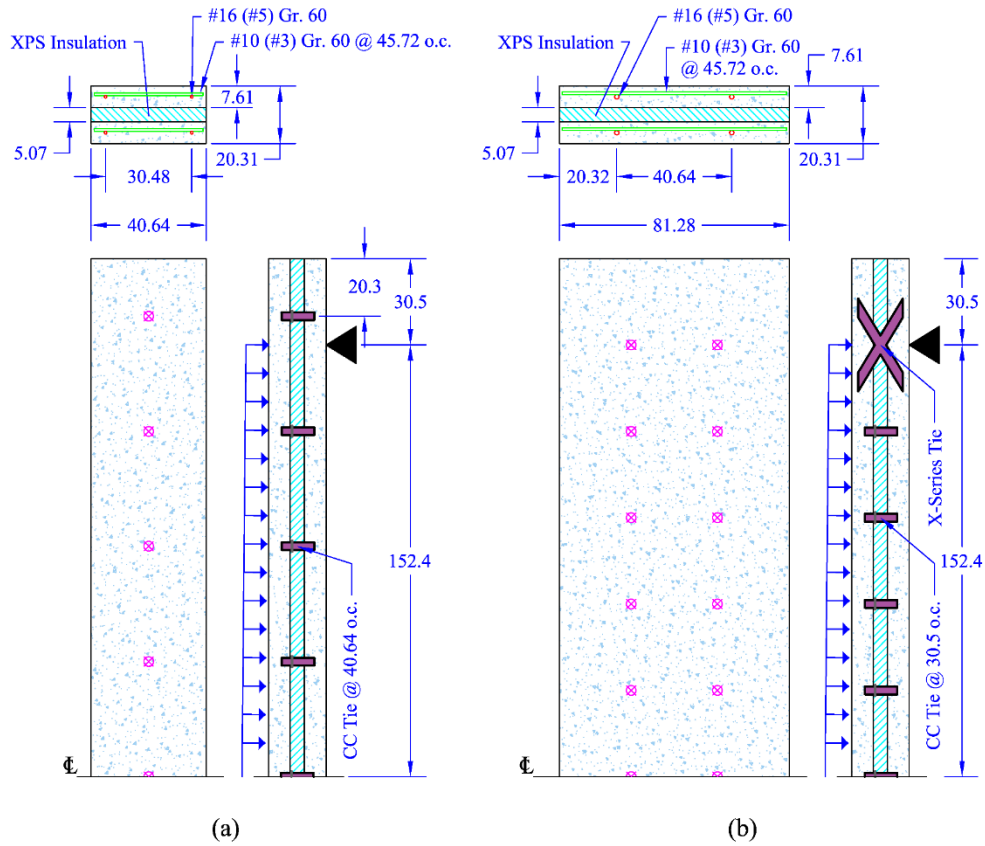
Figure 68. Schematic of experiments (dimensions in cm) tested by (a) Naito et al. [49] and (b) Trasborg [52]

The FE result, in comparison with the experimental result for Naito et al. [49] and Trasborg [52] is shown in Figure 69. The resistance is plotted versus the mid-span displacement. The result also shows the X-series tie and CC tie (near to the support) forces. The FE model predictions shows good agreement with the measured experimental response. Prior to yield milestone, CC ties on both tests, near to supports, reach to its ultimate capacity and proceed with plastic behavior to the peak milestone. X-series tie in Trasborg [52] shows some unloading behavior near to peak milestone. This is may be related to using pure roller support in the FE model and the initial formation for the plastic hinge at the middle which enforces top wythe to reverse its slipping toward the mid-span.

In addition to the previous validations for panels with discrete connections for solid panels and panels with openings, the FE modeling approach provides an adequate level of accuracy for the representation of cartesian connector to shear ties. Therefore, the FE modeling approach is used

to examine the insulated precast panels with discrete connections for a variation of primary to transverse ultimate resistance ratios as shown next in the parametric study section.

(a)   (b)
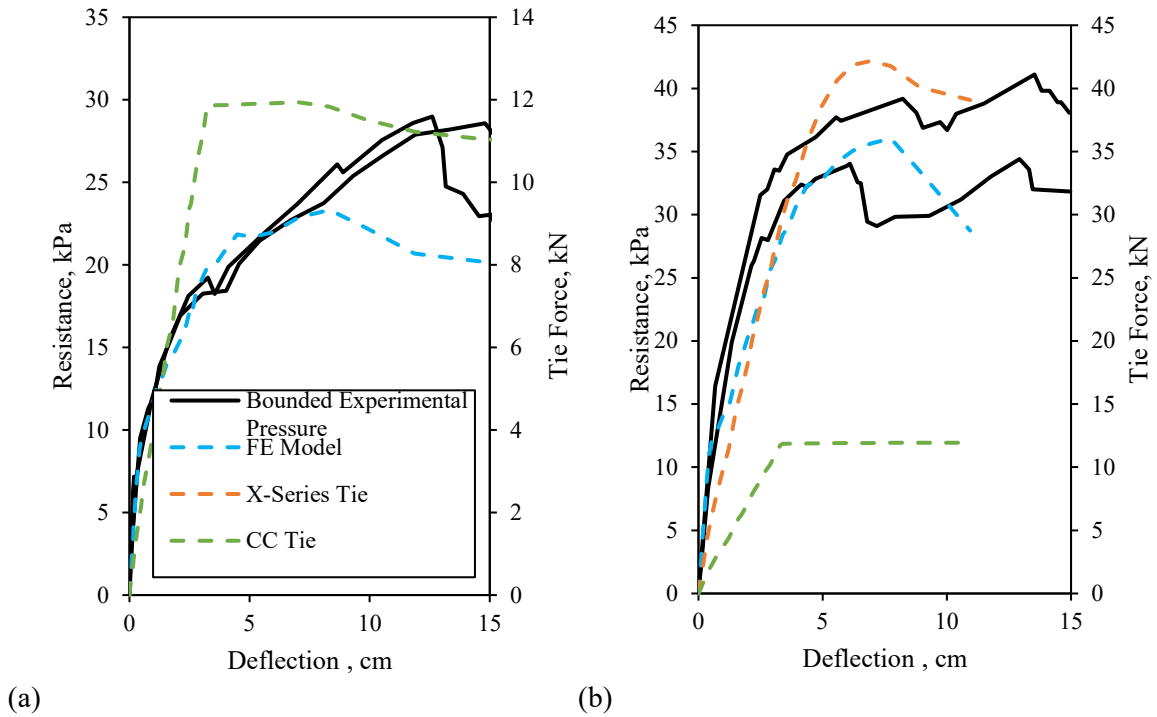
Figure 69. Finite element resistance function and experimental test data for (a) Naito et al. [49] and (b) Trasborg [52]

5.4.   Parametric Study

A parametric study is conducted to examine variations of the ratio of primary to transverse ultimate strength on the resistance functions and limit states of blast-resistant insulated cladding wall panels with discrete connections. The parametric study is based on a prototype panel measuring 9.14 m (30 ft) long, 4.57 m (15 ft) tall and a thickness of 20.32 cm (8 in) with six discrete connections as illustrated in Figure 70. The boundary conditions in the study consist of rollers along the x-axis and pin supports along the y-axis as indicated in Figure 70. This configuration represents a practical case where the tieback connections, used to resist lateral loads, are set to allow thermal expansion in the transverse direction (x-axis) and resist movement in the primary (y-axis). The vertical bar size in Figure 70 is not labeled because reinforcement ratio, and thus ultimate resistance calculations, is varied as part of the parametric study. The transverse reinforcement is not varied

110

and consists of #10 (#3) bars spaced at 45.7 cm (18.0 in.) on center for top and bottom wythes. It should be noted that the vertical bars (running along the y-axis) are typically detailed as the primary flexural reinforcement in accordance with current design practice [15]. Horizontal (along x-axis) reinforcement is included only to resist shrinkage and temperature demands in accordance with ACI 318 [31].

The tested shear ties typically, such as in Naito et al. [53], represent the in-plane shear resistance in one-way direction. The load-deflection, shown in Figure 67, characterizes the in-plane shear resistance for the tie and foam together. As illustrated previously, the tie is considered to resist the flexural demands of insulated panels with discrete connections in the assumed one-way directing only, per the current design practice [15]. Due to its interaction with concrete, the foam can participate in flexural resistance in both directions. Additionally, cartesian connectors in ABAQUS software can identify one type of material behavior. For these reasons, the foam is modeled separately from the tie in the parametric study. Figure 70 shows locations and geometries of the foam and tie connectors, as used in the FE model. Expanded polystyrene (EPS) Type I foam is selected in this study with shear modulus of 1.931 MPa (280 psi) and shear strength of 124.1 kPa (18 psi). Using basic mechanics, the load-deflection for the foam for an area of 40.64 cm by 40.64 cm (16 in by 16 in), equivalent to the area in the test program per Naito et al. [53], is computed as shown in Figure 71. The tie load-deflection then can be calculated back from the tie plus foam load-deflection, i.e. X-series tie is selected (Figure 71). The load-deflection for the tie without foam is idealized, for numerical simplicity, and selected in this study.
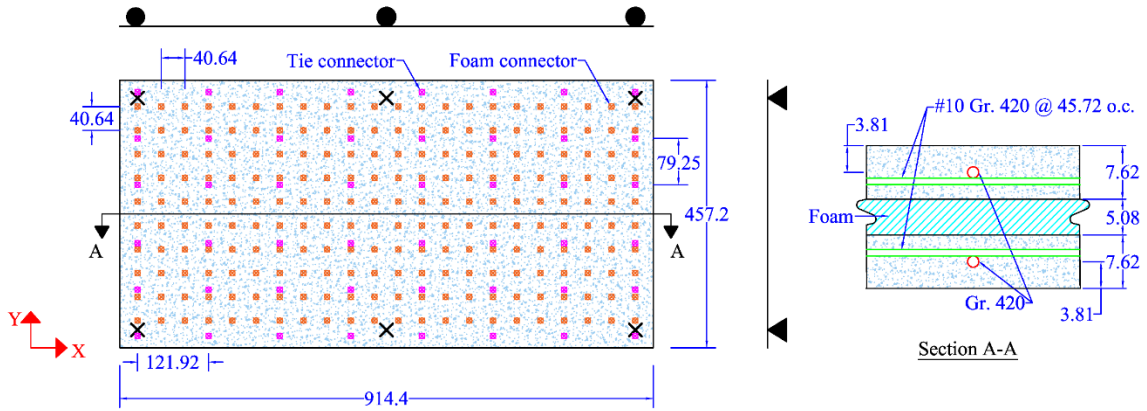
Figure 70. Configurations of insulated precast panel and its boundary conditions (dimensions in cm)
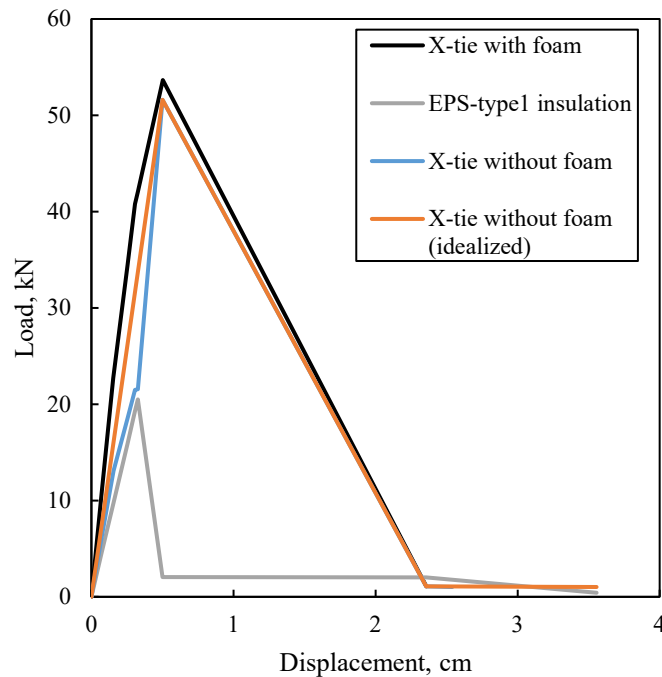
Figure 71. Load-displacement of EPS foam and X-series tie

Like the validated FE model, the parametric study is modeled in ABAQUS [29] using shell

elements (S4) with a uniform mesh size of 10.16 cm (4 in). The parametric study also uses the

concrete material model discussed previously in section 3. A summary of all material properties

used in the study is shown in Table 8. To facilitate more accurate comparison of the model with

realstic panel response, an expected rebar stress-strain curve is obtained from Gombeda et al. [34].

For the purpose of this paper, the curve is scaled to match the minimum yield, tensile strengths and

ultimate tensile strain values prescribed by ASTM A615 [44]. Plots of constitutive properties for

concrete and steel reinforcement are shown in Figure 23a and b, respectively. The elastic-perfectly-plastic stress-strain behavior used in the conventional design approach is also shown for comparison in Figure 23.

It is expected that the foam will be active in both directions during in-plane shear resistance. When the foam fails in one directions, the cartesian connector in the FE model should provide no in-plane shear resistance in the orthogonal direction. To insure the coupling behavior in both directions that is assigned for foam connectors, a simplified preliminary model is developed via ABAQUS software [29] which represents a 40.64 cm by 40.64 cm (16 in by 16 in) two wythes connected with a cartesian connector, i.e. denotes foam connector (Figure 72a), The wythes are modeled to be very stiff to insure a pure behavior for the cartesian connector. The behavior of cartesian connector is defined using a coupled in-plane non-linear load-displacement as shown in Figure 71, i.e. EPS-Type1 insulation. The geometries are selected which reflect similar dimensions as examined for shear ties specimens per Naito et al. [53]. The movement for the bottom wythe is restrained in the three directions, i.e. X, Y and Z direction. The movement for the top wythe is restrained in the Z direction only. A load in the X direction is applied initially with a value larger than the ultimate foam capacity to insure failure of the foam connector. After that, another load (i.e. concurrent with the load in X direction) is applied in the Y direction, which is less than the ultimate foam capacity. The reaction for the model which represents the shear transfer between the two wythe generated by the cartesian connector is shown in Figure 72a and b. The results show that the reaction in X direction (FE Reaction_X Axis) follows the load-displacement per the calculated foam, i.e. EPS-Type1 insulation, which also illustrates failure of the foam connector. No reaction in Y direction (FE Reaction_Y Axis) is noticed, i.e. reaction is almost zero, along the loading history. This is also illustrated in Figure 72b where the load is plotted against loading steps. The loading in Y direction is applied at the load step 500, i.e. after the failure of the foam connector in X direction, and the reaction in Y direction shows negligible resistance throughout the remaining

loading steps. This behavior insures the coupling response in the cartesian connector which is expected from the foam interaction with concrete in both direction.
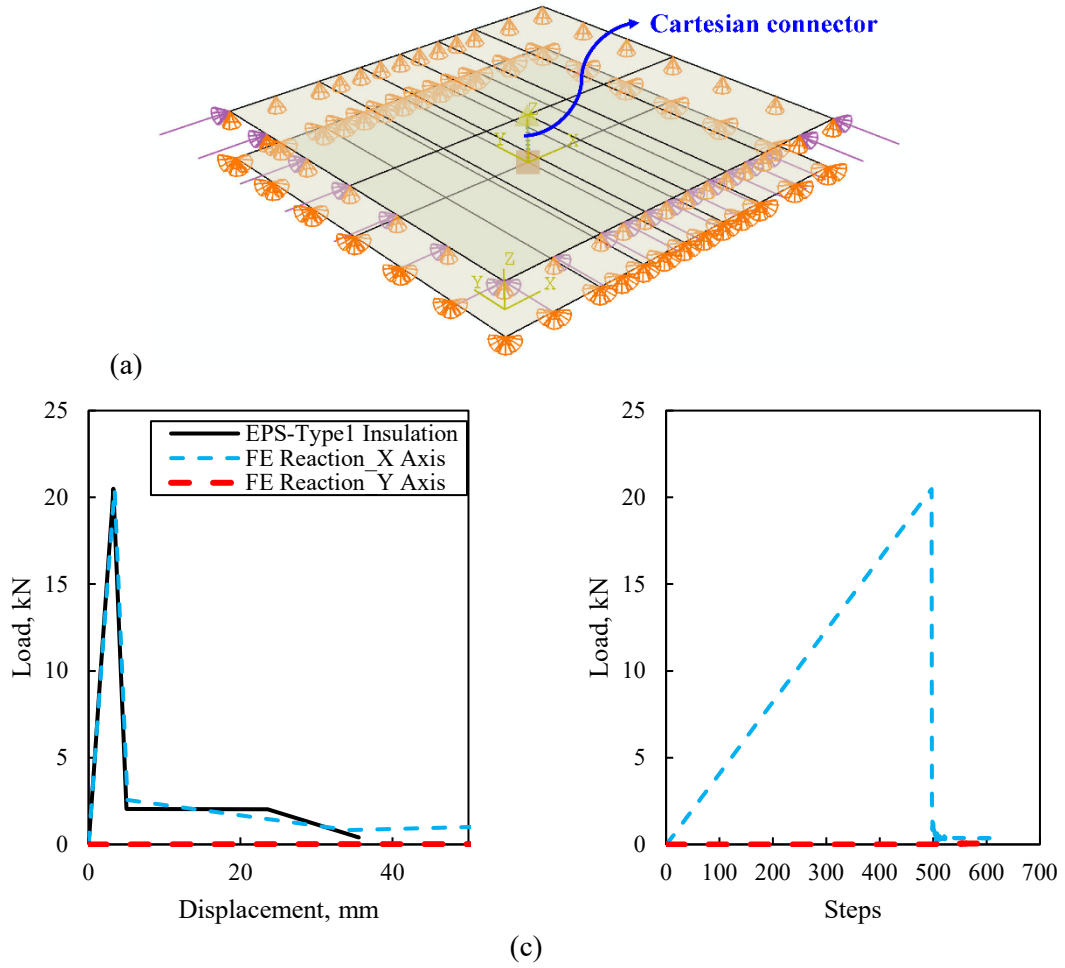
Figure 72. (a) Foam modeling connector, (b) connector load-displacement and (c) connector load vs. loading steps

5.4.1. Varying Primary Ultimate Flexural Resistance

The primary ultimate resistance, w_1, of the prototype panel is varied and calculated considering fully composite action per the one-way assumption [15]. While orthogonal (transverse) ultimate resistance, w_2, is kept constant for the minimum shrinkage and temperature requirements and calculated considering non-composite action. The transverse reinforcement consists of #10 (#3) bars spaced at 45.7 cm (18.0 in.) on center for all cases for top and bottom wythes. Table 16 summarizes all panel design case studies analyzed in this study. Using the strip method,

reinforcement ratio is calculated using Equation 19 where A_s corresponds the area of steel of the in

bottom wythe (i.e., the bar in the top wythe is not included in the reinforcement ratio calculation);

d corresponds to distance from extreme compression fiber to centroid of the extreme tensile

reinforcement; b corresponds to the tributary spacing of the bars. A detailed schematic of the cross-

section configuration is shown in Figure 70. It is assumed that the insulated precast concrete walls

in this study are exposed to weather, and thus the minimum clear cover for each bar is 1.91 cm

(0.75 in.), in accordance with ACI 318-14 [31].

The ratio of primary to transverse ultimate resistance is varied from 4.3 to 12.6. The lower

bound ultimate resistance was selected to ensure that the ratio of nominal moment capacity, M_n, to

cracking moment, M_{cr}, remains greater than 1. This ensures that the nominal moment capacity will

occur on the cracked section and thus mitigates any brittle failure mechanisms or significant

discrepancies when applying the component-specific limit states. The upper bound nominal

moment corresponds to net tensile strain, ε_t, of 0.008 which is approaching the lower bound limit

of 0.005 for tension controlled sections in accordance with ACI 318-14 [31].

The shear transfer is calculated using the strength concept as given in the PCI design

handbook [15] as shown earlier. The shear transfer considers the lesser of either the maximum

compressive strength of concrete or the maximum tensile strength of reinforcement. The shear ties

then must resist the shear transfer in the shear span, i.e. one half of the clear span for simply

supported elements. Following this approach, number of shear ties, N, are calculated using Equation

21 for the half of primary (vertical) direction span and shown in Table 16. It should be noted that,

for modeling simplicity, number of shear tie connectors are kept similar for the given range of

primary to transverse ultimate resistance ratio and load scaling is used to account for the change in

the number of shear ties.

Insulated precast panels with discrete connections are examined in this study. The results

of the finite element model are compared with the ultimate resistance that is calculated using the

current one-way assumption. Figure 73 shows the support conditions and loading diagrams to calculate the current practice flexural resistance (one-way assumption) for each case. The one-way ultimate resistance for each cases is calculated considering the primary, w_1, and transverse axis, w_2 [1]. Table 16 shows the primary, w_1, and the ratio of primary to transverse, w_1/w_2, ultimate resistance for each case. The ratios of w_1 to w_2 are larger than one for the selected cases which reveal that the transverse direction is weaker than the primary direction which may induce the formation of the weaker mechanism. As mentioned previously, the current practice assumes one-way behavior and considers the flexural resistance of the primary (vertical spanning) direction only. To evaluate this assumption, the response of the FE model is compared with the ultimate resistance in the primary direction. The comparison is mainly focused on resistance function, response limits and strain energy.

Table 16. Range of primary to transverse ultimate resistance ratios for case studies

Bar size	#13 (#4)	#16 (#5)	#16 (#5)
d (cm)	16.51	16.51	16.51
b (cm)	39.37	30.48	15.24
ρ (%)	0.20	0.40	0.80
ρ_T (%)	0.097	0.097	0.097
ε_t	0.04	0.011	0.008
N	24	48	94
M_n (kN-m)	240.45	381.91	705.12
M_n/M_{cr}	1.06	1.69	3.11
w_1 (kPa)	13.40	21.28	39.29
w_1/w_2 (kPa/kPa)	4.3	6.8	12.6
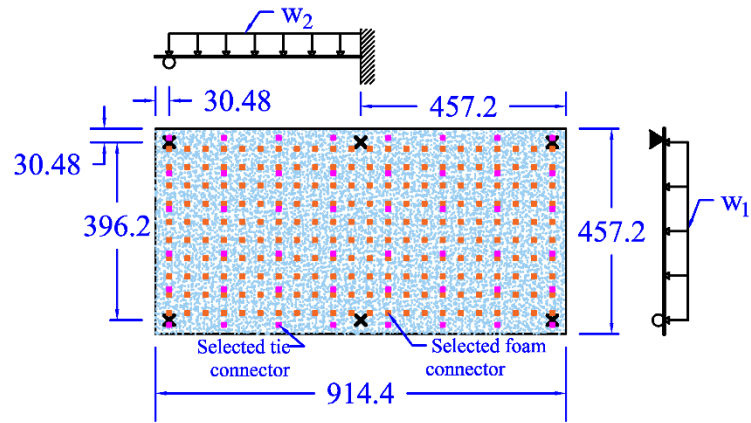
Figure 73. Current practice support conditions (units in cm)

5.5. Analysis Results

This section highlights the analysis results for insulated panels measuring 9.14 m (30 ft) wide, 4.57 m (15 ft) tall with six discrete connections while varying the primary ultimate resistance. The analyses are performed for the range of primary to transverse ultimate resistance ratios that is shown in Table 16. The results are labeled as follows: the first parameter denotes the ratio of primary to transverse ultimate resistance, e.g. w_1/w_2=6.8. The second parameter is added only for the worst scenario when no interaction between foam and concrete which denotes here that the foam resistance is not active, i.e. w_1/w_2=6.8_NoFoam. All other labeling is defined within the related section.

5.5.1. Idealized line supports and discrete connections

The current design approach assumed the discrete connections to behave as idealized line support, as explained earlier. The idealized line support behavior based on this assumption is examined and compared with the discrete connections. The insulated panel with a ratio of w_1 to w_2 equals 6.8 is selected for this comparison. The deflected shape at peak deformation is shown in Figure 74 for the panel with horizontal line support, i.e. Horizontal LS-w1/w2=6.8, vertical line support, i.e. Vertical LS-w1/w2=6.8, and six discrete connections, i.e. 6DC-w1/w2=6.8. Both panels with line supports reach to the expected mechanism based on the defined boundary

117

conditions. The panel with discrete connection reaches to an unexpected mechanism, i.e. bi-directional behavior around the middle support. The resistance functions for these panels are shown in Figure 75. The PDC limit states are included, for comparison with component specific milestone, and averaged for both span directions. Consistent with the deflected shape, the panels with idealized line supports reaches to higher capacity than the relative UFC approach due to the used of realistic material. The panel with discrete connection, designed to span vertically, reached to less strength than the UFC current approach, i.e. w_1, as a result of the unexpected mechanism that leads the panel to fail in the horizontal reinforcement of the top wythe above the middle support. The reduction in strength for the panels with discrete connections occurs due to the change in mechanism from bi-directional to quasi-horizontal (weaker) mechanism as shown in Figure 76. Component specific milestones for the panels with idealized line supports and discrete connections show discrepancy with the current limit states.
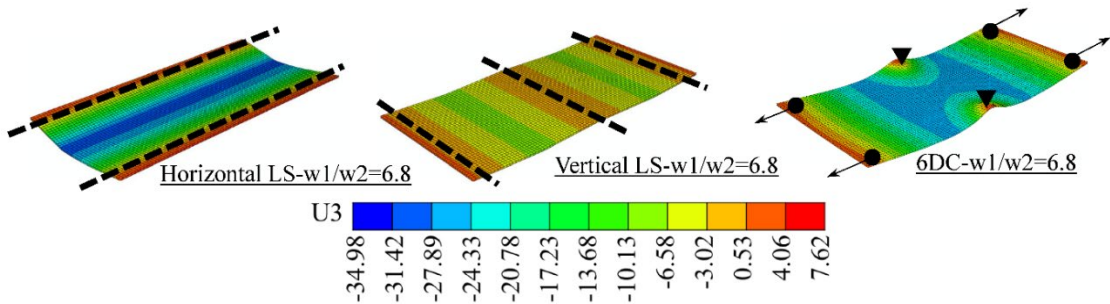
Figure 74. The FE deflected shape at peak for panels with idealized line support and discrete connections (units in cm)
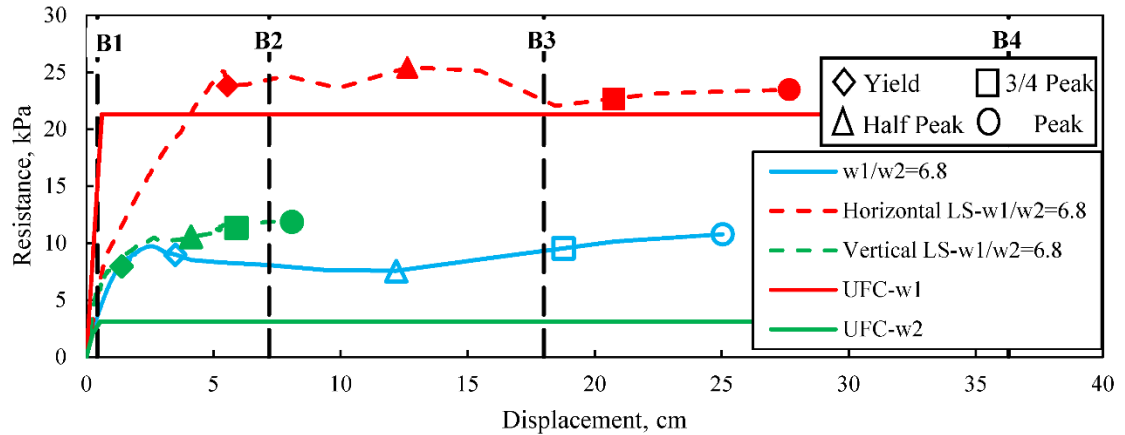
Figure 75. Resistance functions for the panels with idealized line support and discrete connections

w1/w2=6.8 (Yield)　　　w1/w2=6.8 (1/2 Peak)　　　w1/w2=6.8 (3/4 Peak)
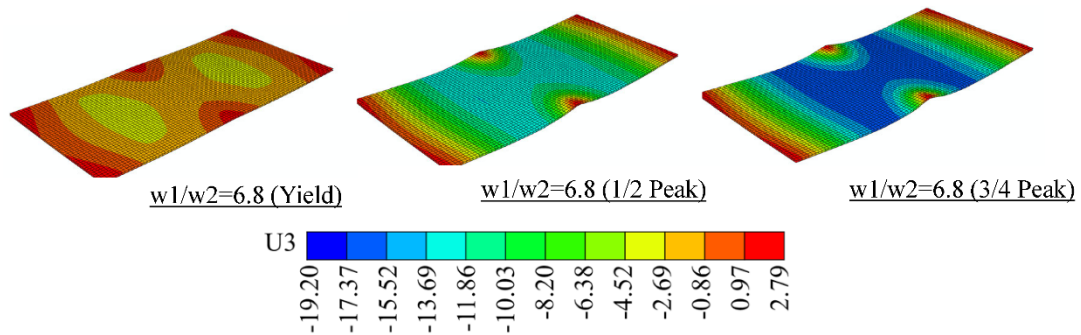
Figure 76. The FE deflected shape at peak for panels with discrete connections for yield, 1/2 peak, and ¾ peak milestones (units in cm)

5.5.2. *Resistance Functions and Deflected Shapes*

As explained earlier, the discrete connection may complicate the response of insulated panels and the one-way assumption may not be achieved. Thus, the effect of discrete connection is examined for the range of primary to transverse ultimate resistance as shown in Table 16. The deflected shape at peak deformation milestone are shown in Figure 77 for the examined insulated panels. Figure 77 shows the deflected shape for the cases where foam is active and foam is not active, i.e. resembles the worst scenario. The deformed shapes for the cases with no foam reveal similar transverse failure mechanism, weaker mechanism. For the cases with activated foam the deformed shapes show similar quasi-transverse mechanism. The failure for the panels with foam occurs at the transverse steel of the top wythe above the mid-connection. The FE resistance

119

functions for the insulated panel are shown in Figure 78a. The normalized resistance to the current one-way assumption, w_1, is shown Figure 78b. The resistance and normalized resistance are plotted against the displacement at the point of interest. The point of interest is measured at the location of maximum displacement at peak response, i.e. at peak deformation milestone (Figure 79). Component specific response limits as well as the prescriptive PDC response limits are shown in Figure 78 for comparison.

Similar resistance functions for the panels with no active foam (Figure 78a), is observed due to the weaker direction mechanism as shown in Figure 77. The results of the panels with active foam are nearly identical due to the consistent deformed shapes at peak deformation. The FE capacity underestimates the assumed one-way capacity for all cases as shown in Figure 78b. This is again due to the formation of the unexpected mechanism relative to the one-way assumption mechanism. Despite the formation of the transverse mechanism the peak displacements for panels with no active foam are able to achieve the PDC's B4 response limit. Panels with active foam reaches to higher capacity than panels with no active foam yet less ductility, i.e. peak displacement lower than the PDC B4. The results here confirms that the transverse is induced due to the use of primary ultimate resistance higher than the one in the transverse direction, i.e. w_1 to w_2 higher than one, as it assumed in the current design practice.
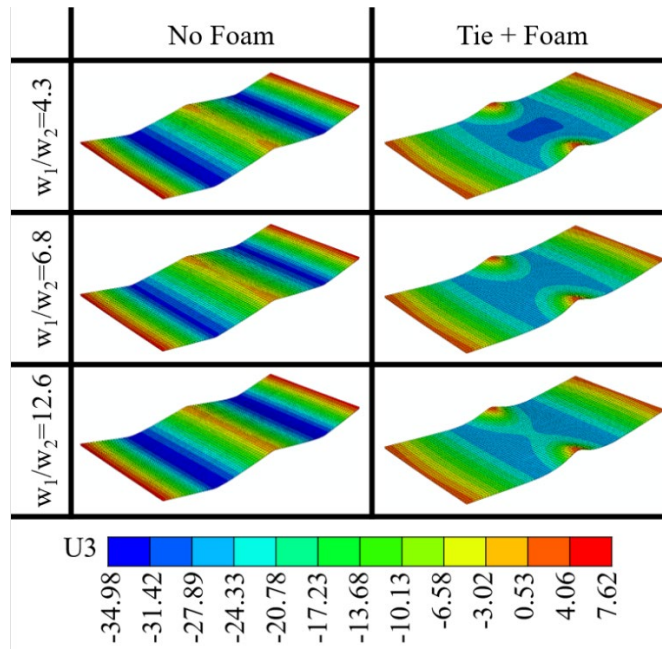
Figure 77. Peak FE deflected shapes for insulated panels with active and non-active foam (units in cm)

(a)

(b)
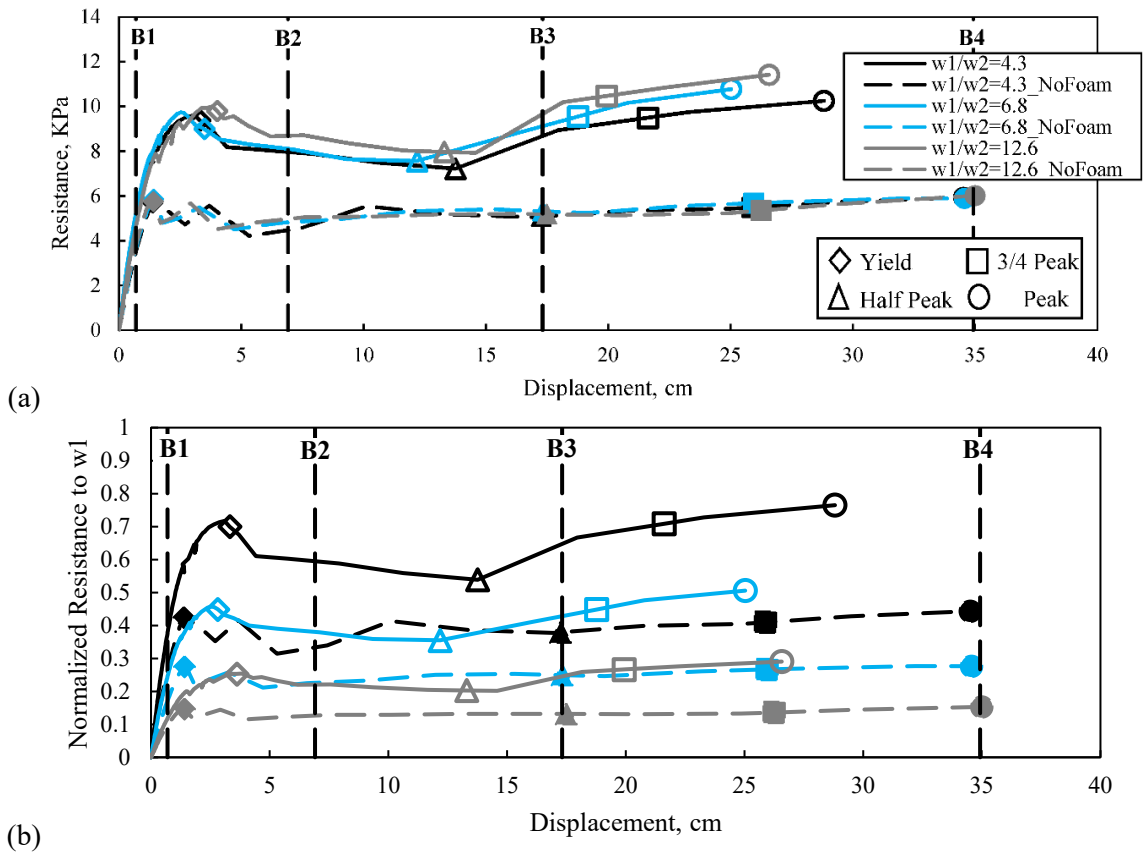
Figure 78. Out-of-plane flexural resistance of the insulated panel: (a) load-displacement resistance functions and (b) normalized to w_1
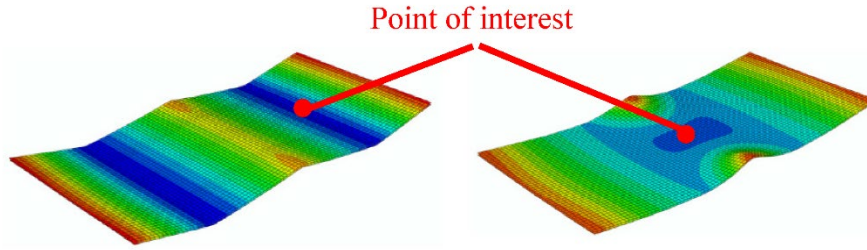
Figure 79. An example for the location of the displacement interest point

The load-displacement for selective connectors for the panels with active foam are shown in Figure 80. The selected connectors consist of foam and shear tie and are located as shown in Figure 73. As explained previously, the ties are considered to resist the flexural demands in the vertical direction only per the one-way assumption. The foam is assumed to resist the flexural demands in both direction. Therefore, 'FoamXX', as shown in the legend of Figure 80, represents the load-displacement for the foam in the horizontal direction. Similar representation is performed for the foam in the vertical direction. The results in Figure 80 shows increasing in load for the tie prior to the rebar first yield milestone where pure two-way deformed shape was observed. After that, reduction in the load is noticed due to the initiating of the quasi-horizontal (weaker) mechanism, shown previously in Figure 76. The selected foam connector, located near the mid-support as shown in Figure 73, shows increasing in load in the vertical direction near to the first yield in rebar milestone. After that reduction in the load is noticed which indicates failure of the foam in the horizontal direction. Since the loading in the foam is coupled in both direction, as illustrated previously, the vertical resistance for the foam connector fails simultaneously with the failure of the foam in the horizontal direction.
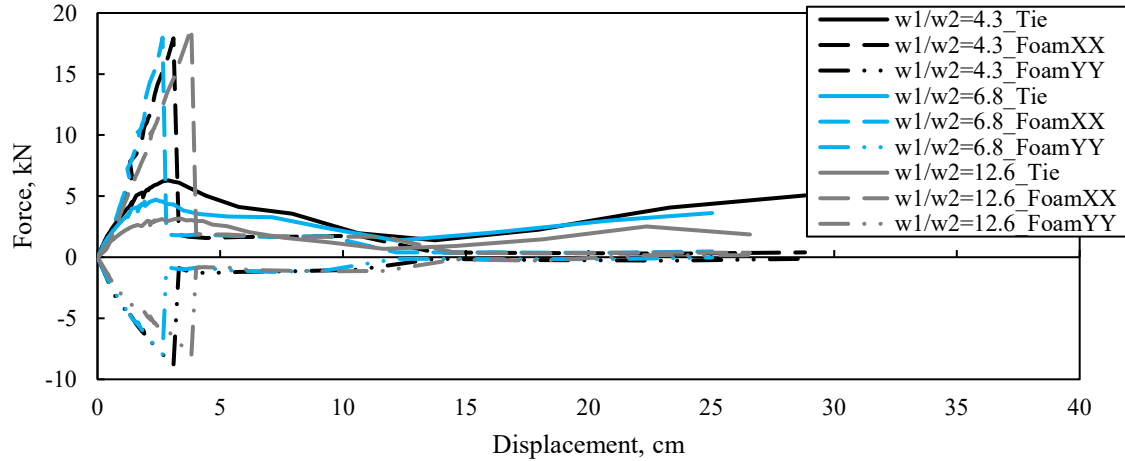
Figure 80. Load-displacement for selected tie and foam connectors.

5.5.3. Connection Reactions

The flexural design for blast-resistant wall panels with discrete connections is conducted with the assumption that the connections will provide the proper integrity to the panel allowing it to form and maintain a ductile flexural mechanism. To assess the effectiveness of this assumption, the reaction of each connection based on the FE study is obtained and compared to the reaction calculated based on the current UFC approach. The maximum reaction determined from the numerical analysis is compared with the UFC reaction in the weaker flexural direction. The reaction demands are based on the relative tributary area of each connection. The capacity of a connection, r, is found using Equation 20.

$$r = \min(w_1, w_2) \times Tributary\ Area \qquad \text{Equation 22}$$

The FE reactions for the insulated panel with active foam are investigated and compared with the UFC approach. Figure 81 illustrates these comparisons for two different connection locations: edge and middle of the panel. Figure 81a shows the reactions are plotted against the point of interest displacement. Middle connections result in higher demands than edge connections, as expected, based upon tributary width differences. The comparison between the UFC approach and the maximum FE reaction of the middle connection is performed using linear correlation as shown in Figure 81b. Cases which fall below and to the right of the bisecting line demonstrate situations

where the UFC approach predicts more reaction force than the FE model and thus the conventional design would satisfy both requirements. The opposite is true for data points above and to the left of the dividing line which illustrates panel configurations which the actual resistance function produces larger connection demands relative to design values. All panels fall into the latter classification as illustrated in Figure 81b. Designing the connections for the lower one-way flexural strength can result in an under prediction of the actual loads on the connection.

(a)   (b)
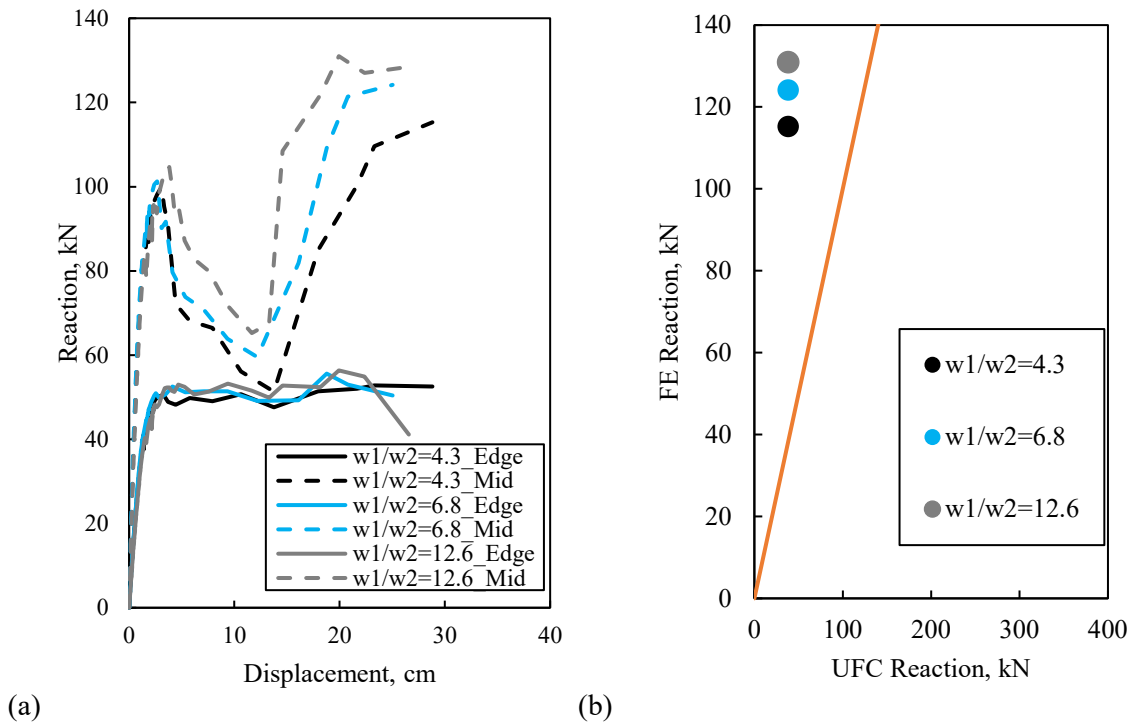
Figure 81. Reactions and linear correlation for insulated panels with active foam

5.6.   Dominant Span Sensitivity Study

The results for the parametric study have shown that the FE strength capacity for the insulated panels always underestimates the strength calculated based on the current one-way and fully composite action assumptions. Because of these assumptions, as explained earlier, minimum reinforcement as well as non-composite action were considered in the horizontal direction. These considerations results in possessing a ratio of primary to transverse ultimate resistance of higher than one which significantly impacts the capacity and induce the unexpected mechanism as

observed previously. The horizontal idealized line support illustrated that the capacity was achieved when the intended mechanism is formed. Therefore, a dominant sensitivity study is performed by strengthen the transverse direction which will results in a ratio of w_1 to w_2 equals or less than one. This is done with the insulated panel with a ratio of w_1 to w_2 equals 6.8 by replacing the minimum reinforcement in the transverse direction with higher amount of reinforcement. Table 17 shows the new arrangement for transverse reinforcement for the strengthen panel, i.e. w_1/w_2=1 and 0.5, It should be noticed that the ratio of w_1 to w_2 couldn't be decreased lower than 0.5 as a result of violating the nominal flexural assumption, i.e. the neutral axis is larger than the wythe thickness, for any additional reinforcement. The deflected shape at peak deformation milestone is shown in Figure 82. The strengthen panel, i.e. w_1/w_2=1 and 0.5, shows different mechanisms from the conventionally design panel, i.e. bi-directional behavior more into the vertical direction. The resistance function, component specific milestone and the current response limits for the strengthen panels are shown in Figure 83. The resistance function for the strengthen panel show significant improvement in capacity and ductility compared with the conventionally design panel. The panel with w_1 to w_2 equals 0.5 almost reach the PDC B4 milestone. The study shows that the intended mechanism couldn't be achieved since the ratio of couldn't be decreased lower than 0.5, as explained earlier.

Table 17. New arrangement of transverse reinforcement for insulated panels

Cases	6DC-w1/w2=1	6DC-w1/w2=0.5
Bar size and spacing	#16 @ 15.88 cm o.c.	#22 @ 12.45 cm o.c.

w1/w2=6.8   w1/w2=1   w1/w2=0.5
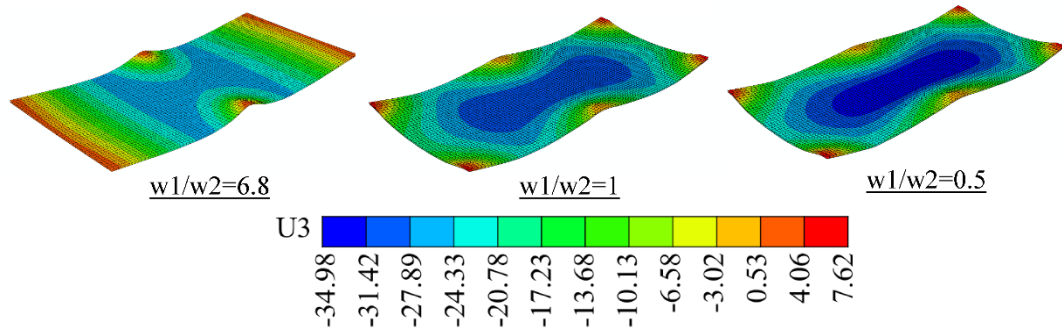
Figure 82. The FE deflected shape at peak deformation for the strengthen panel (units in cm)
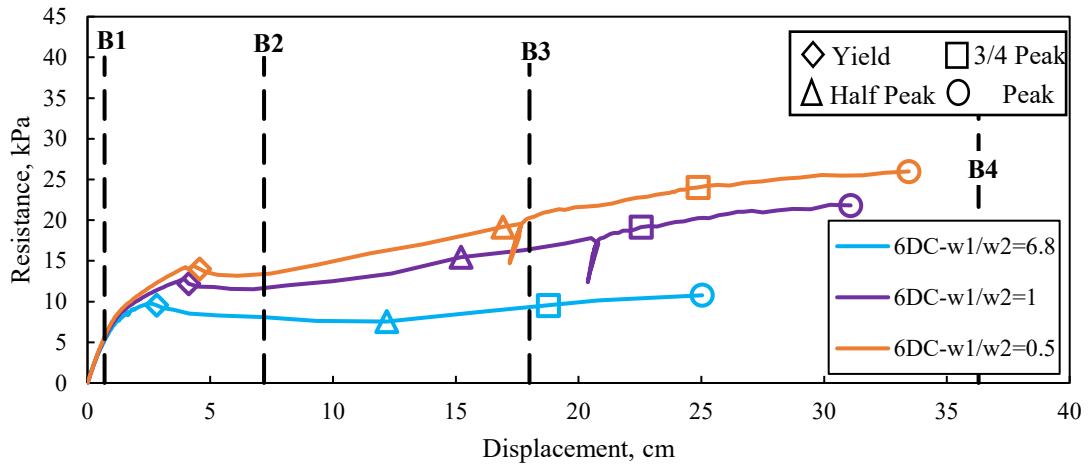
Figure 83. Out-of-plane flexural resistance of the strengthen panel

5.6.1. *Strain Energy*

The strain energy analysis is performed for the strengthen panels, i.e. w_1/w_2=1 and 0.5, and compared with the panel designed following the conventional approach, i.e. w_1/w_2=6.8. Comparison of strain energy provides a means of assessing the dynamic resistance of a structural component. Strain energy is computed as the area under the resistance function up to the desired response limit. Figure 84a illustrates an example for the calculated area (strain energy) under the FE and the current UFC curve for w_1/w_2=6.8 panel up to the desired response limits, i.e. 3/4 peak and PDC B3. The comparison is performed using linear correlation as shown in Figure 84b. Cases which falls below and to the right of the linear line show the UFC strain energy overestimating the FE strain energy and thus, unsatisfying the design requirements. The opposite is correct for the cases fall above and to the left of the linear line. The results for the conventionally designed panel,

126

i.e. w_1/w_2=6.8, shows overestimation for the UFC strain energy compared with the FE strain energy, except for the yield milestone and PDC B1 limit state. Improvement result is observed for the strengthen panels, especially the panel with w_1 to w_2 equals 0.5 where majority of the FE strain energy along the milestones reach to higher values than the UFC approach. The PDC B4 limit and peak milestone fall below and to the right of the linear and thus unsatisfying the design requirement. This may result due to the fact that the PDC limits are not correlated to material limit states, per Gombeda et al. [27].

(a)   (b)
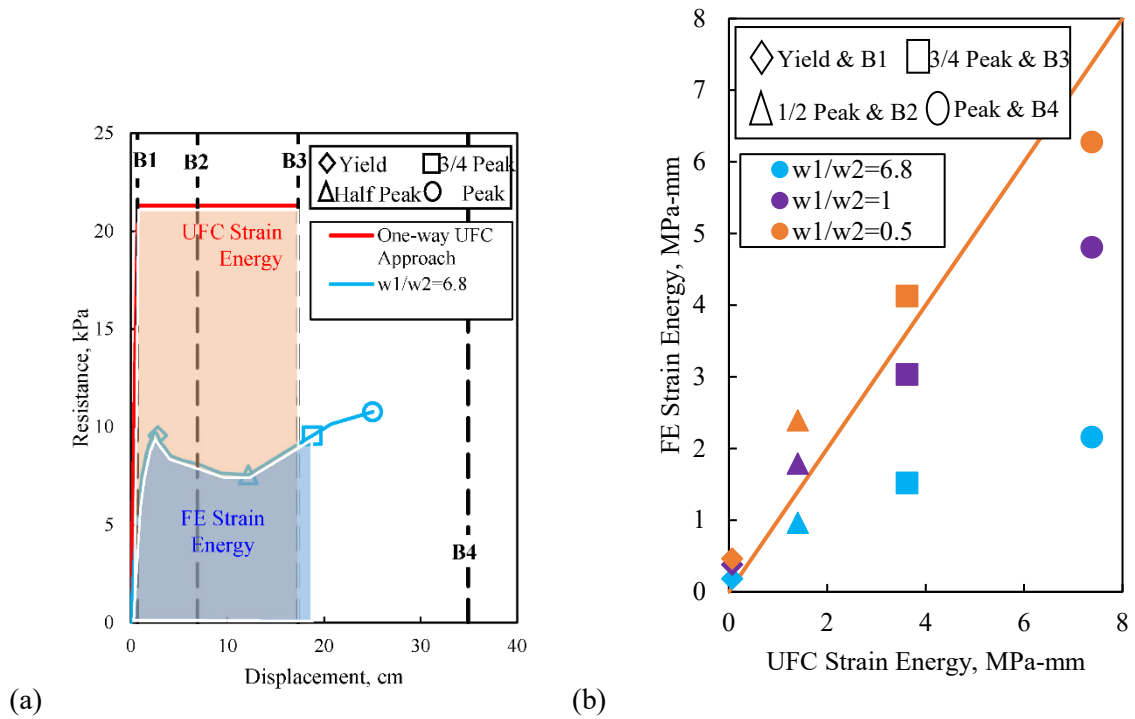
Figure 84. (a) FE and UFC strain energies example and (b) strain energy linear correlation for strengthen insulated panels

6. CONCLUSIONS

The work presented in this dissertation covered four topics about blast-resistant precast concrete wall panels. The conclusion for each topic can be made:

6.1.   Simplified Methodologies for Preliminary Blast-Resistance Design

6.1.1. Summary

This chapter focused on the implementation of a simplified methodology for the rapid assessment of blast-induced damage (i.e using pressure-impulse or *P-I* curves) during the construction bidding process and early design stage for precast concrete wall panels considering the conventional design assumptions. Two simplified approaches were developed: normalization approach and a curve fitting approach. The normalization approach was compared with the traditional SDOF model for a large sample of precast panel configurations and was found to have low error percentages, with 95% of the examined cases having error percentages between +/- 6%. *P-I* curves of 630 precast panel configurations were computed with the curve-fitting approach and also compared with conventional SDOF estimates. The curve fitting approach resulted in wider spread of error with approximately 70% of the cases having error percentages between -13% and +27%.

6.1.2. Contribution

- A spreadsheet-based tool was developed using the normalization which facilitates the inclusion of a broad range of panel constitutive parameters while maintaining ease of implementation for precast concrete producers and design engineers.

6.2.   Solid Panels with Discrete Connections

6.2.1. Summary

A numerical study of precast concrete cladding panels was conducted to examine the effect of discrete connections on the load-deformation response under out-of-plane loads. The study is

conducted using nonlinear finite element analysis using ABAQUS. The models are verified against four experimental research studies and found to provide a good estimate of the observed response. The validated models are used to conduct a parametric study of a prototype wall panel. The number of discrete connections and the primary ultimate resistance of the panel are varied. The ultimate resistance in the transverse direction is maintained for shrinkage and temperature requirements. The computed responses are compared to standard blast design practice which utilize elastic-perfectly-plastic response assumptions. A dominant span sensitivity study is performed which illustrates the ratio of primary to transverse resistance that leads the panel to reach to the intended mechanism as it considered by the current design practice. The study requires strengthening the transverse direction of the panel by replacing the minimum reinforcement with higher amount of reinforcement.

6.2.2. Contribution

- Using the idealized line support, the panel designed to span horizontally fails at the top of middle support which results in lower ductility compared with the panel designed to span vertically. Thus, designing the panel to span vertically is more preferable.

- Strengthening the panel with discrete connections in the primary direction only using a one-way assumption results in the formation of an unexpected mechanism in the orthogonal (weaker) direction for majority of the examined cases. This leads to a significant reduction in panel capacity and ductility.

- The orientation of the discrete connection degrees of freedom can impact the ability of a panel to form the intended mechanism. In some cases where the axial movement in the panel is restrained in the transverse direction and allowed in the primary direction a flexural mechanism will form in the primary direction even though the strength is weaker in the transverse direction.

- The strain energy estimated using the numerical models overestimates the UFC approach when the panel achieves the intended flexural mechanism. For higher ratios of primary to transverse

ultimate resistance, the FE strain energy is underestimated by the UFC approach due to the formation of the unexpected mechanism which also caused reduction in the ductility.

- The bi-directional behavior and the realistic material characteristic caused the connection demands at ultimate to be under predicted by the conventional design.

- Component specific limits are strongly dependent upon material properties and the ratio of primary to transverse ultimate resistance. Significant discrepancy between component specific limits and current practice limits is observed as a results of the unexpected weaker mechanism formation.

- Strengthening the panel by increasing the transverse reinforcement results in higher capacity and ductility. The study reveals that the intended flexural mechanism in the primary direction is only achieved when transverse strength is twice that of the primary direction.

6.3. Solid Panels with Opening(s) and Discrete Connections

6.3.1. Summary

The implications of discrete connections on the load-deformation response of precast concrete cladding panels with opening(s) subjected to out-of-plane-loads was examined in this study. The study is conducted using nonlinear finite element analyses using ABAQUS that has similar framework as the finite element model in chapter three. The models were verified against two experimental research studies from which good comparisons were observed. The validated model was used to conduct a suite of parametric studies on prototype wall panels with varying number of openings and reinforcement configurations and thus the ultimate strength. The computed responses are compared to standard blast design assumptions which utilize idealized boundary conditions, material properties, prescriptive response criteria, and an assumed primary flexural direction, regardless of the discrete connection layout. A dominant span sensitivity study is performed in this chapter which illustrates the ratio of primary to transverse resistance that leads the panel to reach to the intended mechanism as it considered by the current design practice. This

requires strengthening the transverse direction of the panel by replacing the minimum reinforcement with higher amount of reinforcement.

6.3.2. Contribution

- All conventionally design panels with a single opening and two openings examined in this study fail in the transverse direction (the unexpected direction). The failure typically occurs in the regions above and below the opening(s) and is caused by the reduction in resistance resulting from the geometric presence of the opening and the detailing of minimum temperature and shrinkage reinforcement in the transverse direction.

- The ductility of all panels, relative to current prescriptive antiterrorism response criteria, is compromised as a result of the unexpected failure mechanism.

- The maximum magnitude in the reaction function occurs due to the resistance integration of both directions. This behavior as well as using realistic materials overestimates the FE model reactions compared with the current approach reactions and thus lead to unconservative estimate of connections demands.

- Different assumed patterns of force interaction between blast-resistant window(s) and the adjacent concrete regions do not facilitate significant variations in panel response, relative to each other. This may be the result of the unexpected failure mechanism not fully exhausting the effects of this interaction.

- Strengthening the panel by increasing the transverse reinforcement results in higher capacity and ductility. The study reveals that the intended flexural mechanism in the primary direction is only achieved when transverse strength is four times that of the primary direction.

6.4. Insulated Panels with Discrete Connections

6.4.1. Summary

The out-of-plain flexural response of the blast-resistance insulated precast concrete cladding panels is examined via a numerical study that has similar framework as in chapter three and four. The study is performed to investigate the implication of the discrete connections and the current practice assumptions on the resistance function under out-of-plane loads. The models are verified against two experimental research studies and found to provide a good estimate of the observed response. The validated model is used to conduct a parametric study of a prototype wall panel. The ratio of primary to transverse ultimate resistance of the panel are varied. The computed responses are compared to standard blast design practice, i.e. one-way flexural assumption and considering a full composite behavior, which utilize elastic-perfectly-plastic response assumptions. A dominant span sensitivity study is performed in this chapter which illustrates the ratio of primary to transverse resistance that leads the panel to reach to the intended mechanism as it considered by the current design practice. This requires strengthening the transverse direction of the panel by replacing the minimum reinforcement with higher amount of reinforcement.

6.4.2. Contribution

- The capacity of the conventionally designed insulated panels for all range of primary to transvers ultimate resistance ratios underestimates the capacity of the current practice approach, i.e. one-way flexural assumption due to the unexpected weaker mechanism in the orthogonal direction.

- Worst scenario cases for insulated cladding panels are examined where the foam interaction with the wythes is not active. The result for these cases reveals weaker capacity than the cases with active foam and thus underestimates the current practice approach due to the formation of the transverse (weaker) mechanism.

- Foam resistance adjacent to the middle connections fails in the horizontal direction near to the yield milestone which induces the unexpected weaker mechanism.

- Connections reaction that are computed using the numerical approach and considering the realistic material characteristic reveal that connection demands are not achieved when following the conventional design approach based on the weaker flexural direction.

- Strengthening the panel by increasing the transverse reinforcement results in higher capacity and ductility. The study shows that the intended primary flexural mechanism could not be achieved due to the minimal thickness available in the non-composite wythes and the required transverse reinforcement needed.

- The strain energy is examined for the conventional designed panels and the strengthen panels. The results show improvement in strain energy for the strength panels compared with the conventionally designed panel.

REFERENCES

[1] Department of Defense (DoD). UFC 3-340-02 Unified Facilities Criteria: Structures to Resist the Effects of Accidental Explosions. 2014.

[2] Biggs JM. Introduction Desing to Structural Dynamics. McGraw-Hill Book Company; 1964.

[3] Jarrett DE. Derivation of The British Explosives Safety Distances. Annals of the New York Academy of Sciences 1968;152:18–35.

[4] Li QM, Meng H. Pressure-impulse diagram for blast loads based on dimensional analysis and single-degree-of-freedom model. Journal of Engineering Mechanics-Asce 2002;128:87–92. doi:Doi 10.1061/(Asce)0733-9399(2002)128:1(87).

[5] Fallah AS, Louca LA. Pressure-impulse diagrams for elastic-plastic-hardening and softening single-degree-of-freedom models subjected to blast loading. International Journal of Impact Engineering 2007;34:823–42. doi:10.1016/j.ijimpeng.2006.01.007.

[6] Shi Y, Hao H, Li ZX. Numerical derivation of pressure-impulse diagrams for prediction of RC column damage to blast loads. International Journal of Impact Engineering 2008;35:1213–27. doi:10.1016/j.ijimpeng.2007.09.001.

[7] Dragos J, Wu C. A new general approach to derive normalised pressure impulse curves. International Journal of Impact Engineering 2013;62:1–12. doi:10.1016/j.ijimpeng.2013.05.005.

[8] Dragos J, Wu C, Haskett M, Oehlers D. Derivation of Normalized Pressure Impulse Curves for Flexural Ultra High Performance Concrete Slabs. Journal of Structural Engineering 2013;139:120913014027006. doi:10.1061/(ASCE)ST.1943-541X.0000733.

[9] Wang W, Zhang D, Lu FY, Tang FJ, Wang SC. Pressure-impulse diagram with multiple failure modes of one-way reinforced concrete slab under blast loading using SDOF method. Journal of Central South University 2013;20:510–9. doi:10.1007/s11771-013-1513-z.

[10] US Army Corps of Engineers Protective Design Center. Single Degree of Freedom Structural Response Limits for Antiterrorism Design 2008.

[11] Department of Defense (DoD). UFC 3-340-02 Unified Facilities Criteria: Structures to Resist the Effects of Accidental Explosions. 2014.

[12] General Services Administration (GSA). Alternate path analysis & design guidelines for progressive Collapse Resistance. Washington, DC: 2013.

[13] Naito C, Oswald C. PCI Design Handbook: Appendix A: Blast-resistant design of precast, prestressed concrete components. PCI Journal 2014.

[14] Oswald C, Bazan M. Comparison of SDOF Analysis Results to Test Data for Different Types of Blast Loaded Components. Structures Congress 2014, 2014.

[15] Precast/Prestressed Concrete Institute. PCI Design Handbook. 7th ed. Chicago, IL: 2010.

[16] Giovino G, Olmati P, Garbati S, Bontempi F. Blast Resistance Assessment of Concrete Wall Panels: Experimental and Numerical Investigations. International Journal of Protective Structures 2014;5:349–66. doi:10.1260/2041-4196.5.3.349.

[17] Melançon C, Carufel SD, Aoude H. Blast Behavior of One-Way Panel Components Constructed with UHPC, First International Interactive Symposium on UHPC; 2016.

[18] Pantelides CP, Garfield TT, Richins WD, Larson TK, Blakeley JE. Reinforced concrete and fiber reinforced concrete panels subjected to blast detonations and post-blast static tests. Engineering Structures 2014;76:24–33. doi:10.1016/j.engstruct.2014.06.040.

[19] Cramsey N, Naito C. Analytical assessment of blast resistance of precast, prestressed concrete components. PCI Journal 2007;52:67–80. doi:10.15554/pcij.11012007.67.80.

[20] Naito CJ, Dinan RJ, Fisher JW, Hoemann JM. Precast/prestressed concrete experiments–series 1 (volume 1). Interim Report. AFRL-RX-TY-TR-2008-4616. Air Force Research Laboratory; 2008.

[21] McNeice GM. Elastic-plastic bending analysis of plates and slabs by the finite element method 1967:271.

[22] Sakka ZI, Gilbert RI. Structural Behavior of Two-Way Slabs Reinforced with Low-Ductility WWF. Journal of Structural Engineering 2017;143:1–9. doi:10.1061/(ASCE)ST.1943-541X.0001902.

[23] Tabatabaei ZS, Volz JS, Baird J, Gliha BP, Keener DI. Experimental and numerical analyses of long carbon fiber reinforced concrete panels exposed to blast loading. International Journal of Impact Engineering 2013;57:70–80. doi:10.1016/j.ijimpeng.2013.01.006.

[24] Jacques E. Blast Retrofit of Reinforced Concrete Walls and Slabs n.d.:286.

[25] Naito C, Hoemann J, Shull J, Beacraft M, Bewick B, Hammons M. Dynamic Performance of Non-Load Bearing Insulated Concrete Sandwich Panels Subject To External Demands. 2011.

[26] Department of Defense (DoD). UFC 4-010-01 Unified Facilities Criteria: DoD minimum antiterrorism standards for buildings. Washington, DC: 2013.

[27] Gombeda MJ, Naito CJ, Quiel SE. Performance-based framework for evaluating the flexural response of precast concrete wall panels to blast loading. Engineering Structures 2018;168:473–86. doi:10.1016/j.engstruct.2018.04.050.

[28] American Society of Civil Engineers. ASCE/SEI 41-06 Seismic Rehabilitation of Existing Buildings. 2007. doi:10.1061/9780784408841.

[29] ABAQUS analysis user's manual 2017. Johnston, RI, USA: Dassault Systems Simulia Corp.; 2017.

[30] Belarbi A, Hsu TTC. Constitutive Laws of Concrete in Tension and Reinforcing Bars Stiffened By Concrete. ACI Structural Journal 1994;91. doi:10.14359/4154.

[31] Building Code Requirements for Structural Concrete (ACI 318-14). American Concrete Institute; 2014.

[32] Popovics S. A numerical approach to the complete stress strain curve for concrete. Cement and Concrete Research 1973;3:583–99.

[33] Pauw A. Static Modulus of Elasticity of Concrete as Affected by Density. ACI Journal Proceedings 1960;57. doi:10.14359/8040.

[34] Gombeda MJ, Naito CJ, Quiel SE. Visual Damage at Flexural Response Milestones for Blast-Resistant Precast Concrete Panels with Varying Reinforcement. Engineering Structures n.d.

[35] Cashell KA, Elghazouli AY, Izzuddin BA. Failure assessment of lightly reinforced floor slabs. I: Experimental investigation. Journal of Structural Engineering 2011;137:977–88.

[36] ASTM Standard A615-18. Specification for Deformed and Plain Carbon-Steel Bars for Concrete Reinforcement. West Conshohocken, PA: ASTM International; 2018. doi:10.1520/A0615_A0615M-18E01.

[37] PCI Blast and Structural Integrity Committee. Blast Design of Precast / Prestressed Concrete Components 2009.

[38] F12 Committee. Specification for Glazing and Glazing Systems Subject to Airblast Loadings. ASTM International; n.d. doi:10.1520/F2912-17.

[39] Biggs JM. Introduction to Structural Dynamics. McGraw-Hill, Inc.; 1964.

[40] Wang T, Hsu TTC. Nonlinear finite element analysis of concrete structures using new constitutive models. Computers & Structures 2001;79:2781–91. doi:10.1016/S0045-7949(01)00157-2.

[41] Smith ST, Kim SJ. Strengthening of one-way spanning RC slabs with cutouts using FRP composites. Construction and Building Materials 2009;23:1578–90. doi:10.1016/j.conbuildmat.2008.06.005.

[42] Enochsson O, Lundqvist J, Täljsten B, Rusinowski P, Olofsson T. CFRP strengthened openings in two-way concrete slabs – An experimental and numerical study. Construction and Building Materials 2007;21:810–26. doi:10.1016/j.conbuildmat.2006.06.009.

[43] Rusinowski P. Two-way concrete slabs with openings n.d.:127.

[44] ASTM. ASTM Standard A615/A615M-16, Standard Specification for Deformed and Plain Carbon-Steel Bars for Concrete Reinforcement. 2016. doi:10.1520/A0615_A0615M-16.

[45] Pfeifer D, Hanson J. Precast Concrete Wall Panels: Flexural Stiffness of Sandwich Panels. ACI Special Publication 1965;11:67–86.

[46] Frankl BA, Lucier GW, Hassan TK. Behavior of Precast, Prestressed Concrete Sandwich Wall Panels Reinforced with CFRP Shear Grid. PCI Journal 2011:42–54.

[47] Woltman G, Tomlinson D, Fam A. Investigation of Various GFRP Shear Connectors for Insulated Precast Concrete Sandwich Wall Panels. Journal of Composites for Construction 2013;17:711–21. doi:10.1061/(ASCE)CC.1943-5614.0000373.

[48] Naito C, Beacraft M, Hoemann J, Shull J, Salim H, Berwick B. Blast Performance of Single-Span Precast Concrete Sandwich Wall Panels. Journal of Structural Engineering 2014;140. doi:10.1061/(ASCE)ST.1943-541X.0001020.

[49] Naito CJ, Hoemann JM, Shull JS, Saucier A, Salim HA, Bewick BT, et al. Precast/Prestressed Concrete Experiments Performance on Non-Load Bearing Sandwich Wall Panels: Fort Belvoir, VA: Defense Technical Information Center; 2011. doi:10.21236/ADA545204.

[50] Wang T, Hsu TT. Nonlinear finite element analysis of concrete structures using new constitutive models. Computers & Structures 2001;79:2781–91.

[51] Popovics S. A numerical approach to the complete stress-strain curve of concrete. Cement and Concrete Research 1973;3:583–99. doi:10.1016/0008-8846(73)90096-3.

[52] Trasborg P. Analytical and Experimental Evaluation of Precast Sandwich Wall Panels Subjected to Blast, Breach, and Ballisitic Demands. Lehigh University, 2014.

[53] Naito C, Hoemann J, Beacraft M, Bewick B. Performance and Characterization of Shear Ties for Use in Insulated Precast Concrete Sandwich Wall Panels. Journal of Structural Engineering 2012;138:52–61. doi:10.1061/(ASCE)ST.1943-541X.

[54] Gombeda MJ, Trasborg P, Naito CJ, Quiel SE. Simplified Model for Partially-Composite Precast Concrete Insulated Wall Panels Subjected to Lateral Loading. Engineering Structures 2017;138:367–80.

VITA

Omar Mohammed Alawad, son of Mohammed Alawad and Hosah Almuseter was born in March 10, 1987 in Buridah, Saudi Arabia. He earned his Bachelor degree in Civil Engineering in July 2010 from Qassim University. After graduation, Omar worked in a consultant office as a project engineer for three months. In January 2011, Omar received the approval to be one of the faculty members in Qassim University in Buridah, Saudi Arabia and to a scholarship to pursue his graduate study in the United States. He received his Master of Science in Structural Engineering in September 2014 from Lehigh University. Afterward, he pursue his Ph,D. study in August 2014 in Lehigh University in Structural Engineering. He will receive his Ph.D. degree in Structural Engineering in May 2019.